Introductory Climate Science

Global Warming Explained

Terry Sloan

TERRY SLOAN

INTRODUCTORY CLIMATE SCIENCE; GLOBAL WARMING EXPLAINED

Introductory Climate Science; Global Warming Explained
1st edition

ISBN 978-87-403-1408-3
Peer review by Michael J. Hambrey, Emeritus Professor of Glaciology,
Aberystwyth University

CONTENTS

FOREWORD

Climate Change is one of the burning issues of the day (no pun intended) and it is crucial to understand the nature of the reason or reasons for the undoubted average Global temperature change over the past century, or so. A number of text books on the topic have appeared, written in the main by meteorologists, and the conclusion is invariably that man-made emissions are responsible. However, there have been criticisms from some non-meteorologists, that their analyses are, if not flawed, seriously suspect. This is where the present book comes in. It is written by a distinguished elementary particle physicist who has no axe to grind and who is keen to go back to basics and analyse the physics involved.

To say that the book is comprehensive is an understatement. It ranges from the basic science in question, to such topics as the History of the Solar System and the work of the Intergovernmental Panel on Climate Change. Although written as an undergraduate text, and indeed the topics have served that purpose, it can be read by most people who have some knowledge of science; a summary should be prescribed reading for all politicians who have responsibility for the Earth's continued well being.

(Sir) Arnold Wolfendale FRS, 14th Astronomer Royal and former President of the Institute of Physics and the European Physical Society.

PREFACE

This book is intended to explain the basic principles of the science which lies behind the subject of man-made global warming. It is based on a series of lectures given as an optional course for physics undergraduates at Lancaster University. The course was named "The Physics of Global Warming". As befits a scientific study of a subject, quantitative treatments are given and the book contains algebra and formulae. Nevertheless it should be possible for a person with a non-mathematical background to read through these formulae and achieve an understanding of why the increasing concentration of greenhouse gases arising from burning fossil fuels leads to global warming. The term greenhouse gases here means mainly carbon dioxide (CO_2), methane (CH_4) and oxides of nitrogen.

My background is in particle physics and I became interested in climatology when it was hypothesised by some scientists that cosmic rays were the main cause of global warming rather than increasing greenhouse gas concentrations. Attempts were then made by myself and co-workers, all particle or cosmic ray physicists, to corroborate the hypothesis. The conclusion of this work was that while cosmic rays must have some effect on global warming via cloud formation, the effect is too small to be detected and therefore only plays a minor role.

Subsequent to this I became interested in trying to understand why changes in the small concentrations of greenhouse gases could lead to significant global warming. Having achieved at least a qualitative understanding of this, the course referred to above was designed and given. Another reason to be interested in this subject stemmed from reading accounts in the popular press and on the internet which often deny that man-made global warming is occurring. I felt it necessary to gain enough understanding to be able to judge the quality of such accounts. This book aims to allow the reader to be able to separate the science from the pseudo-science which surrounds this subject.

Nowadays, the hypothesis that increasing concentrations of greenhouse gases in the atmosphere cause global warming is almost universally accepted as the paradigm among expert climatologists and it is accepted by all learned societies of the World. The organisation responsible for overseeing and reviewing all the scientific literature which leads us to this conclusion is the Intergovernmental Panel on Climate Change (IPCC). This is a panel of many hundreds of the World's foremost experts on climate science. The work of the panel is described in Chapter 10 and is summarised in 5 publically available Assessment Reports (AR) which have been released so far. The first AR is labelled FAR, the second SAR, third TAR, the fourth AR4 and the latest one released in 2014 is AR5. These reports, running to thousands of pages, are all available on the World Wide Web at http://www.ippc.ch/. The reader is referred to these reports for further details of the theories and measurements and the references to the scientific papers where they are described. This book is meant to serve as a starting primer.

Chapter 1 of the book gives a qualitative (i.e. non-mathematical) overview of the basic reasons why our increased use of fossil fuels will lead to global warming and ultimately a change to the climate. The subsequent chapters describe the main features of the climate and the principles of the science which leads to these conclusions.

In the journey to achieve the understanding to permit me to write this book I have been helped by many people. I am particularly indebted to my colleagues Professor Anatoly Erlykin and Professor Sir Arnold Wolfendale for many stimulating discussions. I am also indebted to Professor Fred Taylor of Oxford University for his book Elementary Climate Science from which I learned much and for his help to further my understanding of the subject. I am grateful also to Professors Joanna Haigh and Giles Harrison for help on many topics. I also thank Professor Sir John Houghton for his assistance in writing Chapter 10. Particular thanks go to Professor Mike Hambrey for his suggestions and his critical reading of the manuscript. Finally I thank my Wife, Jean, for her love and encouragement to carry on even when writing became a chore.

T. Sloan (April 2016).

1 MAN-MADE GLOBAL WARMING – AN OVERVIEW

In this chapter a brief and qualitative overview is given of the science underlying man-made global warming from the increased concentration of carbon dioxide (CO_2) and other so-called greenhouse gases in the atmosphere. These have arisen from the increased burning of fossil fuels since the onset of industrialisation in the 19th century. The explanations in this chapter are covered more fully and quantitatively in the remainder of the book.

A simple model is briefly outlined in the chapter. This simple picture ignores all the many features of the climate other than the effects of increasing levels of greenhouse gases. It serves to show that global warming can be understood without the need for the more complicated models used by climate scientists which are fully documented in the reports of the Intergovernmental Panel on Climate Change (IPCC). However, to obtain a complete and accurate picture, all the features need to be accounted for and these are included in the more complicated models.

We start with a definition of what we mean by the climate. The climate is a long term average over all the large variety of weather variations. The weather represents the fluctuations about this average. For example, the Tropics have a climate which is warm and balmy; however, from time to time a snow storm can occur. The former (what you expect) is the climate but the latter (the fluctuation about the average) is the weather. A mnemonic is that the "climate is what you expect while the weather is what you get".

1.1 INTRODUCTION

Measurements of the average global surface temperature show a rising trend since the 19th century. This is what we term global warming. It is extremely likely that the causes are due to the increasing concentrations of greenhouse gases in the atmosphere from the burning of fossil fuels such as coal, gas and oil. The small probability of doubt in this statement will be discussed in later chapters. These fuels have been produced and used in increasing quantities since industrialisation. Such warming is leading to changes to the climate. The main greenhouse gas is carbon dioxide whose concentration has grown from 280 parts per million (ppm) in the early 19th century when large scale industrialisation began to over 400 ppm now (2016).

In this chapter a simplified overview of the reasons for this man-made global warming is given. This simplified overview summarises the book. The summary omits the mathematics necessary to master fully the picture of increasing greenhouse gas concentrations leading to man-made climate change. It rather gives an overview of the principles involved which, it is hoped, will make the application of mathematical details to the argument in later chapters easier to follow.

Although the vast majority of expert climate scientists accept that the emission of greenhouse gases leads to global warming and with it climate change (IPCC AR5 2013), there are some scientists and non-scientists who deny the connection. The vast majority of these are not experts on climate science. Man-made climate change denial will be dealt with in Chapter 11. It seems clear that to burn off the fossil fuels laid down over hundreds of millions of years in a period of a few hundred years must lead to serious consequences for the atmosphere. Such burning is effectively a slow-motion explosion.

A reason for denial is often given as mistrust of computer models. In this book a simple picture is derived which gives the first order principle on which these models are based. Such a basic picture is readily understandable. Hence we show that there is no need for complicated computer models to understand the basic science behind man-made global warming or anthropogenic global warming (AGW) as it is called. The room for doubt will be discussed in a later chapter.

Figure 1.1 shows the mean global surface temperature anomaly (i.e. difference from the 1961–1990 average global temperature) as a function of time. The curves are the results of different analysis techniques and they have been combined with the temperature records taken from thermometer readings after 1850. Roughly 1000 years ago the temperature was somewhat lower than today and this is sometimes referred to as the Mediaeval Warm Period. The temperature decreased to roughly 1°C cooler than today 300 years ago and this is sometimes referred to as the Little Ice Age.

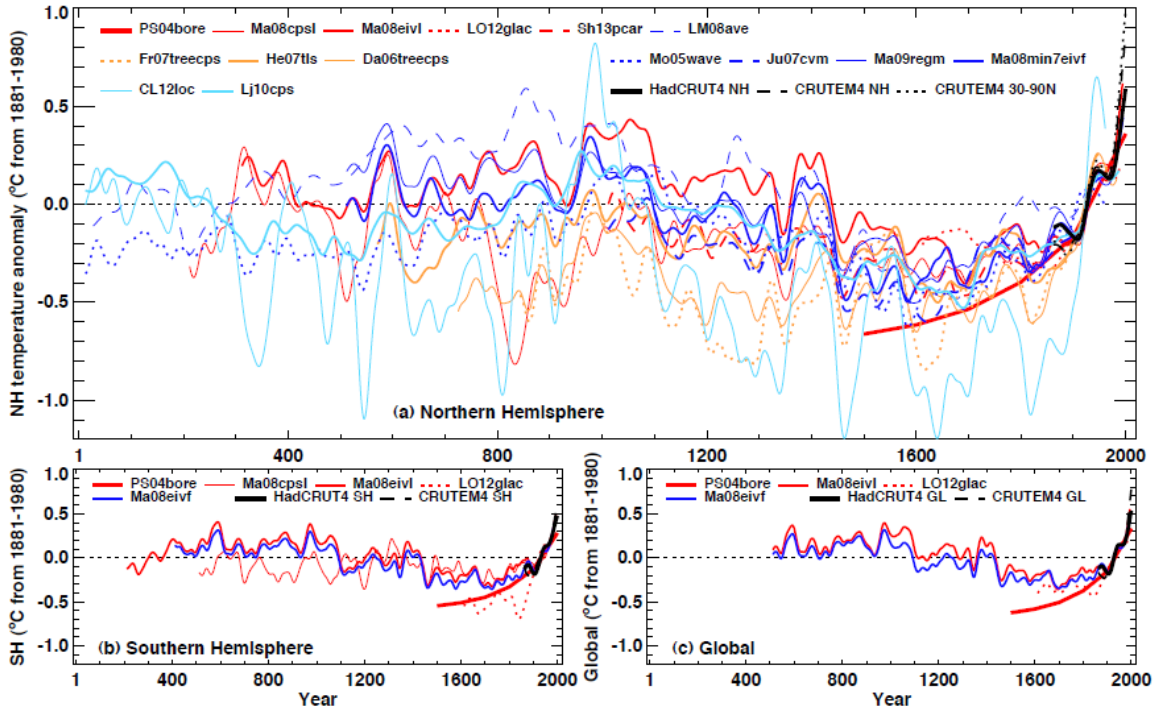

Figure 1.1 The mean reconstructed global temperature anomaly over the last 2000 years against time from various reconstructions in the (a) Northern (b) Southern Hemsipheres and (c) Global (Source IPCC AR5 2013, see this reference for the details of the different reconstructions). The accuracy can be judged from the differences between the different reconstructions.

Fig 1.1 and the reconstruction of Marcott et al 2013 (available at http://cdn.theatlantic.com/static/mt/assets/science/marcott-B-CD.jpg) shows that during the last 10000 years or so the mean global temperature has been relatively stable compared to the large decrease seen in the earlier ice age (see Chapter 9). During this epoch of stable climate mankind has progressed from being a hunter-gatherer into the present society of the 21st century. In other words the stable climate has allowed civilisations to flourish.

Corroboration of the sudden 20th century temperature rise is found in the area of sea ice in the Arctic which is observed to be shrinking due to the warming as shown in Chapter 5 (see figure 5.8b). Additionally, the mean thickness of the Arctic sea ice has been observed to have almost halved between 1970 and 2010 (Lindsay and Schweiger 2015). Conversely,in the Antarctic the sea-ice area has been increasing. This is thought to be due to complex processes from global warming such as the increased delivery of glacial meltwater produced by the rising temperatures. The meltwater is less dense than sea water so that it floats on the sea surface where it freezes more easily than salt water due to its higher freezing temperature. This freezing accounts for the increased Antarctic ice sheet. Further corroboration comes from glaciers all over the World from the Tropics to Polar regions which are shrinking at an accelerating rate because of rising temperatures (see Chapter 5, figure 5.9 taken from Llovel et al 2014). The shrinking of a glacier is illustrated in figure 1.2. There are a few exceptions of growing glaciers. These occur where the increased precipitation falling as snow, expected from global warming, more than compensates for the melting due to rising temperatures. Doubters point to the increase in Antarctic sea ice and the few growing glaciers to justify their view, ignoring the good scientific reasons for such effects.

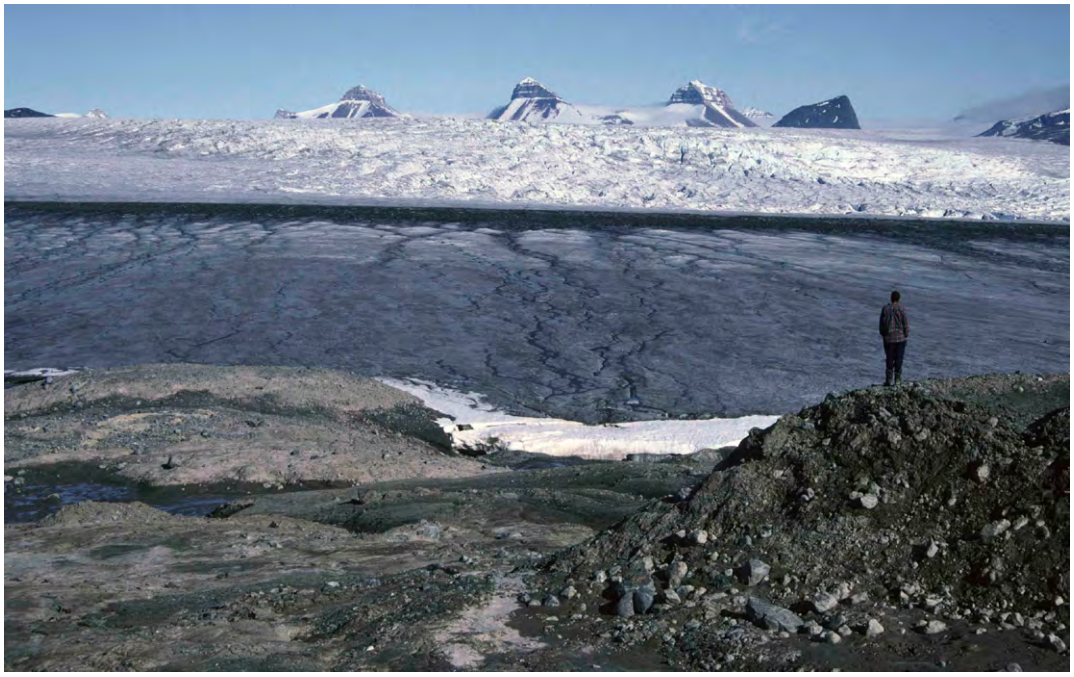

1996

2009

Figure 1.2 Kongsbreen, a tidewater glacies in Svalbard in the Norwegian Arctic, in 1996 and 2009. The person is standing in exactly the same position in each, and the mountains in the background serve as reference points. In the 1996 image glacier ice with its prominent moraine (the line of debris) fills the background. By 2009 a marine embayment has encroached into the glacier from the right. Note also how the mountains are more prominent in 2009, the result of substantial thinning of the glacier. (Photo, by kind permission of M. Hambrey). For more illustrations of melting glaciers see https://en.wikipedia.org/wiki/Retreat_of_glaciers_since_1850.

The main reasons for the sudden warming is widely believed to arise from the increase in the socalled greenhouse gas concentrations in the atmosphere. This name is applied since these gases act as a warming agent in the atmosphere as we shall discuss below. The increase in the concentrations of greenhouse gases since industrialisation is illustrated in figure 1.3.

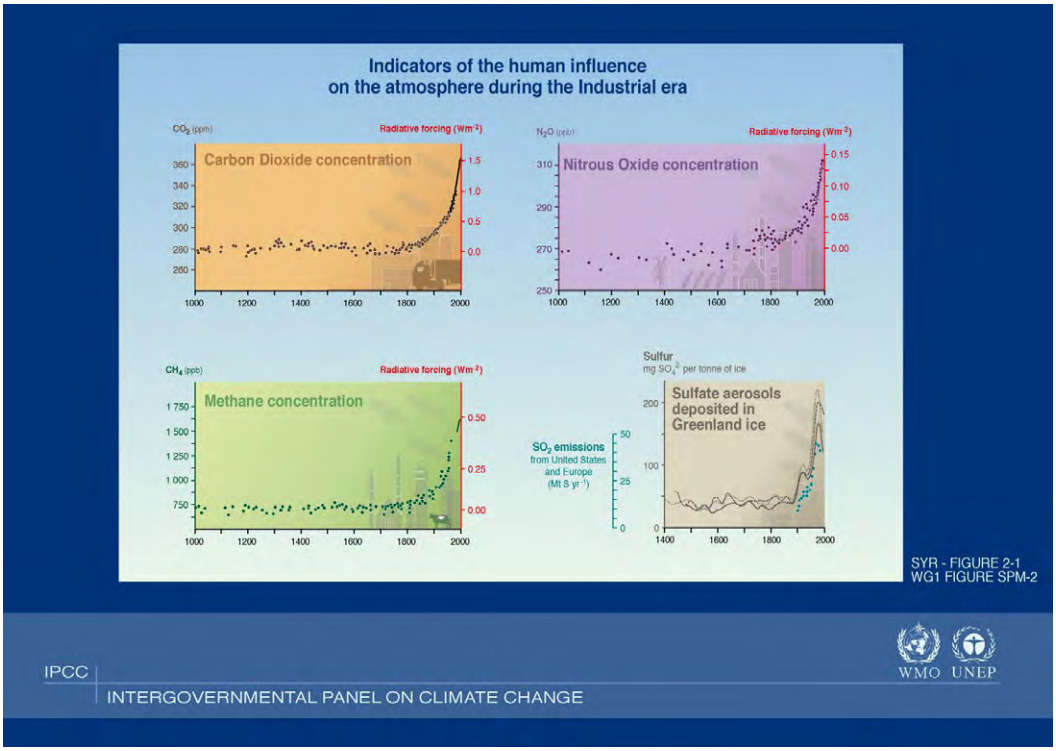

Figure 1.3 Illustrations of the rapid increase in various greenhouse gases since industrialisation began in 1800 (IPCC TAR).

1.2 WHY DO GREENHOUSE GASES CAUSE GLOBAL WARMING?

All bodies radiate energy which is carried away by electromagnetic radiation. For example when you feel the warmth from a heater your body is sensing the emitted radiation. The wavelength and intensity of such radiation depends on the temperature of the body. At low temperatures the radiation is mainly in the invisible infra-red region of the spectrum. The wavelength becomes shorter as the temperature increases. The intensity of the radiation increases rapidly as the temperature of the body increases (as the fourth power of the absolute temperature). Thus the sun at a surface temperature of 5780K radiates in the visible part of the spectrum. However, a warm water radiator at a temperature of order 340K (70°C radiates via infra-red radiation which can be felt on standing next to such a radiator (see endnote 1 page 202). To understand this, think of a block of iron put in a fire. If removed quickly it does not glow and one can only feel the heat radiated (via the infra-red radiation). If left longer in the fire the iron begins to glow with a dull red colour (red is a long wavelength visible radiation). If left longer still the iron glows when it becomes white hot i.e. all colours of the rainbow are being emitted as well as some infra-red radiation.

The Sun radiates its energy into space. Some of this is intercepted and absorbed by the Earth which warms as a result. The Earth then radiates energy into space as a result of the warming. The Earth reaches an equilibrium temperature when the energy absorbed from the Sun is equal to that radiated away. The Earth being much cooler than the Sun radiates its energy as infra-red radiation. As we shall show in later chapters, the temperature at which the Earth would be in equilibrium with the energy falling on it equal to that radiated away would be 255K (i.e. -18°C). Without greenhouse gases in the atmosphere the temperature at the Earth's surface would be close to this value i.e. most liquid water would be frozen and life as we know it would not exist on Earth. The presence of greenhouse gases causes the atmosphere to absorb the infra-red radiation emitted from the Earth's surface so that the atmosphere acts like a blanket around the Earth allowing it to warm to a more comfortable average temperature of 287K (14°C), at which life can exist.

Greenhouse gases are good absorbers of infra-red radiation due to molecular effects which will now be explained. The principal components of the atmosphere (78% nitrogen, 21% oxygen and 1% argon) absorb little of the sunlight incident on the Earth and little of the infra-red radiation radiating from the Earth's surface. However, the more complicated molecules in the trace gases which make up the greenhouse gases (such as water vapour and carbon dioxide) absorb little of the sunlight but are strong absorbers in the infra-red region of the spectrum. Absorption of the infra-red radiation emitted from the Earth's surface by such greenhouse gases causes the atmosphere to warm so that it itself radiates electromagnetic energy both upwards and downwards, with the downward component warming the surface of the Earth.

1.3 A SIMPLE PICTURE OF MAN-MADE GLOBAL WARMING

The greenhouse gases are well mixed in the atmosphere. However, as the height increases the water vapour becomes less important since it freezes out due to the decreasing temperature so that carbon dioxide becomes the largest contributor to the absorption of infra-red radiation. The process of absorption by greenhouse gases is illustrated in figure 1.4. The left hand panel shows the direct sunlight hitting the ground little of which is absorbed in the atmosphere. The infra-red energy radiated from the ground (lowest upward arrow) is absorbed in the layer of atmosphere nearest the ground which then radiates infra-red energy in all directions implied by the upwards and downwards arrows. The downward component warms the Earth's surface while the upward component is absorbed in the next layer. This also warms and radiates infra-red energy both upwards and downwards the downward component warming both the ground and the lower layers of the atmosphere. This continues through successive layers until the height where the atmosphere becomes too thin to absorb the upward going infra-red radiation. At this altitude the upward radiation escapes into outer space.

The situation with an increased concentration of carbon dioxide is illustrated in the right hand panel of figure 1.4. It can be seen from this panel that the height in the atmosphere at which radiation escapes to space increases as the carbon dioxide content of the atmosphere increases since there is more at higher altitude. In other words the effective thickness of the atmosphere increases.

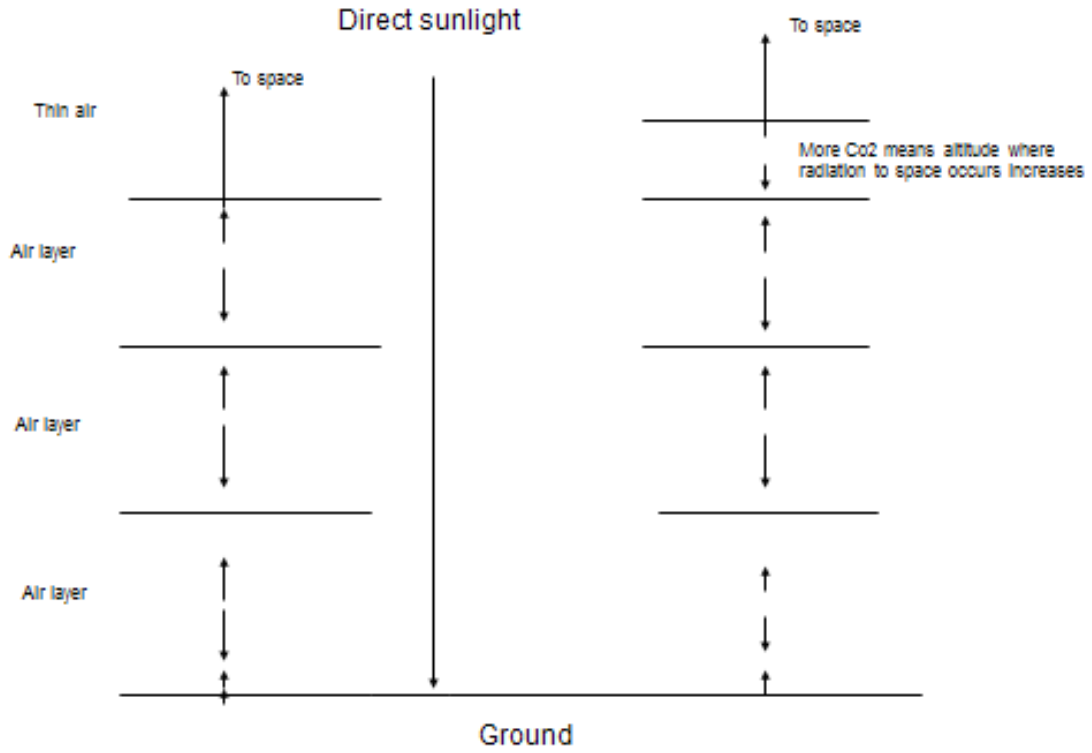

Figure 1.4 The process of absorption of infra-red radiation in the atmosphere. The centre downward arrow indicates the direct sunlight little of which is absorbed in the atmosphere. The left hand panel shows the re-radiation from layers of the atmosphere of infra-red radiation due to warming of the atmosphere from the Earth's surface. In the uppermost layer the atmosphere becomes too thin to absorb the radiation which then escapes into outer space. The right hand panel shows the situation for the increased carbon dioxide content. The altitude at which such radiation to outer space takes place is increased due to the greater level of absorbing carbon dioxide.

The temperature in the troposphere (the lower atmosphere) decreases at a constant rate of roughly 6 degrees per kilometre of altitude. This is known as the lapse rate. Such a constant decrease is imposed by the thermodynamics of the atmosphere and will be described in chapter 3. Thus if the altitude at which radiation to space increases, as a result of increasing greenhouse gas concentration, and the lapse rate is fixed, the temperature at the Earth's surface must increase by simple geometry, as illustrated in figure 1.5 (right hand panel). It can be seen from this figure that as the concentration of greenhouse gases increases the height in the atmosphere at which radiation escapes into space changes from the upper point of the solid line to the upper point of the dashed line. Since the gradient of the lines is fixed (the lapse rate) the temperature at the Earth's surface must increase as this height increases.

In effect, greenhouse gases allow the atmosphere to act like a blanket around the Earth. Addition of more greenhouse gases by the burning of fossil fuels causes the blanket to become thicker resulting in warming of the Earth. This picture will be quantified and discussed in more detail in Chapter 7. As we shall see there this simple picture produces a dramatic increase in global warming from the known increased greenhouse gas concentrations. This increase is greater than that observed. To obtain a more accurate picture, all the other known features of the climate must be accounted for.

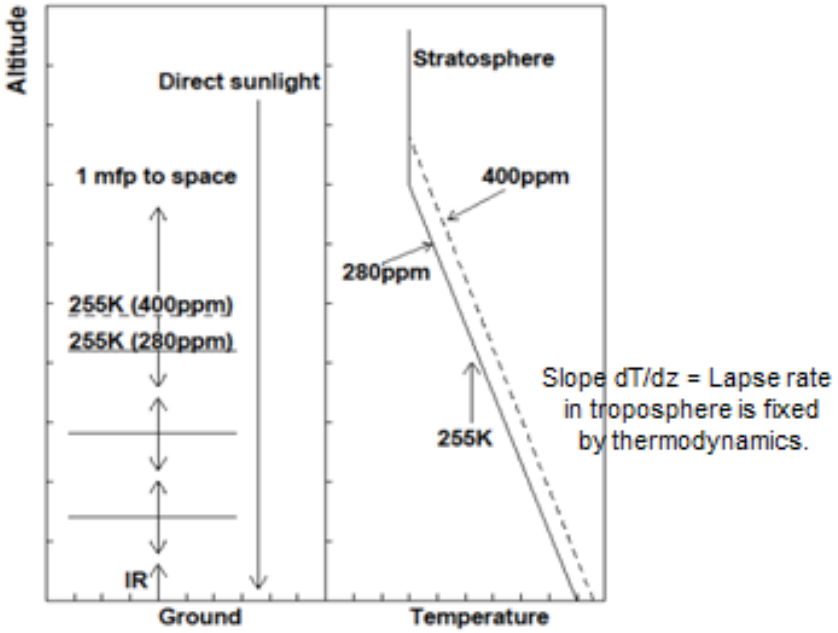

Figure 1.5 Left hand panel shows the increasing height at which radiation to space occurs as the greenhouse gas concentration increases (as in figure 1.4). The right hand panel shows how the fixed gradient (or slope) of the temperature decrease with altitude (dT/dz = the lapse rate) causes the surface temperature to rise.

1.4 THE MORE COMPLETE PICTURE

The grossly simplified picture described above is only a first order process by which increased greenhouse gas concentration lead to global warming. It ignores all other complications which affect the climate. There are many such complications: for example, much of the excess heat is absorbed by the oceans; some of the excess heat circulates in the atmosphere and oceans and is distributed around the globe; the warming is expected to lead to more severe storms which whip up more dust into the atmosphere producing cooling, etc., etc. Further complications arise from feedback mechanisms. These are mechanisms whereby warming produces a change. The change can lead to further warming so that a positive feedback results. The change could produce a cooling effect so that this would be termed a negative feedback effect. An example of a positive feedback is the melting of polar ice. Ice is highly reflective whereas the water to which it melts is less reflective. As a result the melting of ice to water allows more solar energy to be absorbed by the Earth which causes further warming. An example of a negative feedback mechanism is the fact that warming allows the atmosphere to take up more water vapour so that more clouds are produced. These tend to reflect away more of the solar radiation which produces a cooling effect.

All such known processes concerning the climate are modelled by the climatologists in computer simulations known as General Circulation Models (GCMs). These include the take-up of water vapour in the atmosphere due to the warmer air. Figure 1.6 shows the results of such simulations with and without the extra warming (or forcings as they a sometimes called) produced by man-made greenhouse gases. It can be seen that the models agree well with the measurements when man-made forcings are included (upper panel of fig 1.6) whereas the warming is not reproduced if they are not included (lower panel).

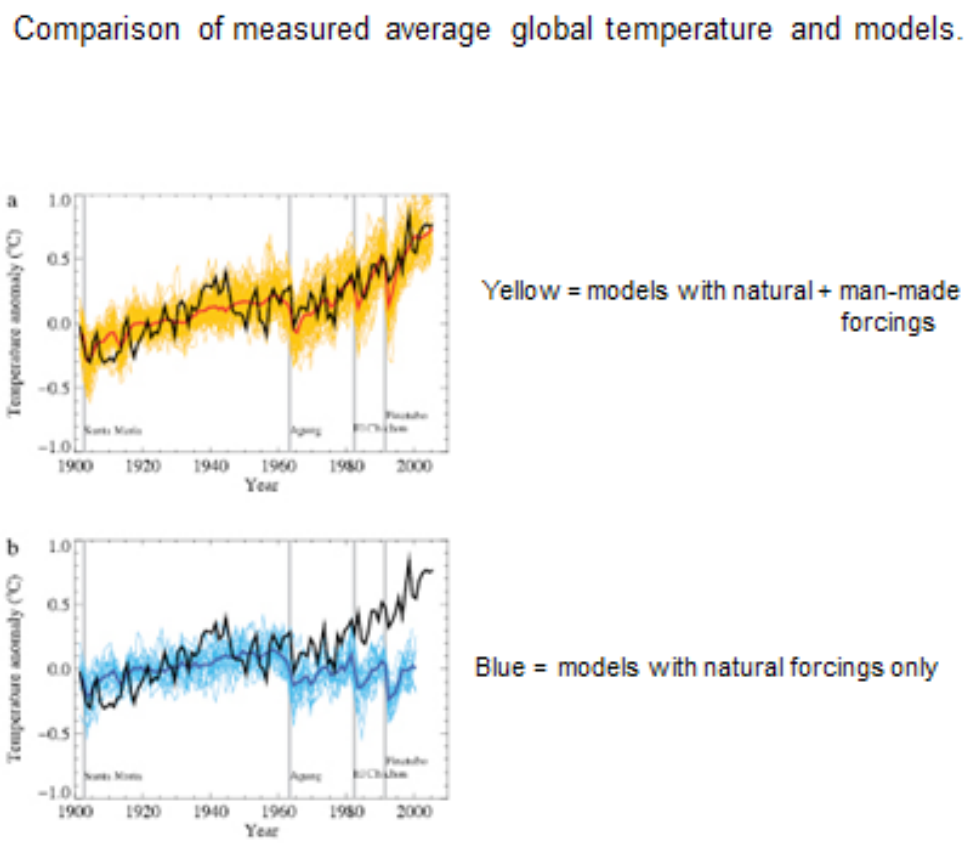

Figure 1.6 The measured mean global surface temperature against time throughout the 20th century (black curve). The yellow and blue curves show the results from many runs of different general circulation models (GCMs) (Based on Chapter 12 of the WG1 report, fig. 12.7 of IPCC TAR). The solid red and blue curves show the averages of all the models.

The Intergovernmental Panel on Climate Change (IPCC) has been reviewing all the scientific work on the climate since its inception in 1989 (see Chapter 10). Its conclusion that mankind is affecting the climate by the burning of fossil fuels has grown stronger with time.

1.5 CONCLUSION

In this chapter the physical basis of man-made global warming due to increasing greenhouse gas concentrations has been described. Since the First Assessment Report (FAR) of the IPCC, confidence has grown in the conclusion that the production of greenhouse gases by mankind's burning of fossil fuels is causing global warming which will lead to changes in the climate. In its latest assessment report (the fifth assessment report IPCC AR5), the IPCC assesses that it is extremely likely that human influence has been the dominant cause of the observed warming since the mid-20th century. Here extremely likely is defined as 95% probable. This statement implies that it is less than 5% probable that more than half the warming is due to natural causes. AR5 points out that such warming is leading to rising sea levels due to the melting of glaciers, the melting of the Greenland and Antarctic ice sheets and to thermal expansion of the oceans. It also points out that the warming will lead to more extreme weather events.

We continue in this book to attempt to understand at a fundamental level the basic scientific principles which have led to these conclusions. Chapter 2 describes the climate system and the principal drivers of the climate. Chapter 3 discusses the atmospheric science needed to understand the arguments. Chapter 4 goes on to discuss the science of clouds. Chapter 5 discusses the global circulation of energy and the monitoring of the climate. Chapter 6 discusses the aspects of molecular spectroscopy which cause greenhouse gases to absorb infra-red radiation while the principal components of the atmosphere (oxygen and nitrogen) absorb little. In Chapter 7 we discuss modelling the climate beginning by quantifying the simple model described above. In Chapter 8 we discuss the measurement of the global average temperature. Chapter 9 describes the history of the Earth and its climate since the formation of the Solar System. Chapter 10 describes the working of the IPCC. Chapter 11 discusses the uncertainty in the conclusion that mankind is changing the climate and the attempts to deny the science made in some quarters.

References

IPCC TAR Figures 1.3 and 1.6 are taken from the Third Assessment Report (TAR) of the Intergovernmental Panel on Climate change (IPCC) available at http://www.ipcc.ch. All other reports of the IPCC (including AR4 and AR5 referred to in this chapter) are also available on this web site.

IPCC AR5 2013, Report of WG1, ("The Physical Science Basis"), of the IPCC in the Fifth Assessment Report figure 5.7.

Lindsay R and Schweiger A 2015, 'Arctic sea ice thickness loss determined using subsurface, aircraft and satellite observations', *The Cryosphere* vol. 9 (2015) pp. 269–283.

Llovel et al 2014, 'Deep-ocean contribution to sea level and energy budget not detectable over the last decade', *Nature Climate Change*, Vol. 4 pp. 1031–1035. DoI 10.1038/NCLIMATE2387.

Marcott SA, Shakun JD, Clark PU and Mix AC 2013, 'A reconstruction of regional and global temperatures for the past 11300 years', *Science* vol. 339 pp. 1198–1201.

Exercises

1. A climate change sceptic stated that CO_2 is only present in the atmosphere at a concentration of 400 ppm (0.04%) and so such a small amount cannot be significant. Write a letter to him explaining why he is wrong. Point out why the increasing level of greenhouse gases is very likely to have serious consequences for the climate.
2. The climate change sceptic also made the statement that the IPCC concentrates on the greenhouse gas carbon dioxide whereas water vapour is a much stronger absorber of infra-red radiation. Write a letter to him to point out how the effects of water vapour are allowed for in the IPCC calculations.
3. A politician was heard to say "I believe that the Earth is warming but it is probably natural. Computer models cannot be trusted to allow you to conclude that the warming is man-made". Explain why his view is oversimplified.

2 DRIVERS OF THE CLIMATE

In this chapter the main drivers of the climate are described. These are the Sun, the water and carbon dioxide cycles, the effects of the greenhouse gases and the effects of heat transfer.

2.1 THE DIFFERENCE BETWEEN WEATHER AND CLIMATE

The weather is the meteorological condition at a particular place at a particular time. The climate at a particular place is the long term average over time.

For example, the tropical regions of the Earth have a warm and balmy climate. However, occasionally there will be a snow storm in the region at a particular time. The snow storm is attributed to the weather, whereas the warm balmy picture we have of the tropics is the climate. To summarise, the climate is what you expect at a particular place, the weather at any time is what you see which includes all the fluctuations about the average climate.

2.2 OVERVIEW OF THE CLIMATE

The climate is influenced by many factors. These are summarised in figure 2.1.

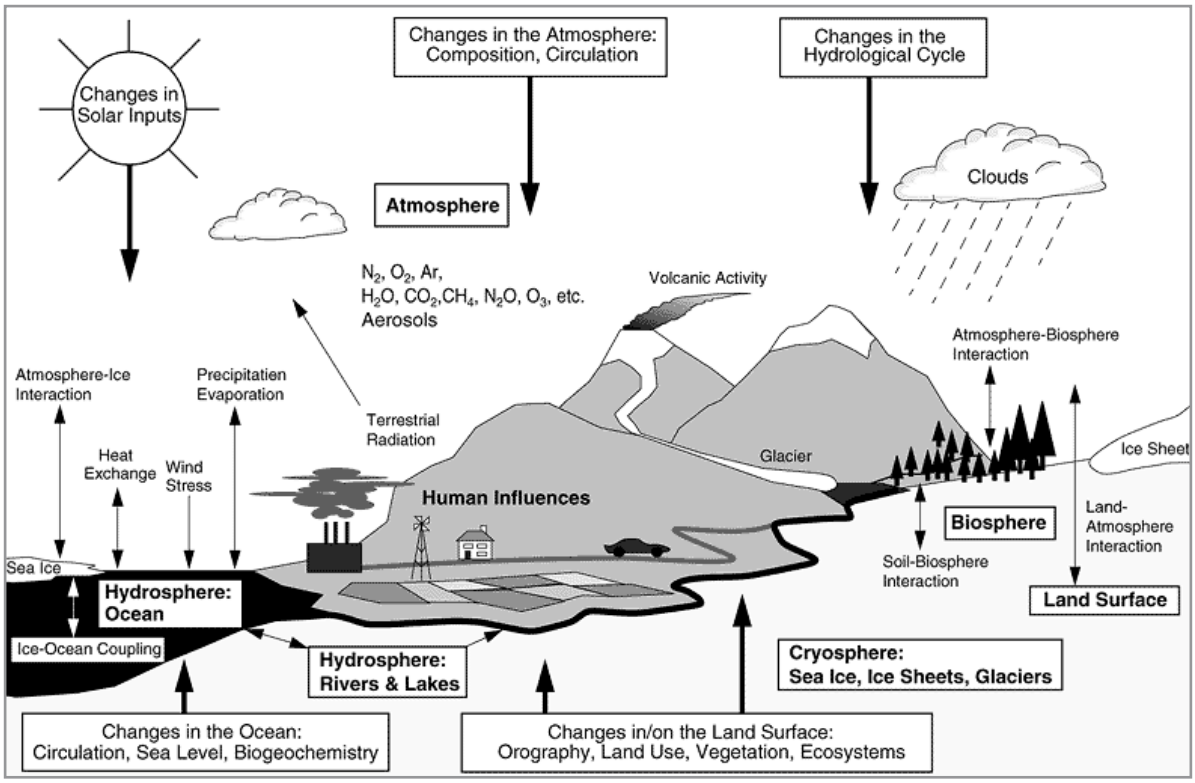

Figure 2.1 Schematic view of the components of the climate system (bold), their processes and interactions (thin arrows) and some aspects which may change (bold arrows). (IPCC 2001).

The Sun is the principal energy source which drives the climate. Its surface temperature is 5780k and it emits a total of 4 10^{26} W of power mainly by thermal radiation. Averaging this over a sphere containing the orbit of the Earth around the Sun (radius 1.5 10^{11} m) shows that at the Earth's orbit radius we receive solar radiation at the rate of 1366 W/m^2. This figure is known as the solar constant.

The Earth is approximately a sphere with radius R, i.e. area $4\pi R^2$. Hence each square metre of the Earth's surface receives on average ¼ of this radiation since the area of the disc intercepting the sunlight is πR^2. Roughly 30% of the radiation is reflected (mainly by the clouds) so that the energy falling on the Earth averaged over its surface is 1366(1-0.3)/4=239 W/m^2. The Earth is a warm body as a result of this energy and so the Earth itself radiates energy into space. Equilibrium is reached when the energy radiated is equal to the energy falling on the Earth since energy is conserved.

More of this energy falls directly at the Equator than at the poles of the Earth. However, the energy is somewhat equalised by the circulation of air currents (winds) in the atmosphere and by ocean currents. The oceans cover 71% of the Earth's surface and they contain much more stored energy than the atmosphere because of their greater mass. However, this energy is circulated more slowly by the slower moving ocean currents than by the winds in the atmosphere.

Evaporation from the surface of the oceans with subsequent precipitation as rain or snow followed by run-off back to the oceans defines the hydrological cycle of the Earth. Clouds are an intermediary of this cycle. The cycle is shown in figure 2.2.

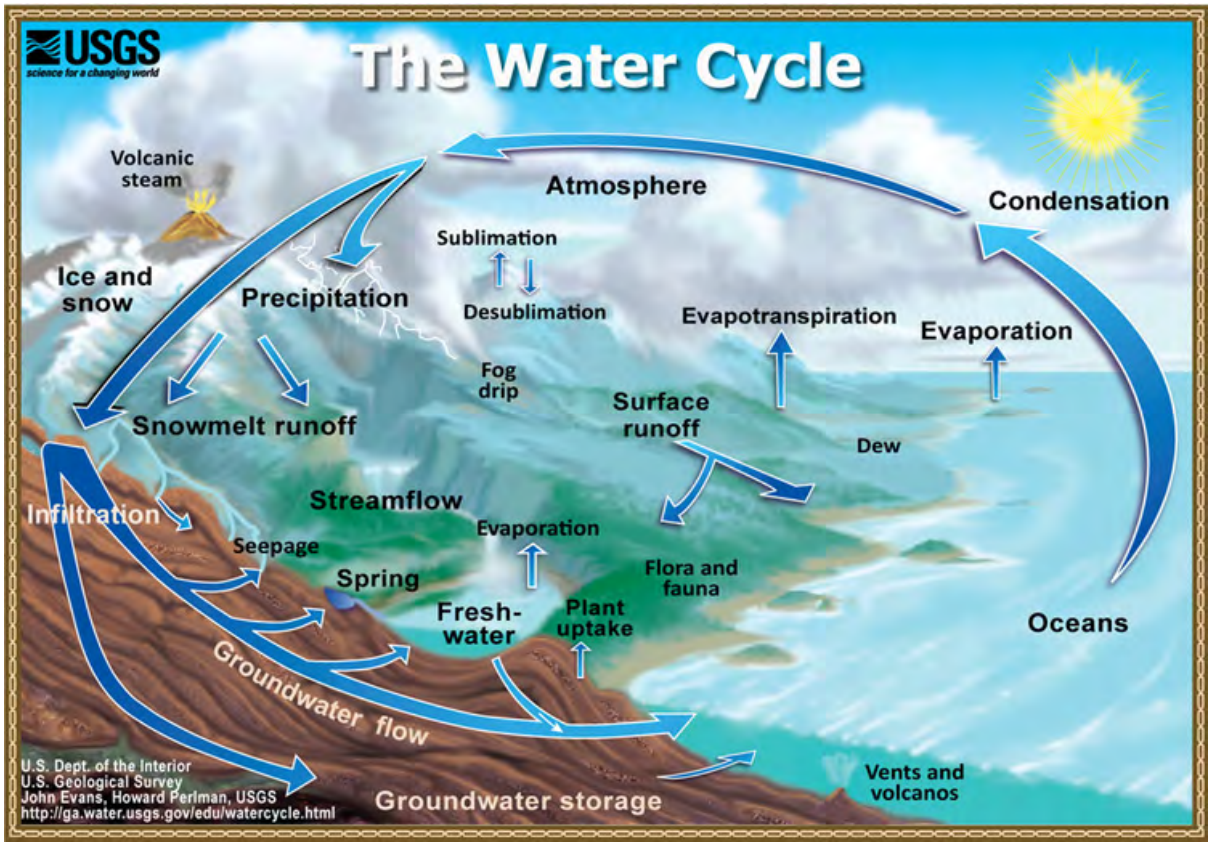

Figure 2.2 The hydrological cycle -. the recycling of water on the Earth (source John Evans and Howard Perlman, US Geological Survey http://ga.water.usgs.gov/edu/watercycle.html, photo courtesy Howard Perlman).

Air consists of 78% nitrogen (N_2) and 21% oxygen (O_2) and 0.93% argon (Ar). Simple monatomic and diatomic molecules such as these do not strongly absorb infra-red energy since molecular vibrational modes in them are not excited by such radiation. On the other hand such vibrational modes are excited in trace gases which are triatomic such as carbon dioxide (CO_2, concentration 0.04%) and water vapour and so they are very strong absorbers of infra-red radiation. The ability to absorb infra-red radiation means that these gases allow warming of the atmosphere and so they are known as greenhouse gases. The physics underlying the absorption of radiation by molecules of these different gases will be described in Chapter 6. The density of the air in the atmosphere falls approximately exponentially with altitude. The temperature also is variable with altitude falling approximately linearly up to the stratosphere. This will be discussed in Chapter 3.

Carbon dioxide (CO_2) is well mixed and cycles in the atmosphere. Figure 2.3 shows the CO_2 cycle. The atmosphere currently contains 730 Giga-Tonnes of CO_2 (1 Giga-Tonne = 10^{12} tonnes = 1 GT) and the oceans 38000 GT. CO_2 is slightly soluble in water so that the oceans take up an extra 90 GT per year. Of this 88 GT per year is re-evaporated. The CO_2 cycle has been put out of equilibrium by the burning of fossil fuels (6.3 GT per year) and to a lesser degree (0.2 GT per year) by agricultural activity.

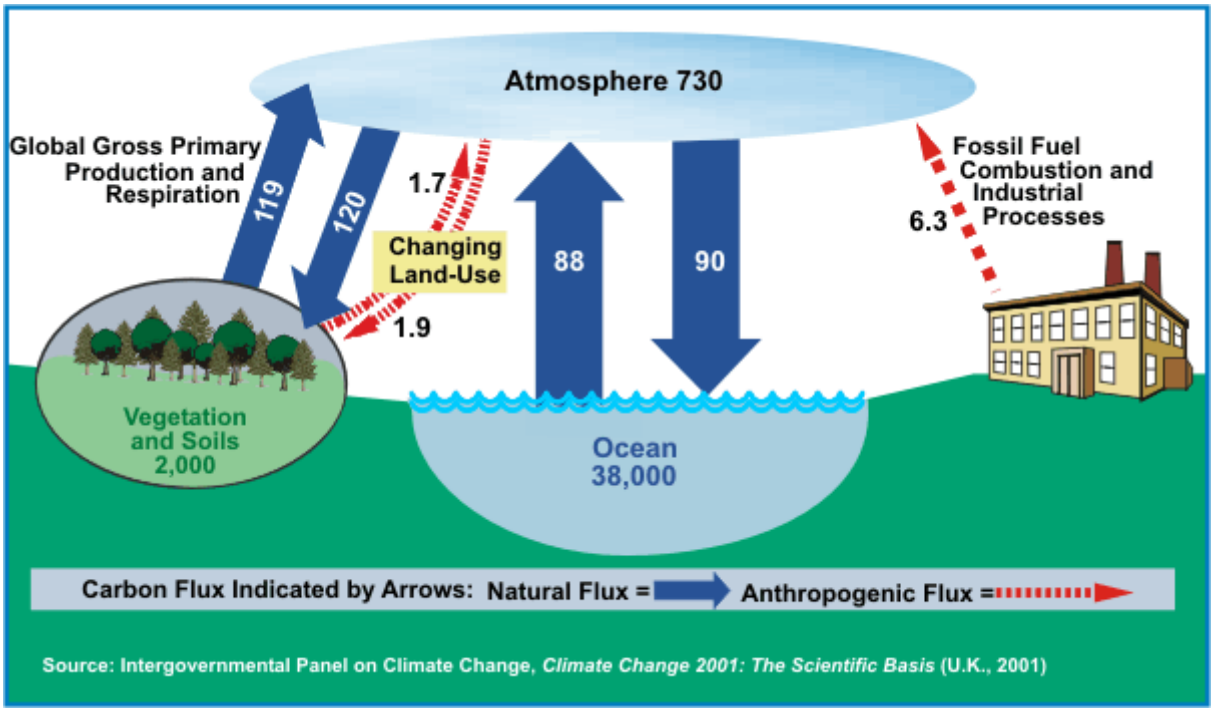

Figure 2.3 The CO_2 cycle, the numbers on the arrows show the fluxes of CO_2 in Giga-Tonnes (GT) per year. The remaining numbers show the total CO_2 stored in GT (IPCC 2001).

Other greenhouse gases include methane (CH_4) and oxides of nitrogen. The increase in greenhouse gas concentrations since industrialisation in the 19th century is evident from figure 2.4. The increase has disturbed the equilibrium of the carbon cycle, established since the end of the last ice age (about 12000 years ago) causing the Global Warming discussed in this book. We shall see in later chapters how this happens.

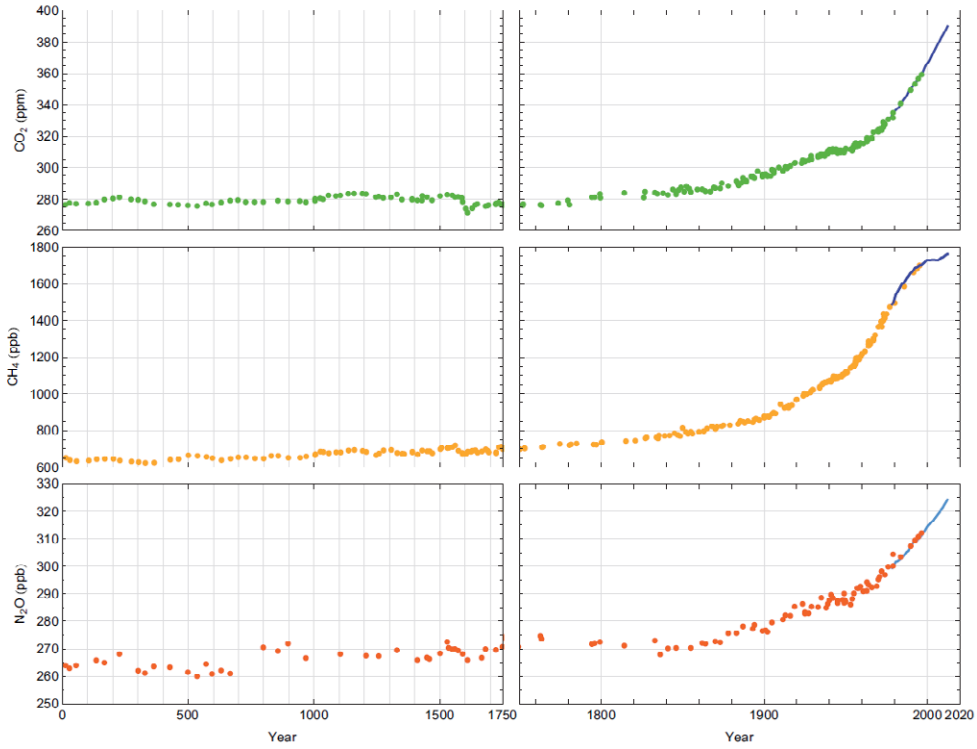

Figure 2.4 The greenhouse gas concentrations as a function of time since industrialisation (right hand plots) and earlier (left hand plots). (IPCC1 2013).

The increase in CO_2 in fig 2.4 has been shown to be from the burning of fossil fuels rather than from natural causes from the isotope ratios (IPCC2 2013). The proportions of the isotopes of carbon, ^{14}C and ^{13}C, in the atmosphere have been observed to decrease as the CO_2 content has increased since industrialisation. Fossil fuels contain little or no ^{14}C which is radioactive with a half-life of 5700 years. It will have decayed away in the hundreds of million years ago since the fossil fuels were laid down (see chapter 9). The photosynthesis of ^{13}C into plants occurs at a lower rate than the dominant isotope ^{12}C. Hence photosynthesis leads to plants and trees being deficient in this isotope. This was also true for fossilised plants from which fossil fuels are derived. The natural CO_2 in the atmosphere is diluted by that from fossil fuel burning which is deficient in the isotopes ^{13}C and ^{14}C. This causes the observed decrease in these isotopes in the atmosphere. The deficiency in these isotopes is hence a characteristic finger print of fossil fuel burning and is known as the Suess Effect (Suess 1955).

2.3 HEAT ENERGY TRANSFER

Heat energy is transferred by three processes, namely, conduction, convection and radiation.

Conduction occurs when two bodies are in contact. In this case the atoms in the hotter body collide with those in the cooler body where they touch to transfer kinetic energy to them. This energy diffuses to the cooler body so that the cooler body heats up.

Convection occurs when heat energy is transferred via a fluid from one body to another e.g. hot air rises from a radiator transferring energy from a hot surface to a cooler one above.

Thermal radiation is the emission by a warm body of electromagnetic radiation. All bodies emit electromagnetic radiation in amounts which depend on their temperature. This is known as thermal radiation. A body which is a perfect radiator is known as a black body. The emission from such a body was derived by Planck who showed that a black body at temperature T K emits electromagnetic energy at wavelength between λ and $\lambda + d\lambda$ at the rate given by $S(\lambda)d\lambda$. Here $S(\lambda)$ is the power density i.e. the energy emitted per unit area of the body per unit solid angle per unit wavelength range. It is derived from the Planck's formula which is plotted on figure 2.5.

The wavelength λ_{max} at which the radiant energy is maximum is obtained by setting $\frac{dS}{d\lambda} = 0$ in Planck's formula. This gives $\lambda_{max}T$ =a constant = 0.0028 mK (known as Wien's Law). The total energy radiated is obtained by integrating Planck's formula over wavelength to give Stefan's Law I.e. $E = \sigma T^4$ where σ = Stefan's constant = 5.67 10^{-8} Wm^{-2} K^{-4}.

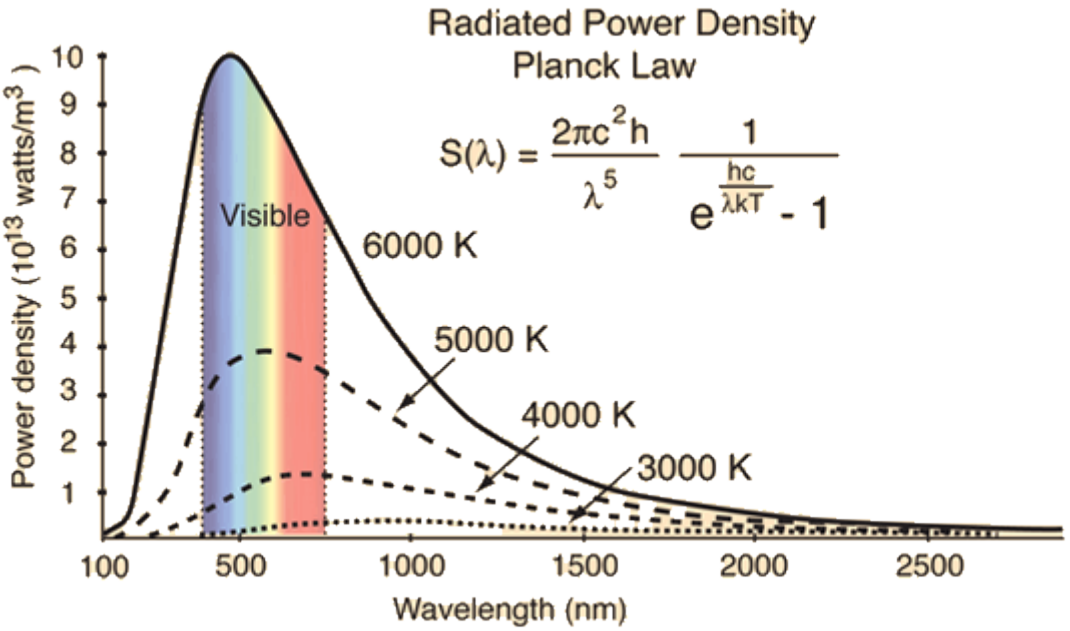

Figure 2.5 The spectrum of electromagnetic radiation emitted by a black body for different temperatures, T, in degrees absolute (K), from the Planck formula for S(λ) (inset). Here h is Planck's constant and c the velocity of light. The area under each curve gives the total energy radiated which increases as T^4 (Stefan's Law). The wavelength at the peak increases inversely as T (Wien's Law) (source http://hyperphysics.phys-astr.gsu.edu/bbrc.html).

Thermal radiation falling on a body is absorbed, increasing the temperature of the body. As it warms the body itself will emit thermal radiation until it reaches an equilibrium temperature where the energy absorbed is equal to the energy re-emitted. This is a consequence of the conservation of energy enshrined in the first Law of Thermodynamics.

Practical bodies are not black bodies i.e. are not perfect emitters or absorbers of thermal radiation. In practice thermal radiation is emitted at a rate $e\sigma T^4$ where e is the emissivity of the surface of the body. This is the fraction of the energy emitted by a black body at the same temperature. In a similar way the surface will only absorb a fraction, a, of the thermal radiation falling on it where a is known as the absorptivity of the surface. Kirchoff's Law states that the absorptivity a is equal to the emissivity e.

Kirchoff's law can be proved as follows. Suppose a body with emissivity, *e*, and absorptivity, *a*, is placed in an enclosure whose walls are at temperature *T*. The body would warm absorbing fraction *a* of the radiation falling on it. If *a* is greater than *e* then the body would absorb energy faster than it could emit it. In consequence it would heat up to a temperature greater than the walls of the enclosure. This violates the second law of thermodynamics since heat is being transferred from a cold body to a hotter body without any external work being done. Similarly if *a* is less than *e* heat would be transferred to the walls without the performance of work in violation of the second law. Therefore *a* must equal *e*. This means that good emitters of thermal radiation are also good absorbers.

2.4 THE SUN

The Sun is the principal energy source which powers the climate. It is a relatively small sized star which radiates a total power of 4 10^{26} W produced by thermonuclear fusion reactions in its core (see figure 2.6). The pressure in the core is large due to the gravitational pull on the material above it so that the density at the core is 15 times that of lead. The temperature at the core is of order 15 10^{6} K. At these pressures and temperatures the collisions between nuclei are so violent that they overcome the repulsion between the like-charged ionized nuclei. This allows nuclear fusion reactions to be sustained. The principal reactions which generate most (85%) of the solar energy convert four protons into a helium nucleus releasing a total of 26 MeV of energy (1eV= 1.6 10^{-19} J). This energy goes into the binding of the helium nucleus. A variety of other thermonuclear reactions is responsible for the remaining 15% of the solar energy.

In this principal reaction series a deuteron ($^{2}_{1}H$ the heavy isotope of hydrogen) is produced In the first reaction

$$p + p \rightarrow {}^{2}_{1}H + e^{+} + \nu$$

here p is a proton or the nucleus $^{1}_{1}H$.. The produced deuterons can then interact with further protons to produce the light isotope of helium ($^{3}_{2}He$) by the reaction

$${}^{2}_{1}H + p \rightarrow {}^{3}_{2}He + \gamma.$$

Pairs of $^{3}_{2}He$ can then interaction to produce the tightly bound isotope $^{4}_{2}He$ and two protons by the reaction

$${}^{3}_{2}He + {}^{3}_{2}He \rightarrow {}^{4}_{2}He + p + p.$$

In this way 4 protons react to produce a helium nucleus. The first of these reactions proceed via the weak nuclear interaction and has a rather small cross section as a result. Had this been a strong interaction process, the interaction cross section would have been much larger and the Sun would have burnt up all its nuclear fuel long ago.

A number of other fusion reactions occur but this series is the main one. The reactions generate the weakly interacting neutrinos (ν) which have been detected experimentally. The detected rate is that expected from such processes confirming this picture of solar energy generation (Olive et al 2014). The neutrinos in the process described above are rather low energy and are therefore difficult to detect. Those detected on the Earth are usually of a somewhat higher energy from processes which generate the remaining 15% of the solar energy. These were first detected in an experiment pioneered by Ray Davies et al (B.T. Cleland et al 1998) for which Davies shared the 2002 Nobel Prize in Physics. Davies actually saw about a factor 3 smaller rate than the billions per second expected. This deficit was subsequently shown to be due to the subtle property of neutrino oscillations, the demonstration of which led to the award of the 2015 Nobel Prize to A. MacDonald and T. Kajita from the SNO Collaboration (SNO 2013).

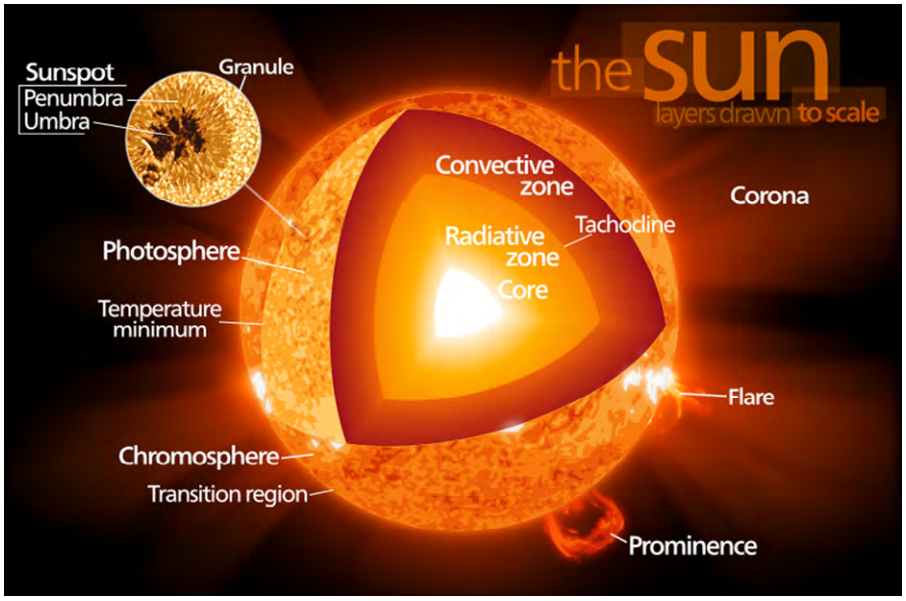

Figure 2.6 Artist's impression of the solar interior (source http://en.wikipedia.org/wiki/Sun published by Kelvinsong) showing the dense high temperature core in which the nuclear fusion reactions occur. The density then decreases with radius. As their name suggests the heat energy from the core is mainly passed by thermal radiation in the radiative zone and by convection in the convective zone thence to the surface.

The heat generated at the core of the Sun takes millions of years to diffuse to the surface. The surface of the Sun is at a temperature of 5780K radiating most of its energy into space as electromagnetic radiation. A small amount of energy is also emitted into space as streams of charged particles known as the solar wind.

Figure 2.7 shows the energy spectrum of the radiation from the Sun. It is close to a black body spectrum with deviations due to absorption of radiation in the photosphere (the solar atmosphere). The solar constant (defined above) has been measured by various satellites located outside the Earth's atmosphere. The current best estimate (Frôhlich 2012) is that the solar constant is 1366 W/m^2 and varies by 0.5 W/m^2 from solar maximum to solar minimum in its 11 year cycle. (See http://science.nasa.gov/media/medialibrary/2009/03/31/01apr_deepsolarminimum_resources/irradiance.jpg).

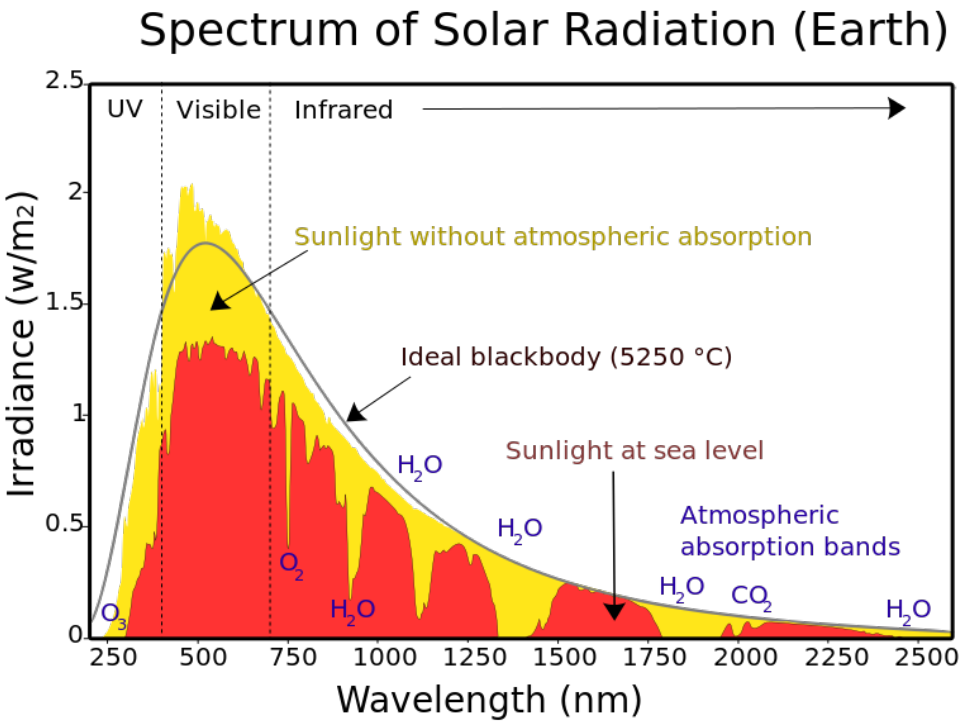

Figure 2.7 The solar spectrum measured above the atmosphere (yellow shaded region) and that calculated from Planck's formula for a perfect blackbody at the solar surface temperature of 5780 K (black curve). The deviations of the yellow region from the black curve are caused by effects in the photosphere (the solar atmosphere). The red shaded region shows the spectrum measured at sea level. Note the bands of strong atmospheric absorption labelled O_3, O_2, H_2O and CO_2 (the substances responsible for each bands). (Image prepared by Robert A. Rohde as part of the Global Warming Art project, published under the GNU Free Documentation License.)

2.5 WARMING OF THE EARTH'S SURFACE DUE TO GREENHOUSE GASES.

The Sun, at a surface temperature of 5780K, emits thermal radiation with a peak wavelength in the visible region of the electromagnetic spectrum (see figure 2.7). The Earth is warmed by this radiation but to a lower temperature. At this temperature the thermal radiation is mainly in the infra-red region of the spectrum (see figure 2.8). As stated earlier the principal components of the atmosphere (nitrogen and oxygen) do not absorb infra-red radiation but the greenhouse gases are strong absorbers. This is illustrated in figure 2.8 which shows the fraction of radiation absorbed in the atmosphere as a function of wavelength.

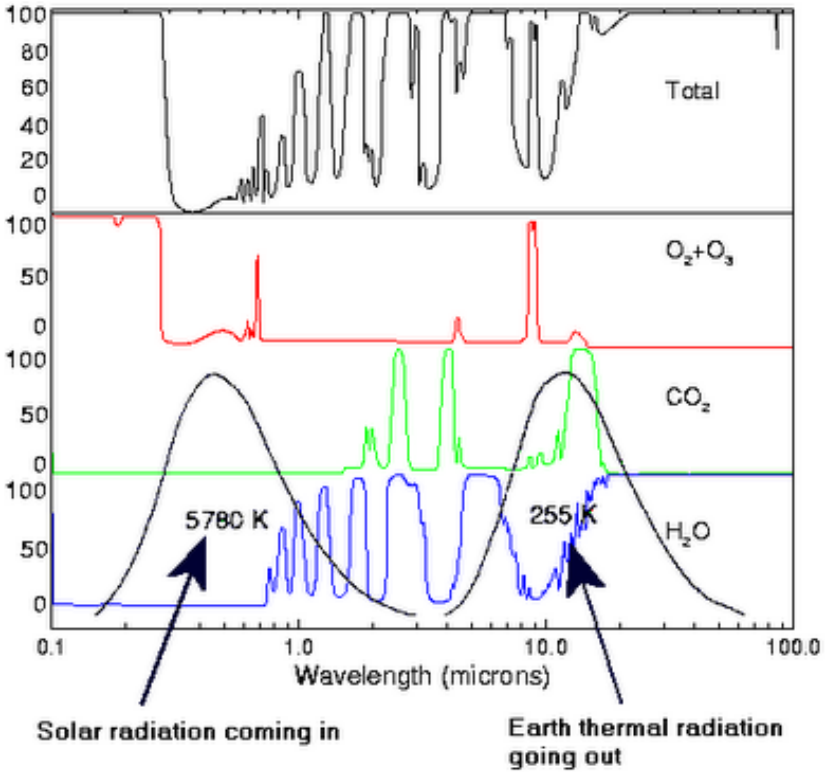

Figure 2.8 The fractions of the radiation absorbed in a one atmosphere thick column of air attributed to the different gases as a function of wavelength of the radiation. The upper panel gives the total absorbed fraction. The red green and blue curves in the lower panel show the contributions to the absorbance from the greenhouse gases water vapour, carbon dioxide and ozone. The lower black curves show the spectra of the thermal radiation emitted from the Sun (left hand curve) and from the Earth (right hand curve, NB not to scale). The total absorption fraction (upper curve) shows that the atmosphere absorbs most of the infra-red radiation from the Earth's surface apart from the small amount in the gap between wavelengths 8–12 microns (see Peixoto and Oort 1992).

To understand the effects of greenhouse gases let us first consider a hypothetical case of a perfect black body of radius equal to that of the Earth in orbit at the Earth's orbit radius. For simplicity we consider such a body to be without atmosphere or oceans and assume that the solar energy, H, falling on it is distributed evenly throughout the body. The body will warm from the solar energy falling on it, reradiating this energy as thermal radiation. By conservation of energy the body will reach an equilibrium temperature, TK, at which the energy radiated (σT^4) exactly balances that falling on it i.e. $H = \sigma T^4$. We showed above that the average heat energy falling on unit area of the Earth's surface is $H = 239$ W/m^2. Hence for this value of H the equilibrium temperature will be $T = (H/\sigma)^{1/4} = 255$ K.

Now if this body had an atmosphere consisting of only nitrogen and oxygen then its surface would have a very cold temperature since the thermal infra-red radiation would radiate directly into space without being absorbed in the atmosphere. The temperature would be somewhat higher than 255K because of the emissivity of the surface. For example, water has an emissivity of 0.96 and most of the Earth's surface (71%) is covered by water. With such an emissivity the temperature would be a little higher than 255K but would still be too low to allow liquid water to exist. It would therefore be unable to support life as we know it.

Adding a small concentration of greenhouse gases to the atmosphere makes it almost a perfect absorber of infra-red radiation (see figure 2.8). At lower altitudes the air will absorb most of the infra-red radiation emitted from the Earth's surface i.e. the atmosphere becomes almost a black body. At higher altitudes the air becomes too thin to absorb the thermal radiation which is emitted to outer space. It is at such altitudes that, to maintain thermal equilibrium, the energy radiated to outer space must match that falling on the Earth from the Sun to conserve energy. The Earth viewed from outer space appears to radiate as an almost black body with an effective temperature of 255 K. This is known as the effective radiation temperature.

Hence small quantities of greenhouse gases allow the atmosphere to act like a blanket warming the planet. We shall see in Chapter 7 how this warming changes with greenhouse gas concentration.

This process is illustrated in figure 2.9 which shows direct sunlight impinging on the Earth. This is mainly in the visible part of the spectrum and so little is absorbed. The infra-red energy radiated from the Earth is, however, absorbed in the air by the greenhouse gases since it is in the infra-red part of the spectrum. Imagine the atmosphere as a series of layers. Each layer warms because of the absorbed radiation and as a result reradiates thermal energy some downwards and some upwards. The upward radiation warms the layers above and the downward radiation those below with some reaching the Earth's surface, warming it. At a high altitude absorption ceases since the air is at too low a density and the upward thermal radiation escapes into outer space. The temperature at this altitude as viewed from outer space is the effective radiation temperature i.e. T_E=255K i.e. the temperature at which the incident radiation balances the outgoing radiation.

The downward energy reaching the Earth's surface provides the warming which makes the Earth warm enough to keep water liquid, allowing life to exist.

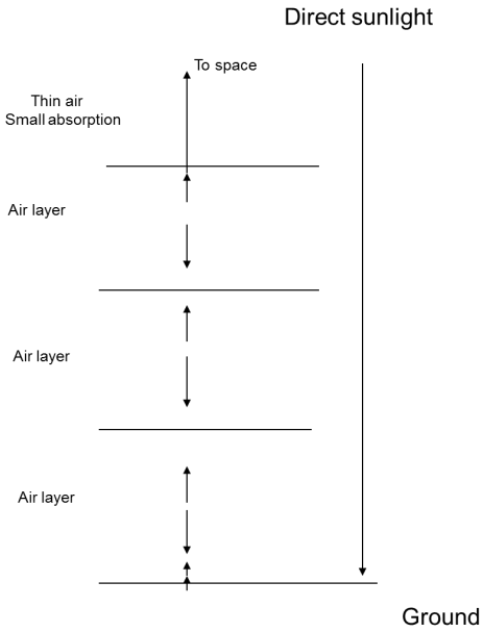

Figure 2.9 Shows the pattern of radiation between layers of the atmosphere. Direct sunlight (right hand arrow) warms the Earth's surface with almost no absorption in the atmosphere. The surface reradiates infra-red radiation which is then absorbed in the atmosphere. The air itself then radiates from layer to layer until at the top of the atmosphere the air is too thin to absorb and the radiation passes to outer space. Water vapour also plays a part in the absorption of infra-red radiation. It is, however, largely frozen out at the high altitude where radiation to space occurs.

2.6 CONCLUSION

The energy budget of the Earth has been discussed in this chapter. We have shown that, without greenhouse gases in the atmosphere, the average surface temperature of the Earth would be too low to allow liquid water to exist. In this case, the Earth would not support life as we know it. The presence of greenhouse gases allows the surface of the Earth to warm to a more comfortable temperature (averaging to approximately 14°C or 277K) allowing the existence of life as we know it. We go on to discuss how the increasing quantities of greenhouse gases will cause further warming of the planet i.e. global warming.

References

Cleland B.T. et al 1998, "Measurement of the solar neutrino flux with the Homestake Chlorine detector", Astrophysical Journal, Vol. 496, pp. 496–526.

Frôhlich C. 2012, "Total solar irradiance observations", Surveys in Geophysics, Vol. 33 pp. 453–473.

Olive K.A. et al (Particle Data Group) 2014, 'Review of Particle Physics', Chin. Phys. Vol. C38, 090001.

IPCC 2001 Fig 1.1 of Chapter 1 "The Climate System, an Overview", of the report of Working Group 1 in the Third Assessment Report (TAR).

IPCC1 2013 Figure 6.11 of the report of WG1 in AR5 of the IPCC.

IPCC 2 2013 Figure TS.5 in the report of Working Group 1 WG1 in AR5.pdf available at https://www.ipcc.ch/

Piexoto J.P. and Oort A.H. 1992, 'Physics of Climate', American Institute of Physics, New York. ISBN 0-88318-711-6 (case) – ISBN 0-88318-712-4 (perfect).

Suess H.E. 1955 "Radiocarbon concentrations in modern wood", Science (3166) Volume 122 pp. 415–7.

SNO 2013, "Combined analysis of all three phases of solar neutrino data from the Sudbury Neutrino Observatory" by the SNO Collaboration, Physical Review C88, 025501.

Exercises

1. Assuming that the sun is a perfect black body calculate the power of the total radiated energy of the sun given its temperature of 5780K. Estimate how long would it continue to burn if all its mass could be converted to energy at the same rate? Its expected lifetime is of order 10^{10} years. Why is this so much less than your previous estimate?
2. Define the term "solar constant". To what extent is it actually constant? Derive its value from the answer to the previous question.
3. a) What is meant by the term "the effective emitting temperature of the Earth"? Show that if the Earth acted as a perfect black body without greenhouse gases in the atmosphere the temperature at the surface would be the effective emitting temperature of 255 K. Assume that the Earth reflects a fraction 0.3 of the incident radiation (the reflected radiation is known as the albedo).
   b) what would the emissivity of the Earth have to be for the Earth's mean effective emitting temperature to be at its present surface temperature of 14 degrees C? Is this a reasonable value for the emissivity?
4. Explain briefly how green house gases allow warming of the Earth to a more comfortable temperature than the effective radiation temperature.
5. Show from the Planck formula (see figure 2.5) that the wavelength, λ, at which the value of $S(\lambda)$ is maximum at temperature T K follows the relationship

$$\lambda T = \frac{hc}{5k} \frac{e^{\frac{hc}{\lambda kT}}}{e^{\frac{hc}{\lambda kT}} - 1}.$$

   Here k, h and c are Boltzmann's constant, Planck's constant and the velocity of light, respectively. Under what conditions does Wien's Law hold? (Wien's Law states that the wavelength of maximum emission λ constant/T). Show that the value of the constant is 0.0028 mK.

Input data
Mean surface temperature of the sun is 5780 K
Mass of the sun is 2 10^{30} kg.
Radius of the Sun is 6.96 10^{8} m.
Mean distance of the Sun to the Earth is 150 10^{9} m
Stefan's constant is 5.7 10^{-8} W m^{-2} K^{-4}
Planck's constant is 6.63 10^{-34} Js
Boltzmann;s constant is 1.38 10^{-23} JK^{-1}
Velocity of light is 3.0 10^{8} ms^{-1}

3 THE ATMOSPHERE

One of the most important aspects of the climate is the atmosphere which is described in this chapter. The various layers of the atmosphere and their characteristics are described and are shown in figure 3.1.

3.1 STRUCTURE OF THE ATMOSPHERE

Figure 3.1 shows the variation of temperature and pressure with altitude in the atmosphere. The most important layer from the point of view of the climate is the lower atmosphere, known as the troposphere. In this layer the temperature falls approximately linearly with altitude at a rate known as the lapse rate. The rate of decrease is roughly 6°C per km of altitude (as discussed later). In the next layer, the lower stratosphere, the temperature is almost constant and independent of altitude. The region where the troposphere merges into the stratosphere is known as the tropopause. The upper part of the stratosphere contains an ozone layer which absorbs the very short wave ultra-violet radiation from the Sun, warming the layer. This radiation is hazardous to life. The ozone layer is generated by the action of the solar ultra violet with oxygen in the atmosphere in which oxygen, O_2, is converted to ozone, O_3. The next layer is the mesosphere in which little energy is absorbed since the density is low and it is shielded from the solar wind by the Earth's magnetic field. Hence the layer cools with altitude. In the next layer, the thermosphere, energy is absorbed by ionization from the solar wind which leaks through the Earth's magnetic field. Hence in this layer the temperature increases with altitude. (The solar wind is a stream of energetic charged particles emitted from the Sun). The different layers are labelled in figures 3.1. Note that the pressure falls approximately linearly on a log scale i.e. it falls approximately exponentially with altitude. We discuss these features in greater detail below.

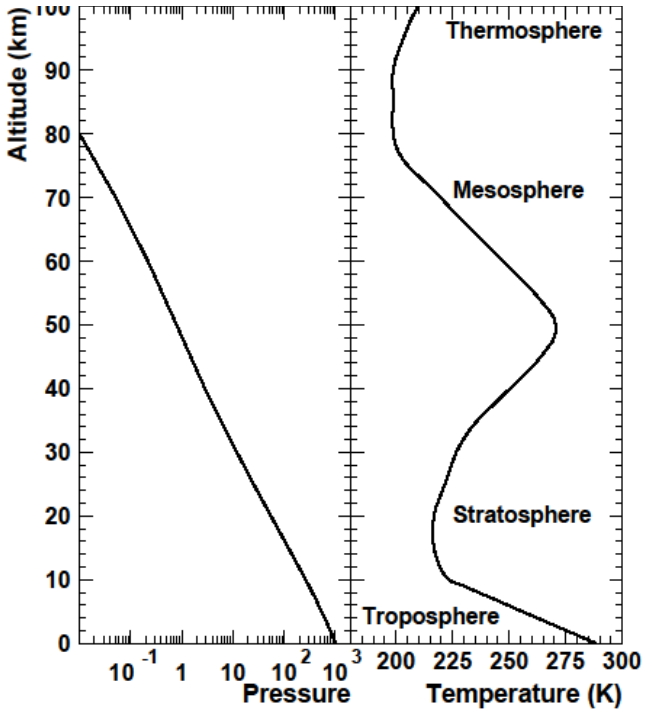

Figure 3.1 The atmospheric pressure (log scale) versus altitude (left hand panel) and temperature (right hand panel).

3.2 VARIATION OF PRESSURE WITH ALTITUDE

Figures 3.1 show that pressure falls with altitude. In Box 3.1 we show that the pressure, P, falls approximately exponentially with altitude as $P = P_0 e^{-\int_0^z dz/H}$, where P_0 is the pressure at the Earth's surface.

Box 3.1 Proof that the pressure as a function of altitude is $P = P_0 e^{-\int_0^z dz/H}$

Consider a horizontal slab of atmosphere of density ρ and thickness dz and unit area, in hydrostatic equilibrium as shown in figure 3.2. The pressure on the lower face is greater than that on the upper face by an amount dP due to the weight of the air above i.e. the increase in pressure on the lower face

$$dP = -\rho g dz \qquad 3.1$$

where g is the acceleration due to gravity. The negative sign allows for the fact that pressure decreases for positive values of dz. We assume that air is approximately an ideal gas at temperature T K so that for 1 mole of the gas $PV=RT$, where P is the pressure, V is the volume of the gas and R is the Universal gas constant per mole. For a mass m of the gas $PV=mRT/M$ where M is the molecular weight, so the density of the gas

$$\rho = \frac{m}{V} = \frac{Mg}{RT} \qquad 3.2.$$

Substituting for ρ from equation 3.2 into equation 3.1 gives

$$\frac{dP}{P} = -\frac{Mg}{RT} dz = -\frac{dz}{H} \qquad 3.3$$

where $H=RT/Mg$ is known as the scale height.

Integrating from z=0 where the pressure is P_0 to height z where pressure is P gives

$$P = P_0 e^{-\int_0^z z/H \, dz} \qquad 3.4.$$

The scale height, H, in equation 3.4, is temperature dependent and so is not constant with altitude (see fig 3.1). Furthermore equation 3.4 is an approximation since air containing water vapour behaves only approximately as an ideal gas. The reason for this is that the water vapour can evaporate or condense depending on the conditions of pressure and temperature. Nevertheless a plot of log P against altitude, z, is approximately linear as shown in figure 3.1. This shows that the fall-off of pressure with altitude is approximately exponential. The deviations from linearity arise from the temperature dependence of the scale height H and the other approximations. At ground level where the temperature T is approximately 290K the scale height H=8.5 km. It falls to 5.8 km in the mesosphere where the temperature drops to below 200K.

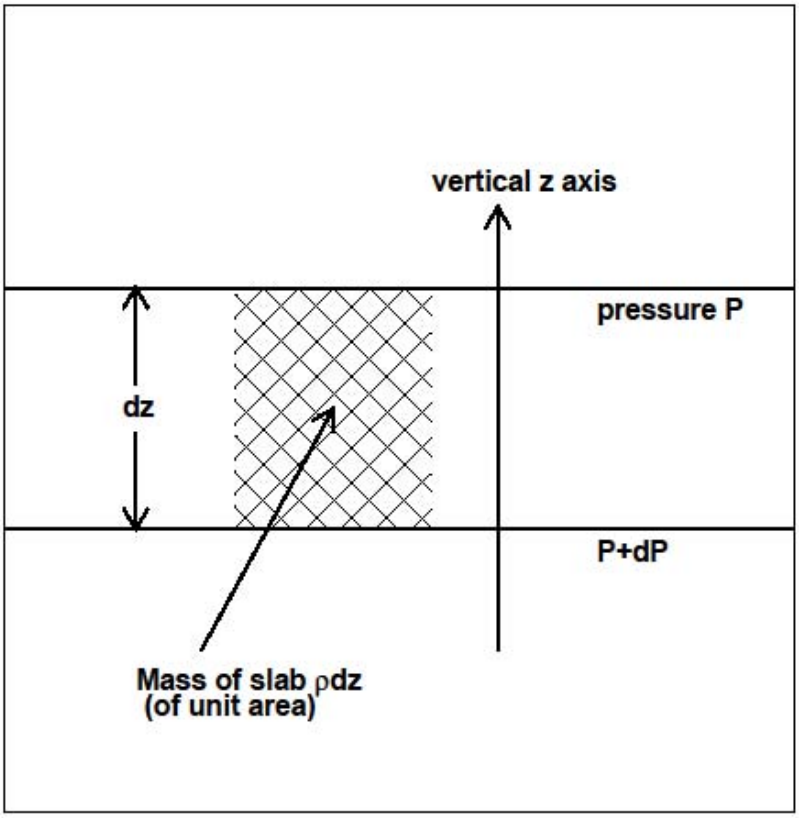

Figure 3.2 A horizontal slab of atmosphere of unit area and thickness *dz* in hydrostatic equilibrium so that the pressure on the upper face is *P* and on the lower face is *P+dP*.

The units of pressure are Pascals (Pa) where 1 Pa = 1 Newton/m^2. Hectopascals are sometimes used where 1 hPa = 100 Pa. Another unit is the mbar which is equal to the hPa. The standard atmosphere is defined as the pressure which supports a column of mercury of height 760 mm (or 760 torr, the old unit of pressure). This is a pressure of 1013 mbar, or 1013 hPa. Another unit is the weight of the atmosphere per unit area which is close to 1013 g/cm^2.

3.3 VARIATION OF TEMPERATURE WITH ALTITUDE IN THE TROPOSPHERE – THE LAPSE RATE

The temperature falls linearly with altitude in the troposphere at the lapse rate $dT/dz \sim 6$ K/km. The reason for this is that the main transport of heat in the troposphere from the surface of the Earth is by convection. The Earth's surface warms due to the solar energy falling on it. This warms the air. The warm air rises and expands since the pressure is lower at higher altitude. As a result it cools. Hence the temperature falls with altitude. However, at high enough altitudes the atmosphere becomes less dense and convection decreases so that radiation becomes the dominant process for heat loss. At such altitudes the troposphere gives way to the stratosphere. In Box 3.2 we show that for dry air, assumed to be an ideal gas, the lapse rate is given by $dT/dz = g/c_p = 10\text{K/km}$ where c_p is the heat capacity per unit mass of air. The effects of moisture in the air reduce this value to 6K/km.

Box 3.2 Proof that the lapse rate $dT/dz = -g/c_p$ for dry air.

Consider a parcel of 1 mole of dry air of volume V at pressure P rising from ground level. As it rises it expands due to the lower pressure at higher altitude. From energy conservation $dQ = C_V dT + PdV$ where dQ is the external heat entering the parcel, C_V is the molar heat capacity at constant volume, dT is the temperature change as the parcel expands by volume dV and PdV is the external work done by the parcel of air as it expands. Now conduction and radiation of energy from the parcel will be small so $dQ \sim 0$, so that $PdV = -C_V dT$. For 1 mole of an ideal gas $PV = RT$ where $R = C_P - C_V$ is the Universal gas constant (with C_P the molar heat capacity at constant pressure). So that for small changes

$$PdV + VdP = (C_P - C_V)dT.$$

We saw above from hydrostatic equilibrium that $dP = -\rho g dz$ i.e. $VdP = -V\rho g dz = -Mgdz$ where M is the molecular weight of air i.e. $-C_V dT - V\rho g dz = (C_P - C_V)dT$

i.e. $\frac{dT}{dz} = -\frac{Mg}{C_p} = -\frac{g}{c_p}$

where we have taken the heat capacity per unit mass c_p as the molar heat capacity C_P divided by molecular weight, M. Note that for moist air the assumption that $dQ \sim 0$ is invalid due to latent heat as the moisture condenses or evaporates with changes of temperature and pressure.

Putting in the values of c_p=1000 J/kg/K and g=10 m/sec^2 gives dT/dz=10K/km.

The calculation in Box 3.2 is for an ideal atmosphere in perfect equilibrium without updrafts or horizontal pressure gradients and without moisture. Radiosonde (balloon) measurements show that the temperature increases at roughly the lapse rate of 6 K/km up to the stratosphere at a height of approximately 10 km. However, fluctuations about a pure linear behaviour occur due to local meteorological conditions. The variation with height also shows seasonal dependence (Taylor 2005).

3.4 THE STRATOSPHERE

At higher altitude the density of the air becomes low enough that the energy transfer by convection is reduced to be smaller than the energy transfer by thermal radiation. This is the layer of the atmosphere known as the stratosphere.

Consider the stratosphere layer at temperature T_S in which we can neglect heat convection and conduction (see figure 3.3). At this height the air density is low enough that most of the thermal infra-red radiation from the Earth below passes through the layer with only a small fraction absorbed. The fraction absorbed is a, the absorptivity of the layer. The layer is at an altitude greater than that at which radiation from below to space occurs, so the energy impinging on the layer per unit area will be that being radiated from the Earth below i.e. σT_E^4 W/m^2 where T_E=255K is the Earth's effective radiation temperature (see section 2.5). Hence the energy absorbed by the layer is $a\sigma T_E^4$. The layer will radiate thermal energy $e\sigma T_S^4$ both upwards and downwards where e is the emissivity of the layer. However, $a=e$ from Kirchoff's Law. By conservation of energy the energy radiated by the layer must be equal to that absorbed i.e. $2e\sigma T_S^4=a\sigma T_E^4$ with $a=e$ where the factor 2 comes from the fact that thermal radiation is emitted from both sides of the layer. Hence $T_S=T_E/2^{1/4}$ = 215K. This argument is applicable to any sublayer of the stratosphere. Hence its temperature is approximately constant.

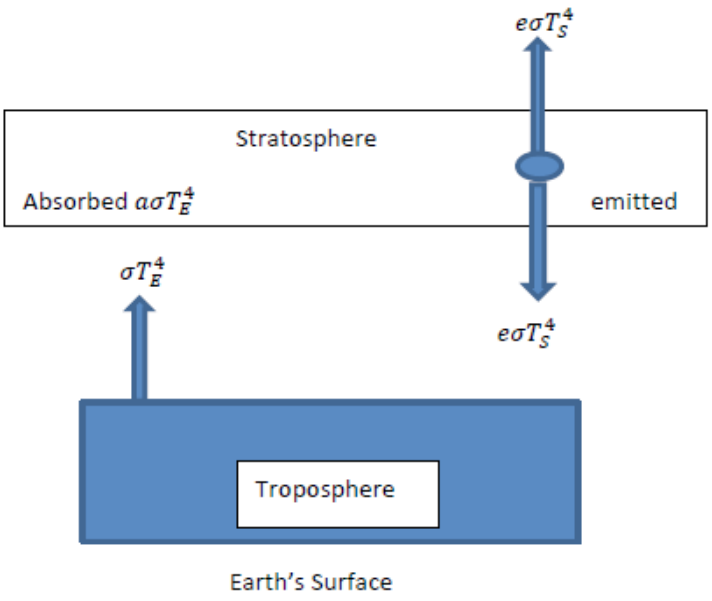

Figure 3.3 Model of stratospheric radiation. The troposphere radiates energy at the effective radiation temperature. T_E = 255K. A small fraction, α, of this is absorbed in the stratosphere and reradiated at temperature T_S with emissivity e.

It can be seen from figure 3.1 that the temperature in the stratosphere is approximately constant. Deviations from this come from meteorological conditions imposed by pressure gradients etc.

This calculation neglects all complications such as meteorological and seasonal effects. This could account from the slight deviation of the stratospheric temperature in fig. 3.1 from the above calculated value.

3.5 THE OZONE LAYER

Figure 3.1 shows that the temperature in the stratosphere is approximately constant at altitudes between roughly 10km to 20km. At higher altitudes the ozone layer exists in which there is strong absorption of solar short wavelength ultraviolet light. The absorption of this energy leads to a temperature rise in the upper stratosphere. Short wave ultraviolet radiation is hazardous for plants and animals living on the Earth's surface. The ozone layer thus provides vital protection for these.

Ozone is created in the stratosphere by the ultraviolet light falling on it. An energetic ultraviolet photon can break apart an oxygen molecule into two oxygen atoms (O) by the process

$$O_2 + h\nu \rightarrow O + O$$

where the photon is indicated by $h\nu$. A liberated oxygen atom can then become attached to an oxygen molecule to yield an ozone molecule i.e. $O + O_2 \rightarrow O_3$.

The ozone molecules which are formed act as strong absorbers of ultraviolet photons which dissociate them back to oxygen, being absorbed in the process. The process reaches an equilibrium when the amount of ozone created is the same as that destroyed by the solar ultraviolet radiation.

This equilibrium was broken in the 20th century by the release of chlorofluorocarbons (CFCs) into the atmosphere mainly from spray cans and refrigerators. It was demonstrated that these could catalytically destroy ozone (Molina and Rowland 1974). The discovery of a hole in the ozone layer in the Antarctic has been linked to this process. The CFCs are thought to diffuse into the upper atmosphere and release the chlorine in the presence of nacreous clouds in the cold conditions of Antarctica. The chlorine then reacts to destroy the ozone molecules. This led to the Montreal Protocol, signed by all members of the United Nations (UN) in 1987, to limit the use of CFCs to prevent further damage to the ozone layer and to allow the equilibrium to be restored. Because of the lifetime of these substances in the atmosphere, it is thought that it may take about 50 years to restore the damage to the ozone layer. Since the Montreal Protocol came into effect the ozone hole has shrunk in size showing that the equilibrium is being restored.

3.6 THE ATMOSPHERIC ELECTRIC CIRCUIT

Figure 3.4 shows a diagram of the atmospheric electric circuit (for a review see Harrison 2004). The upper layer of the atmosphere above the thermosphere (see figure 3.1) becomes charged to a positive potential of order 300 kV due to the action of the solar wind. This layer is known as the ionosphere. The solar wind is a stream of low energy charged particles from the Sun which ionize the upper layers of the atmosphere before they come to rest. Higher energy charged particles from galactic cosmic rays also interact in the upper atmosphere down to much lower levels of order 10–30 km in altitude since they are more energetic than the solar wind particles (see section 4.7 and figure 4.5). Their interactions produce streams of other particles which decay mainly to electrons and muons many of which penetrate down to the Earth's surface. The ionization produced by these energetic particles allows an electric current to flow through the air from the ionosphere to ground. The total current over the Earth's surface is 1800 amps (i.e. approximately 3 picoamps per square metre). The return current to complete the circuit is thought to arise from point discharges under clouds, charge precipitation and lightening discharges. This maintains the equilibrium of the ionosphere (see figure 3.4).

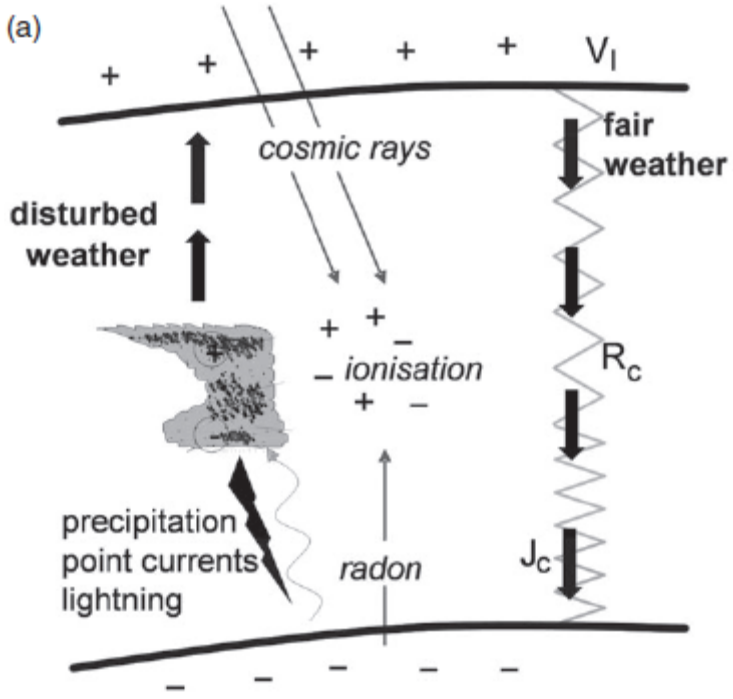

Figure 3.4 The atmospheric electric circuit. The diagonal thin arrows and the arrow marked radon (for ionization from surface radioactivity) show the incoming ionization which is actually isotropic in direction. The solid arrows show the directions of the current flow (Harrison et al. 2015).

The formation of lightning is thought to proceed as follows. In stormy weather conditions, the clouds become charged so that electric fields of order of between 10–100 KV/m are generated between individual clouds or between a cloud and the ground. Such fields are smaller than the field of order 3000 KV/m needed to cause spontaneous breakdown of the air. Lightning discharges are thought to be initiated from the production of an electron of energy of order of a few MeV from a galactic cosmic ray or from a radioactive decay which normally loses energy by ionizing the air. The energy loss becomes smaller for higher energy electrons. Such an electron will be accelerated in the electric field of the cloud. If the energy gained from the acceleration is greater than the energy loss by ionization then the electron will gain enough energy to knock out a further electron in collision with another atom so that a cascade develops. Thus a lightning bolt is formed over distances of order hundreds of metres. Figure 3.5 shows a simulation of this process (Dwyer 2010).

3.7 CONCLUSIONS

In this chapter the variations of temperature and pressure with altitude in the atmosphere have been discussed since these are important to understand from the point of view of the climate. Other important features such as the ozone layer and the electric circuit of the Earth were also discussed. Such topics have effects on the weather and so indirectly affect the climate.

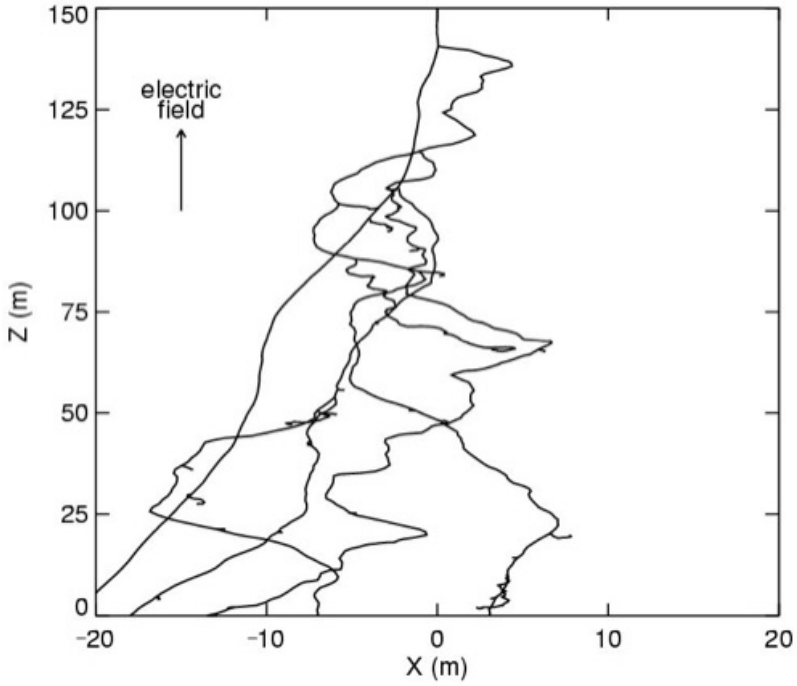

Figure 3.5 shows simulated electron tracks in the vicinity of a thunder cloud (Z vertical coordinate against X) This shows how one electron can produce several more over a distance of order 100m. In this way a lightning discharge develops by an avalanche process. The deviations of the electrons from straight line paths are caused by interactions with air atoms (picture by kind permission of J. Dwyer).

References

Dwyer J. 2010 "Diffusion of runaway electrons and implications for lightning initiation", Journal of Geophysical Research Space Physics Vol. 115 Issue A3, DOI:10.1029/2009JA014504, and references therein.

Harrison R.G. 2004, "The global atmospheric and climate", Surveys in Geophysics vol. 25 (issues 5–6) pp. 441–484, doi:10.1007/s10712-004-5439-8 (2004).

Harrison R.G., Nicholl K.A. and Ambaum M.H.P., 2015, "The microphysical effects of observed cloud edge charging", Quarterly Journal of the Royal Meteorological Society (2015) DOI:10.1002/qj.2554.

Molina M.J. and Rowland F.S. 1974 "Stratospheric sink for chlorofluoromethanes: chlorine-atom catalysed destruction of ozone", Nature vol. 249 pp. 810–812.

Taylor F.W. 2005, 'Elementary Climate Physics', First Edition, Oxford University Press.

Exercises.

1. Why does the temperature of the lower atmosphere (the troposphere) decrease with height? Define the term lapse rate and show that its value is given by g/c_p for a dry atmosphere on Earth stating any assumptions you make. Here g is the acceleration due to gravity and c_p is the heat capacity per unit mass of air. What are the effects of water vapour on the lapse rate?
2. The temperature in the lower stratosphere is approximately constant as a function of height because the overlying atmosphere is optically thin. Explain what is meant by the term optically thin. Estimate the temperature of the Earth's stratosphere given that the effective temperature at which the Earth radiates to space is 255K.
3. Use the values of temperature against altitude in figures 3.1 to estimate the scale height, H, at several different altitudes. Hence plot a graph showing H as a function of altitude. Explain the assumptions you have made in deriving the graph. How accurate do you think the graph is likely to be? What is the average value of H? Occasionally we use this average value as a constant for the atmosphere. What uncertainties do we incur using this assumption?

4 THE PRINCIPLES OF CLOUD FORMATION

Clouds are very important from the point of view of the climate since they are the biggest contributor to the reflection of solar radiation from the Earth. For this reason they have a large effect on the Earth's energy budget. To understand clouds we must first understand surface tension and vapour pressure. From this we must go on to understand how water droplets form from a collection of water molecules, overcoming the effects of surface tension and vapour pressure. These effects are explained in this chapter, as well as the possible effects of ionizing radiation.

4.1 INTRODUCTION

Clouds come in many different forms as illustrated in figure 4.1. The different forms are due to local meteorological conditions. They are mainly confined to the troposphere with rarer occurrences of stratospheric clouds. Among the latter are nacreous clouds which appear rarely in the polar regions in winter months. The latter have been implicated in the chemical processes which led to the formation of the Antarctic ozone hole induced by the use man-made halocarbon substances.

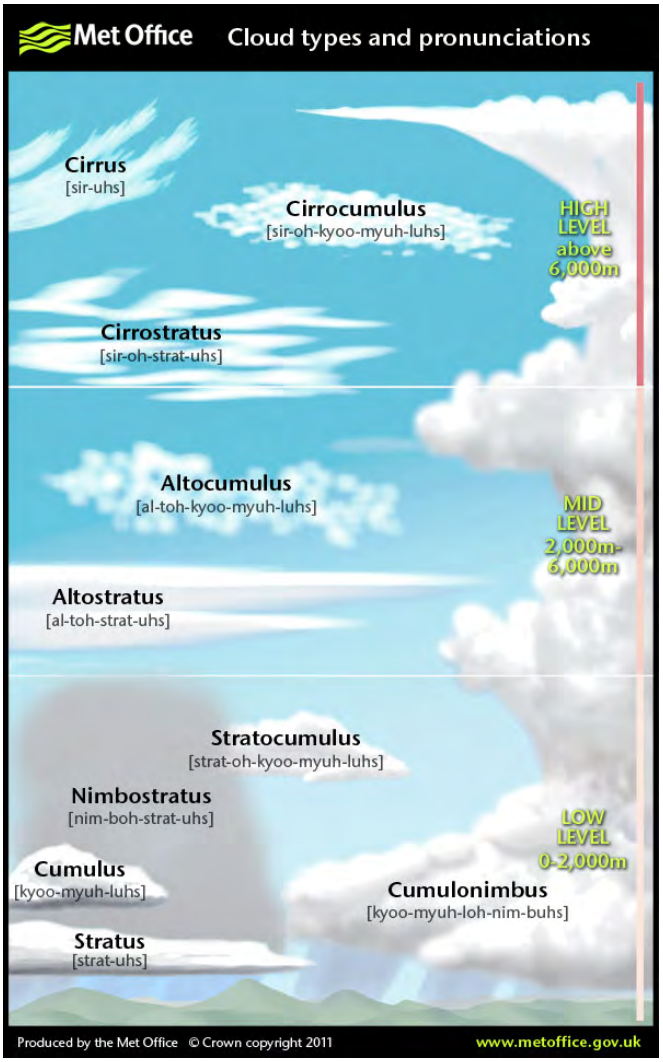

Figure 4.1 Shows a diagram of the different cloud forms as a function of altitude (courtesy of the Met Office © Crown copyright 2011, contains public sector information licensed under the Open Government License v1.0).

Clouds play an important part in climate physics to the extent that they make a large contribution to the Earth's albedo i.e. the fraction of the solar energy falling on the Earth which is reflected into space. It is this aspect of clouds on which we will concentrate here. Roughly 30% of the energy falling on the Earth from the Sun is reflected back into space with ⅔ of this albedo fraction coming from clouds. The remainder is reflected from the atmosphere and from the Earth's surface.

Clouds consist of water droplets or ice crystals of size 10–30μm falling so slowly under gravity that they appear from the ground to be at a constant altitude. The rate of fall is set by the viscosity of the air. In this chapter we consider the mechanism by which these droplets form. They are thought to condense from water vapour in the atmosphere nucleated by small particles known as aerosols or Cloud Condensation Nuclei (CCN). CCN are of size less than 1μm and are needed to overcome the effects of the surface tension of water. To understand the mechanism we discuss surface tension and vapour pressure and then use this to describe the growth of CCN into water droplets in clouds.

4.2 CONSTITUENTS OF CLOUDS.

The water droplets in clouds are of size 10–30μm. These fall under gravity at a constant velocity known as the terminal velocity (see Box 4.1). This velocity is reached when the upward force (due to the viscosity of the air) matches the downward force of gravity. At this velocity the net force on the droplet is zero so that the acceleration is zero (by Newton's Laws of Motion). Note that the viscous drag force increases with the velocity of the droplet.

Box 4.1 The terminal velocity of a small droplet is given by $v_T = \frac{2r^2\rho g}{9\eta}$

for a drop of radius *r*, density ρ in air of viscosity η, where *g* is the gravitational acceleration.

This can be seen as follows. The viscous force, *F*, on a small sphere moving at velocity *v* in a fluid of viscosity η is given by Stokes' formula

$$F = 6\pi r\eta v \qquad 4.1.$$

This was proved by George Gabriel Stokes in 1851. The acceleration of the sphere becomes zero when the downward gravitational force (mg) becomes equal to this viscous force in equation 4.1 i.e. the velocity becomes constant at the value v_T known as the terminal value

i.e. $mg = \frac{4}{3}\pi r^3\rho g = 6\pi r\eta v_T$

so that $v_T = \frac{2r^2\rho g}{9\eta}$ 4.2.

Note that this formula is accurate for smooth flow at low velocities. The transition from smooth to turbulent flow is characterised in fluid mechanics by the dimensionless Reynolds number,$Re = \rho vr/\eta$. Fluid mechanics shows that turbulence becomes important when *Re* becomes greater than of order 100 and the formula in equation 4.2 then breaks down.

Applying the formula in equation 4.2 shows that the downward terminal velocities of droplets in clouds of sizes 10–30μm is small (of order 1 cm/sec). Raindrops are much larger than cloud droplets with diameters from 0.5–5 mm. They are formed by cloud droplets coalescing into larger drops as they collide. These travel more rapidly than cloud droplets so that the Reynolds number (see Box 4.1) is large. The flow is therefore turbulent and equation 4.2 is not valid. The velocity of raindrops varies from 1–10 m/sec. Raindrops are not larger than 5 mm in diameter since for larger sizes the turbulent viscous forces become so great that they overcome the surface tension forces holding the drop together which then breaks into smaller ones during the fall.

4.3 SURFACE TENSION

A force exists in a liquid surface due to the attraction of the molecules for each other. This provides the surface tension of a liquid. An object which breaks the surface of the liquid will feel a force due to the surface tension perpendicular to the liquid edge and parallel to the liquid surface. The magnitude of this force is called the surface tension, σ newtons/metre. At the liquid surface interface with a solid there will be an angle of contact which depends on the relative strength of the forces between the liquid-solid molecules and the liquid-liquid molecules (see figures A4.2 and A4.3).

Consider a film of liquid with surface tension, σ, in the frame with side, L, shown in figure 4.2 which has a moveable side (right hand arm). An external force $F=2\sigma L$ needs to be applied to the moving side to overcome the surface tension force and prevent the arm from moving to the left(the factor 2 arises since there are two sides to the film). If the moving arm is displaced by dx in the direction opposite to the force the work done is $Fdx=2\sigma Ldx$. This is stored as potential energy in the film. The change of area due to the displacement is Ldx. Integrating over the area, the total potential energy per unit area stored in each surface of the film is then σ.

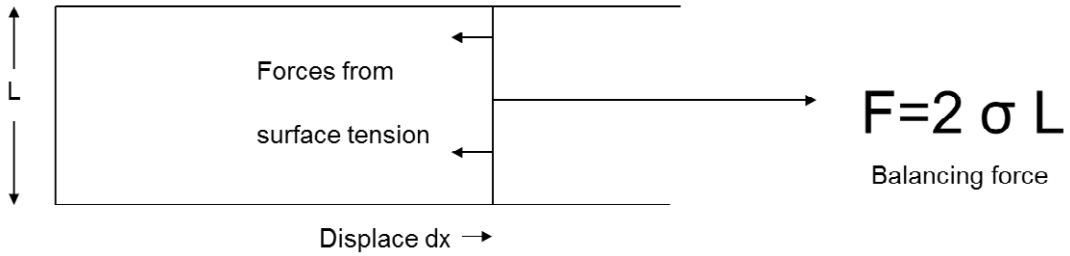

Figure 4.2 A liquid film (e.g. a soap solution) stretched in a frame with side of length L. The right hand side of the frame is moveable. The force F=2σL balances the surface tension force tending to shrink the film.

4.4 VAPOUR PRESSURE

The molecules of all materials (solids or liquids) can escape through the surface of the material creating the vapour pressure of the material. This is the partial pressure in the gas from the molecules of the vapour. If the material is present the vapour pressure reaches a maximum known as the saturation vapour pressure. This is reached when the number of molecules escaping through the surface of the material equals the number returning (as the molecules are in random motion because of collisions with other molecules in the surroundings). If the vapour is present alone it can have pressures greater than the saturation vapour pressure and it is then said to be supersaturated.

The vapour pressure is more relevant for liquids than for solids. As the temperature increases the molecules become more energetic and can break through the surface more easily. Hence the saturation vapour pressure increases with temperature. The rate of change of vapour pressure with temperature is given by the Clausius-Clapeyron equation $dP/dT = L/(T\,\Delta v)$ where L is the specific latent heat of vaporization of the liquid (per mole), T is the absolute temperature and Δv is the molar volume of the vapour (Lue 2009). Integrating this equation shows that the saturation vapour pressure varies exponentially as T. When the vapour pressure in a liquid is equal to the surrounding atmospheric pressure the liquid boils.

For water we speak of the humidity of the air which is a measure of the of water vapour pressure in the air. The relative humidity of the air is the ratio of the vapour pressure of water vapour in the air to the saturated vapour pressure.

In the atmosphere there is continual circulation of the air with local parcels of more humid air than in others. These parcels are isolated from a liquid surface and so the relative humidity can become greater than 100% i.e. the parcel is said to be supersaturated. For example, supersaturation occurs if the parcel drifts into a region of lower temperature. We show below that clouds will form in such a parcel of supersaturated air.

4.5 THE FORMATION OF CLOUD DROPLETS FROM CCN

To form a water droplet in a cloud, molecules of the vapour must stick together. This happens naturally for small numbers of molecules because of their strong electric dipole moments. However, when enough molecules gather together the surface forms and surface tension comes into effect. This prevents further growth of the collection of pure water molecules.

This can be seen as follows. The vapour pressure outside a curved liquid surface (such as a spherical droplet) is different from that over a flat surface. The reason for this is that inside a curved liquid surface of radius, r, an excess pressure exists due to the surface tension, σ, of the liquid. This excess pressure is given by $2\sigma/r$ (see Appendix 4.1). Thus inside a droplet there is an excess pressure which increases as the radius decreases. Due to this excess pressure molecules can escape more easily through a curved surface than through a flat surface. Hence the vapour pressure outside the curved surface of a droplet is increased in comparison to that outside a flat liquid surface. The Kelvin equation relates the vapour pressure outside a spherical drop of radius r, $P(r)$, to that outside a flat liquid surface, $P(\infty)$. This is $P(r) = P(\infty)\exp(\frac{\alpha}{r})$. where $\alpha = 2\sigma M/(\rho\, RT)$ with ρ ,M, T and R the density, the molar mass, the absolute temperature of the liquid and the universal gas constant, respectively. This equation is derived in Appendix 4.2.

For the collection of molecules to grow, the external vapour pressure must be greater than the saturation vapour pressure outside the forming droplet. However, r will be small for the droplet. Hence according to the Kelvin equation the necessary external water vapour pressure will need to be impossibly high to allow the droplet to grow. This is the case for droplets of pure water in clean air.

However, the collection of water molecules can attach itself to a speck of impurity (a CCN) and this will allow the droplet to grow. This can be seen as follows. The real atmosphere contains many specks of impurities such as dust particles, salt particles from evaporated sea spray, sulphates etc. Such impurities act as a solute in the forming droplet lowering the vapour pressure according to Raoult's law. This states that the vapour pressure of a solution of a solute is the vapour pressure of the pure solvent multiplied by its molecular fraction. This is an empirical law which can be understood from the tendency of the solute molecules to block the surface of the solution inhibiting the evaporation of the liquid so that the saturation vapour pressure is lowered.

In a putative droplet forming around a CCN, if there are N molecules of water and n solute ions then the vapour pressure is lowered by a $\frac{N}{N+n} = \left(1+\frac{n}{N}\right)^{-1} \approx 1-\frac{n}{N}$ (for $n<<N$) according to Raoult's rule. Suppose the solute has mass m and Molecular weight m_S, then the number of solute ions dissolving in the droplet will be $n = iN_A m/M_S$ where N_A is Avogadros' number and i is the number of ions per dissolving molecule (the dissociation factor introduced by Van't Hoff, see Lue 2009). The quantity i depends on the solubility of the solute in water. If water molecules dominate in the CCN then the number of water molecules in it will be $m_W N_a/M_W$ where the mass of the droplet is $m_W = 4/3\pi r^3\rho$. We see therefore that the effect of the impurity is to lower the vapour pressure by a factor f given by

$$f = 1-\frac{3imM_W}{4\pi r^3\rho M_S} = 1-\frac{b}{r^3}. \qquad 4.3$$

The solute will therefore depress the saturation vapour pressure from the value given by the Kelvin equation by the factor f in equation 4.3. Hence the total saturated vapour pressure outside the aerosol will be

$$P_v(r) = P_V(\infty)e^{\frac{a}{r}}\left(1-\frac{b}{r^3}\right) \qquad 4.4$$

This function is plotted as the saturation ratio $S(r) = P_V(r)/P_V(\infty)$ in figure 4.3. For solutes which are completely soluble such as salt in water the Van't Hoff factor i will be 2 since there are two ions per dissolved molecule. For ammonium sulphate $(NH_4)_2\ SO_4$ which produces 3 ions per molecule it will be 3.

The peak value of the vapour pressure, S_{crit}, occurs when S_{crit}, occurs when $\frac{dS}{dr} = 0$. This is known as the critical value above which droplets can grow spontaneously. This can be understood as follows.

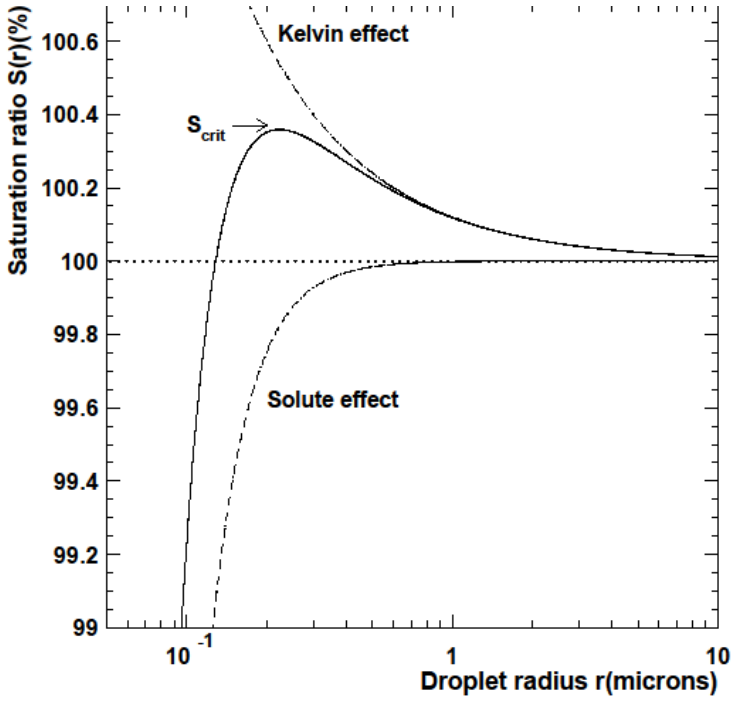

Figure 4.3 The variation of the ratio of the vapour pressure to the saturated vapour pressure outside a droplet as a function of its radius when it contains a solute (solid curve known as the Kohler curve). The lower dashed curve shows the term from Raoult's Rule and the upper dashed curve the behaviour for pure water from the Kelvin curve. The solid curve is computed with α=0.0012 μm (the value expected from equation A2) and b=2 10^{-5} μm^3. This is a typical value of b which requires a speck of solute of size of order 0.02μm, typical of aerosol particle size.

The droplet forming around the CCN will grow to a size which depends on the vapour pressure of the surrounding air as follows. Suppose the forming droplet exists in a region of air where the water vapour pressure S is below S_{crit} i.e. $S < S_{crit}$. If its size is to the left of the Kohler curve at this value of S then the vapour pressure outside it (equal to the value on the Kohler curve at this size) is smaller than that in the surrounding air. Water vapour molecules will diffuse towards it and it will grow to a diameter where its own vapour pressure matches that of the surrounding air i.e. to a size which is on the Kohler curve at the size for this value of S. On the other hand if the aerosol size is to the right of the Kohler curve the vapour pressure outside it will be greater than that in the surrounding air. Water molecules then diffuse away from it so that it evaporates until it is of a size such that the vapour pressure matches that of the surrounding air, again on the Kohler curve. Hence the droplet size will automatically adjust to lie on the Kohler curve when $S < S_{crit}$.

Now take the case when the surrounding air is at a vapour pressure $S > S_{crit}$. The saturated vapour pressure outside the droplet will always be less than that in the surrounding air independently of its size. Hence it will grow by the diffusion of water vapour to it, eventually forming a drop which can grow further into a cloud droplet.

With enough CCN in such a supersaturated region cloud droplets will form and a cloud will appear.

The growth rate of a droplet in a region with $S > S_{crit}$ depends on many factors. These include the degree of supersaturation of the surrounding air, the rate of diffusion of water vapour in the air and the rate at which the latent heat from condensation is conducted away from the growing particle. It is estimated that it takes of the order of 1 hour for a droplet to grow into a cloud droplet once it has entered the region of supersaturated air. A complicated argument shows that the growth rate, *dr/dt*, varies inversely as the radius of the droplet. Hence, the growth rate slows markedly as the cloud droplets increase in size so that for sizes greater than of order 30μm the increase in size comes mainly from the coalescence of droplets by collision. If the density of the droplets is high, coalescence takes place frequently to produce drops which are large enough to fall as rain.

If the CCN are frozen the growth rate is increased because the vapour pressure outside a solid ice crystal is lower than that outside a water droplet and external water molecules can stick to it.

4.6 THE EFFECT OF ELECTRIC CHARGE ON THE FORMATION OF WATER DROPLETS

If a cluster of water molecules is electrically charged the electrostatic potential energy decreases the stored energy from surface tension. This has the effect of offsetting some of the increased vapour pressure of a small uncharged drop expected from the Kelvin formula. Hence ionization facilitates the formation of a water droplet. It is this principle which is exploited in the detection of charged particles in a cloud chamber.

Figure 4.4 Shows tracks consisting of condensed water droplets along the trails of ionization from α particles in a cloud chamber. The end of the needle is a radioactive α particle source (photograph from the Thomas Jefferson National Accelerator Facility – Office of Science Education; available at http://education.jlab.org/glossary/cloud-chamber.html).

Figure 4.4 shows a cloud chamber in operation detecting the tracks of charged α particles. The air in the cloud chamber is supersaturated with alcohol vapour at a level of order 400% more than the saturation level. Furthermore, the air inside of the chamber is extremely clean otherwise condensation on impurity specks occurs by the process described above and not on charged clusters of molecules. At these levels of supersaturation droplets form on the ionization trail left by a fast charged particle and these quickly grow at such a large supersaturation level so that each track becomes visible.

4.7 COSMIC RAYS AND CLOUD FORMATION.

The first suggestion that cosmic rays could have an influence on the climate via influencing cloud formation came from Ney (1959).

The Earth is bombarded by Galactic cosmic rays (GCR). The primary particles are mainly energetic protons and some heavier nuclei with a spectrum which falls roughly as E^{-3} where E is the primary energy. The GCR are much more energetic than the particles in the solar wind. They are energetic enough to penetrate the Earth's magnetic field and interact with air nuclei in the upper atmosphere at altitudes of order 20 km. These interactions produce secondary particles. Figure 4.5 shows a schematic diagram of the interaction of a GCR in the atmosphere illustrating how the secondary particles are produced. The secondary particles are mainly charged π^+, π^- or neutral π^0 mesons and some neutrons and protons. The charged mesons can either go on to produce further mesons by interaction with air molecules or decay to charged muons and neutrinos. The muons only interact weakly or electromagnetically and often they reach the ground. The neutral π^0 mesons quickly decay to gamma ray photons which produce electron-positron pairs by interactions with air molecules. These can produce further photons by the bremsstrahlung process which can go on to produce further pairs. In this way a cascade or shower develops.

The secondary particles producing ionization in the troposphere are mainly the muons and the electrons and positrons. Of order 65% of the ionization at cloud height (of order 3000 m) comes from muons (the so called hard component of cosmic rays) and the remainder from electrons (the so called soft component since they were originally observed to be absorbed in lead). These proportions become 75% and 25% at the Earth's surface with some addition due to radioactivity from the Earth's surface (Greisen 1942).

The intensity of the GCR primaries varies with the solar activity and hence shows the classic 11-year solar cycle. The reason for this is that the solar magnetic field deflects the lower energy GCR so that at times of high solar magnetic field the total GCR flux is less and vice versa at times of low magnetic field. The solar magnetic field varies with the 11-year cycle.

GCR have been monitored by a series of neutron monitors around the globe since the International Geophysical Year of 1957. The neutrons are produced in the interactions in the upper atmosphere and diffuse through the air to ground level. Since neutrons are produced by somewhat different processes from those producing the mesons they are an imperfect proxy for ionization in the atmosphere. This can be seen by comparing the modulation due to the 11 year solar cycle of the neutrons and the ionization at similar magnetic latitudes. The average solar modulation fraction of the Climax Neutron Monitor is 17% compared to the average fraction for all ionizing particles of 6% (Sloan et al 2011) and to the modulation for muons of order 2% (Ahluwalia 2011). This arises because the primary GCRs responsible for producing neutrons, muons and electrons have different energies and so respond differently to the solar magnetic field. The extensive neutron monitor data are often used as a proxy for the atmospheric ionization. It is evident from the different responses to the solar cycle that this is an inexact proxy.

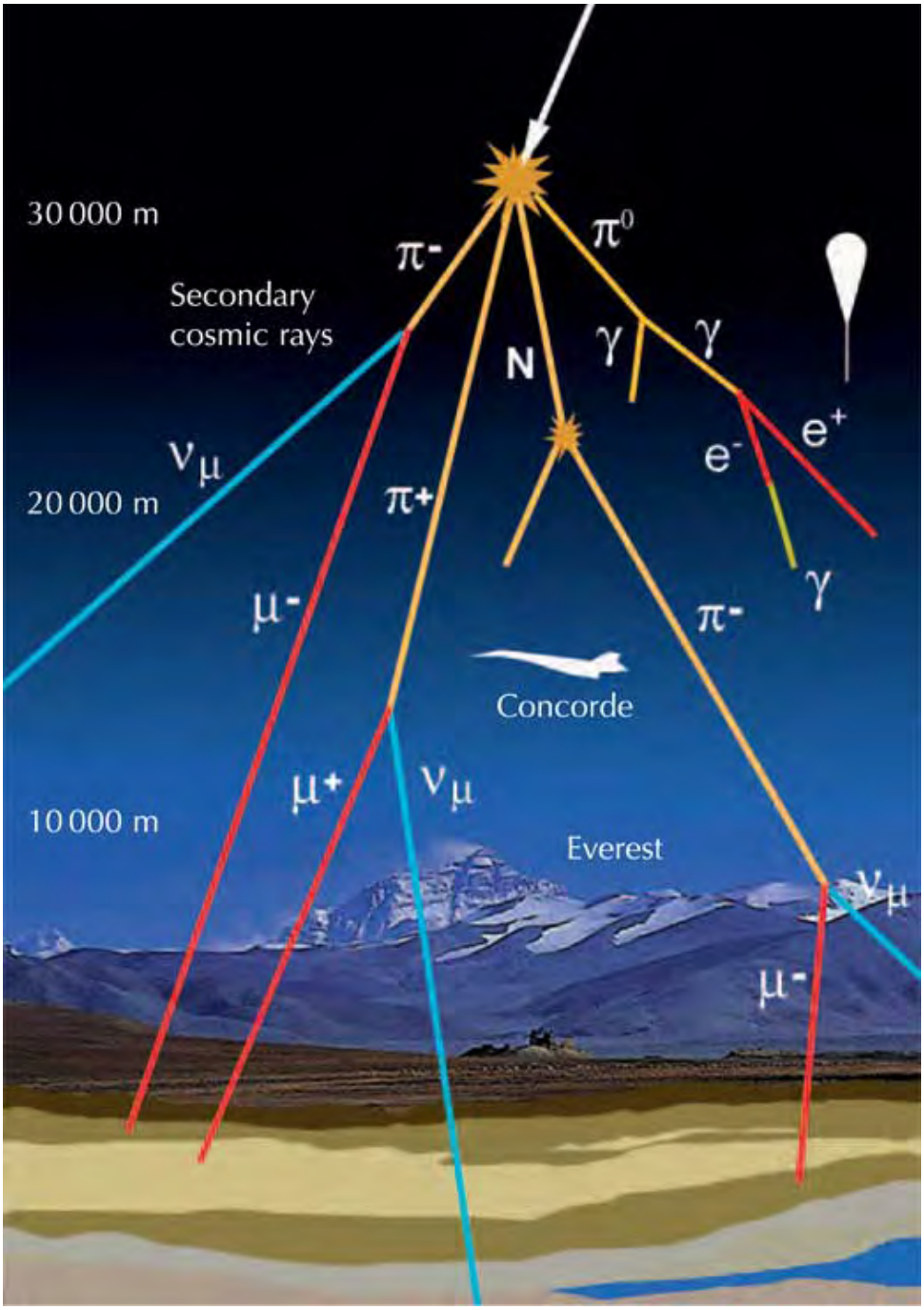

Figure 4.5 Shows a schematic diagram of a galactic cosmic ray (the uppermost arrow) interacting in the atmosphere to produce a shower of secondary particles: mainly π^+, π^- or π^0 mesons. The π^0 mesons quickly decay each to 2 γ ray photons. These convert to electron-positron pairs in the air which produce further photons by the bremsstrahlung process so that a cascade of γ, e+ and e- develops. The π^+ and π- mesons sometimes interact to produce further mesons so that another type of cascade develops. These mesons also decay to $\mu^+\nu_\mu$ and $\mu^-\overline{\nu_\mu}$. The ν particles only interact weakly and play no further part. The μ^+ and μ^- particles are charged particles with long range so that they cause ionization in the troposphere (the so-called hard component). The electron-positron pairs from π° decay also cause ionization (the soft component) (Source http://www.astromart.com/news/news.asp?news_id=1425).

4.8 THE HYPOTHESIS THAT IONIZATION AFFECTS CLOUD FORMATION

An apparent correlation between the solar modulation of the cosmic ray rate, as measured from the Climax neutron monitor, and the low level cloud cover, measured from the ISCCP IR data (Rossow and Schiffer 1999),during the period 1983–1995 was noted (Svensmark and Friis-Christenson 1997, Marsh and Svensmark 2000). Here the neutron monitor data were used as a proxy for the ionization rate in the atmosphere. These authors observed a dip in the low level cloud cover between 1983 and 1995 which followed closely the decrease in the neutron monitor rate due to the 11-year solar cycle. They used this correlation to hypothesise that that there was a strong connection between the production of clouds and ionization from cosmic rays, assuming that more ionization would produce more cloud. They went on to show that, if this were a global phenomenon, it would explain most of the global warming seen in the twentieth century (Svensmark 2007). Svensmark argues that the cosmic ray rate has been shown to have decreased during the twentieth century (McCracken and Beer 2007) so fewer cosmic rays implies less low cloud i.e. more solar radiation penetrating to the surface of the Earth i.e. more warming. However, the correlation was shown to be rather localised covering only a fraction of the globe (Voiculescu et al 2006). Hence the effect can only be used to explain a fraction of the global warming seen in the twentieth century.

4.9 ATTEMPTS TO CORROBORATE THE HYPOTHESISED CONNECTION BETWEEN COSMIC RAYS AND THE CLIMATE

Figure 4.6 shows the ISCCP IR data used by Marsh and Svensmark 2000 for 1983–2011. This includes the following solar cycle (solar cycle 23 peaking in 2002) which passed since the observation of the correlation in 1983–1995 (solar cycle 22). The data show a gradual decrease in low level cloud cover during the following solar cycle from 1995–2010 but there is no dip similar to the one seen from 1983–95. Hence the following solar cycle does not corroborate the Marsh and Svensmark hypothesis. Furthermore, the hypothesis is not corroborated by another set of cloud data from the ISCCP project (Kristjansson 2002) where the correlation is not observed. Hence the dip could be an artefact of the method of measurement of the cloud anomaly.

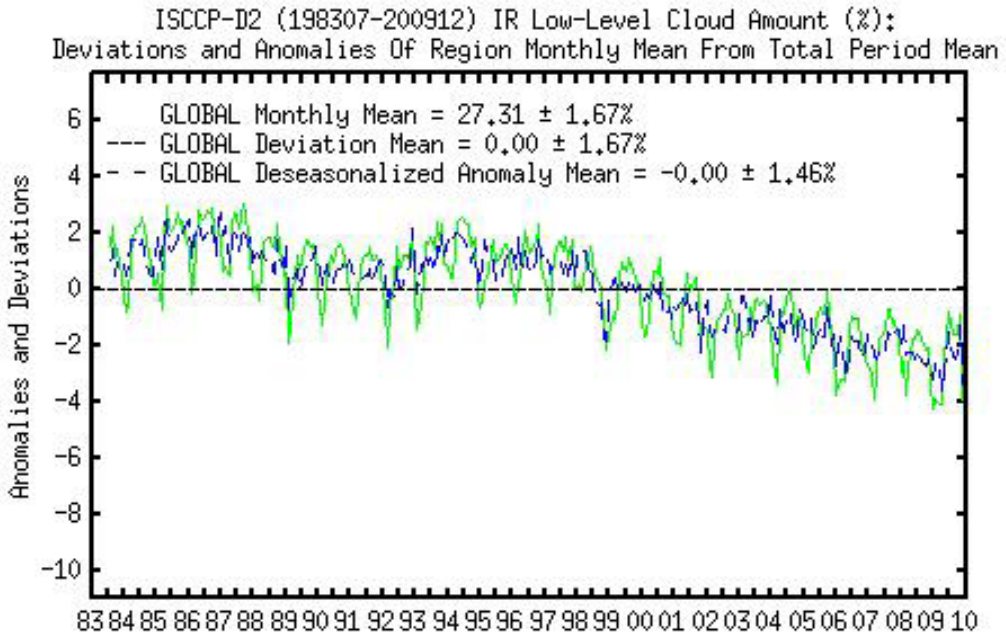

Figure 4.6 The global monthly averaged low level cloud anomaly (deviation from the average) against time (source http://isccp.giss.nasa.gov/climanal7.html see ISCCP 2016). The green curve shows the average monthly value before seasonal correction, the blue after seasonal correction.

An examination of the dip in the low level cloud cover in cycle 22 (1987–94) showed that its magnitude was independent of magnetic latitude. If clouds were being influenced by cosmic rays the decrease should have been greater at the magnetic poles than at the magnetic equator since the solar modulation of the ionization from cosmic rays is greater at the poles than at the equator. A statistical analysis of the failure to find a magnetic latitude dependence of the effect showed that less than 23% of the decrease comes from the changing cosmic ray rate at 90% confidence level (Sloan and Wolfendale 2008).

Figure 4.7 shows the variation of the mean global surface temperature compared to the equivalent Climax neutron monitor rate as a function of time since 1890. The equivalent neutron monitor rate has been derived from the ^{10}Be data from ice cores (McCracken and Beer 2007). Here the data have been smoothed by taking an 11-year running mean to illustrate the overall trend and eliminate the effects of the 11-year solar cycle on the neutron data.

From figure 4.7 it can be seen that the cosmic ray rate decrease occurred in the first half of the twentieth century when the rate of increase of temperature was small. In the second half of the century the cosmic ray rate change was small while the temperature increased rapidly. Hence the changing cosmic ray rate correlates badly with the rise in temperature. From this it was shown that the contribution of the changing cosmic ray rate is less than 14% of the twentieth century global warming (Sloan and Wolfendale 2011). Laboratory studies of the effects of ionization on aerosol (CCN) formation show a finite effect but this is too small to have a significant impact on global warming (CLOUD 2011).

The IPCC conclude in its AR5 from these and other studies that there is no robust connection between cosmic rays and global warming.

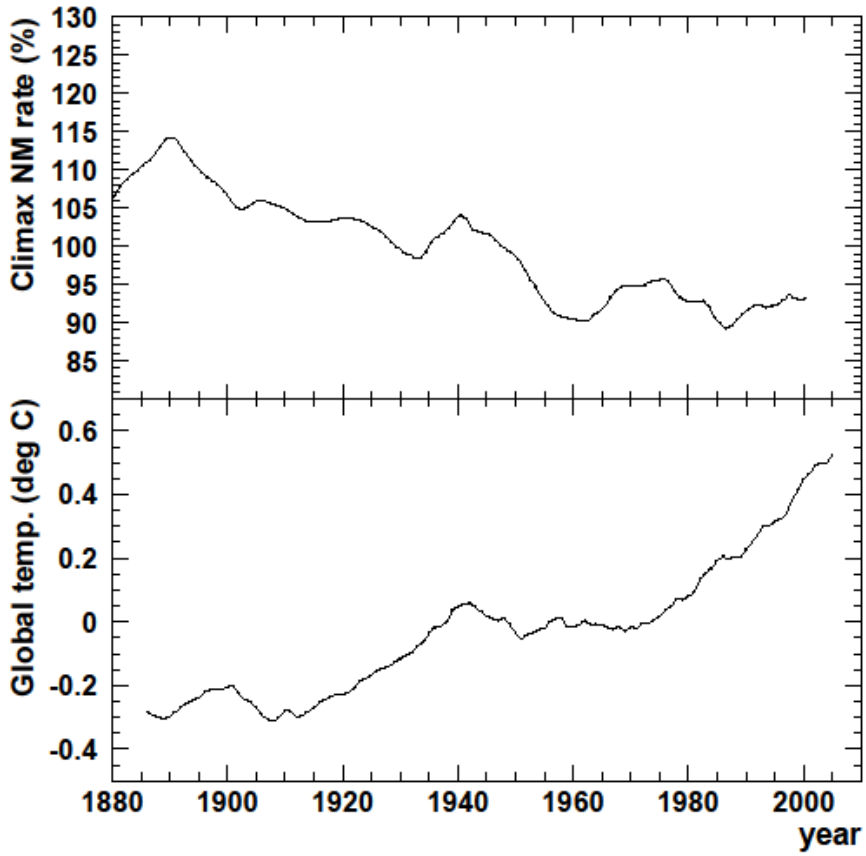

Figure 4.7 (Upper panel) shows the smoothed cosmic ray rate as measured in the Climax neutron monitor and the lower panel shows the average global temperature against time (Sloan and Wolfendale 2011).

4.10 CONCLUSIONS

In this chapter the main features underlying the formation of clouds have been described. It should be possible to appreciate now why one of the largest uncertainties in climate modelling comes about because it is difficult to quantify such formation on a global basis.

APPENDIX 4.1 THE PRESSURE INSIDE A CURVED SURFACE DUE TO SURFACE TENSION

This can be understood from an element of the curved surface of the liquid which has surface tension σ shown in figure A4.1. Consider the forces due to the surface tension at the midpoint of each edge of the element of the surface. The force on the left hand edge in the x direction is F_L and on the right hand edge is F_R. This force in the y direction at the midpoint on the forward edge is F_F and on the back edge is F_B. The radius of curvature of the element between the two midpoints in the x direction is R_x which subtends angle $\delta\vartheta_x$ at the centre of curvature of this line and is R_y in the y direction subtending angle $\delta\vartheta_y$ (as shown in figure A1). The forces F_L, F_R, F_F, F_B have components in the downward direction of $F_L=F_R=\sigma R_y\delta\vartheta_y/2$ and $F_B\delta\vartheta_y/2$. Now the surface tension forces (σ times arc length) are $F_L=F_R=\sigma R_y\delta\vartheta_y/2$ and $F_F=F_B=\sigma R_x\delta\vartheta_x/2$. The total downward force on the element is the sum of all these forces which is $\sigma R_y\delta\vartheta_y\delta\vartheta_x + \sigma R_x\delta\vartheta_y\delta\vartheta_x$. Now $\delta\vartheta_y\delta\vartheta_x = \delta y\delta x/R_yR_x$ where δx and δy are the lengths of the side of the element. The pressure across the surface is the total force on the element divided by its area $(\delta y\delta x)$. Hence the pressure across the surface is given by ΔP given by

$$\Delta P = \sigma\left(\frac{1}{R_x}+\frac{1}{R_y}\right) \qquad \text{A4.1}$$

For a spherical surface of radius R, $R_x=R_y=R$ so that $\Delta P=2\sigma/R$. For a soap bubble there are two sides to the film so that the pressure inside a soap bubble is $2\Delta P=4\sigma/R$.

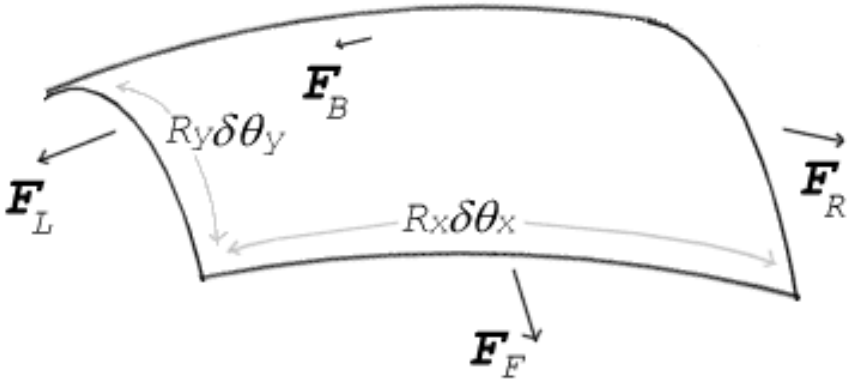

Figure A4.1. A small element of the curved surface of arc lengths $d\theta_x$ and $d\theta_y$ in the x and y directions showing the surface tension forces along each edge. The x axis is from left (L) to right (R) and the y axis from front (F) for back (B). R_x and R_y are the radii of curvature of the arcs.

APPENDIX 4.2 DERIVATION OF THE KELVIN FORMULA

Kelvin showed that the vapour pressure, $P(r)$, outside a spherical surface of radius, r, compared to that over a flat surface, $P(\infty)$ is given by

$$P(r) = P(\infty)e^{\frac{2\sigma M}{r\rho RT}} \qquad \text{A4. 2}$$

Where σ is the surface tension of the liquid which has density ρ, M is the molar mass of the liquid, T is the absolute temperature and R is the universal gas constant.

Proof

When a liquid is in contact with a solid surface a meniscus forms with a contact angle between the solid and the liquid as illustrated in figures A4.2 and A4.3.

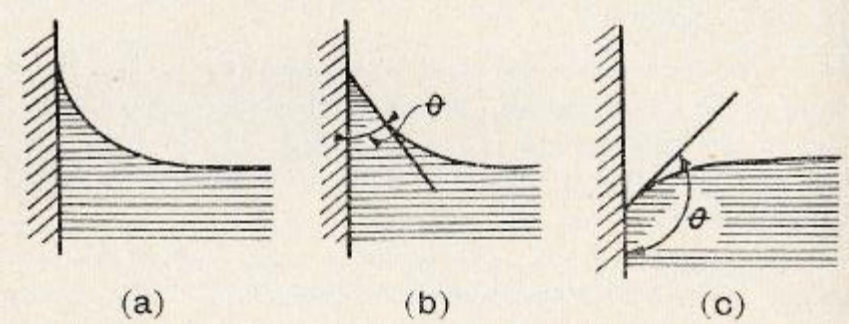

Figure A4.2 illustrates the contact angle, θ, between the liquid and the solid. In cases (a) and (b) the attraction between the molecules of the liquid and those in the wall is greater than that between the liquid molecules giving a small angle of contact. In case (c) the attraction between the molecules of the liquid is greater than that between those the liquid and walls. (Source of diagram Temperley 1953).

We consider here an ideal liquid in which the attractive forces between the molecules of the liquid is much greater than those between the liquid and the walls of the tube. In this case the angle of contact will be nearly π radians and the meniscus will have concave shape pointing downwards as in figure A4.2(c). Consider a fine bore tube suspended vertically in a liquid as illustrated in figure A4.3.

For a fine bore tube, of radius *r*, and a liquid with a high surface tension, σ, and a contact angle near π radians, the meniscus will be hemispherical. The surface tension force is $2\pi r\sigma$ (circumference times surface tension). This will depress the meniscus as shown for the blue tubes in figure A4.2. The pressure force in the liquid tending to equalise the levels is ($\pi r^2 \rho g h$) where h is the height of the meniscus below the flat surface and g is the gravitational acceleration. In equilibrium these two forces are equal i.e.

$$h = \frac{2\sigma}{r\rho g} \qquad \text{A4.3.}$$

The vapour above the curved surface is at a height h below that of the flat surface. The vapour pressure above the curved surface will then be increased to $P(\infty)e^{\frac{h}{H_v}}$ where $P(\infty)$ is the vapour pressure above the flat surface and $H_v = Mg/RT$ is the scale height of the vapour (with M molecular weight of the vapour, R the universal gas constant and T the absolute temperature, see Box 3.1). Substituting for H_v and h from equation 4.3 gives the vapour pressure over the spherical surface of radius r, $P(r)$ i.e.

$$P(r) = P(\infty)e^{\frac{2\sigma M}{r\rho RT}} \qquad \text{A4.2}$$

Note that in using the value of the scale height, H_v, we implicitly assume that the vapour behaves like an ideal gas. This means that the equation A4.2 is an approximation.

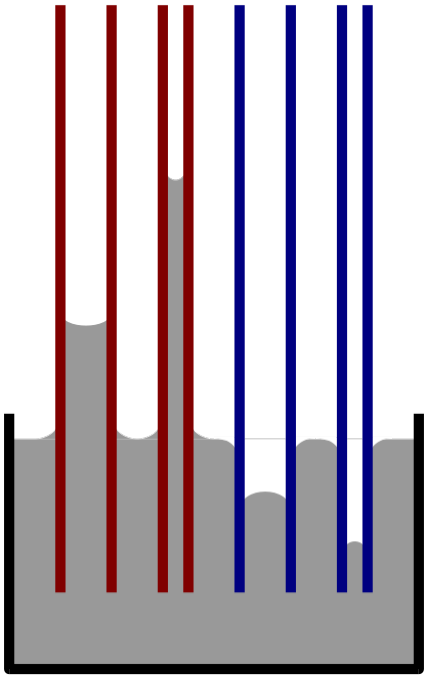

Figure A4.3 Four tubes suspended in a liquid. The red rubes have small contact angles e,g, as water in a clean glass tube. The blue tubes have contact angles close to π radians e.g. as mercury in glass. (Source https://en.wikipedia.org/wiki/Surface_tension).

References.

Ahluwalia H. 2011, "Timelines of cosmic ray intensity, *A*ρ, IMF and sunspot numbers since 1937", Journal of Geophysical Research volume 116 (2011) A12106.

CLOUD (2011), J. Kirkby et al., "Role of sulfuric acid, ammonia and galactic cosmic rays in atmospheric aerosol nucleation", Nature, Volume 476, pp. 429–433.

Greisen K. 1942, "The intensities of the hard and soft components of cosmic rays as functions of altitude and zenith angle", Physical Review volume 61 pages 212–221.

ISCCP 2016, figure obtained from International Satellite Cloud Climatology Project (ISCCP) maintained by the ISCCP research group at NASA Goddard Institute for space studies, New York, NY, USA, see Rossow W.B. and Schiffer R.A. 2005, Bulletin of the American Meteorological Society, volume 80, pages 2261–2288.

Kristjansson JE, Staple A, Kristjansen J and Kaas E (2002), "A new look at possible connections between solar activity, clouds and climate", Geophysical Research Letters volume 29 page 2107.

Lue L 2009 "Chemical Thermodynamics" published by Bookboon, ISBN 978-87-7681-497-7.

Marsh N and Svensmark H (2000), "Low cloud properties influenced by cosmic rays", Physical Review Letterrs volume 85 page 5004.

McCracken KG and Beer J (2007), "Long term changes in the cosmic ray intensity at Earth 1429–2005", Journal of Geophysical Research volume 112 A10101.

Ney E.P. 1959, "Cosmic rays and the weather", Nature volume 183 (1959) 451–452.

Rossow WB and Schiffer RA 1999, "Advances in understanding clouds from ISCCP", Bulletin of the American Meteorological Society Vol. 80 page 2261.

Sloan T., Bazilevskaya G.A, Makhmutov V.S., Stozhkov Y.I., Svirzhevskaya A.K. and Svirzhevsky N.S. "Ionization in the atmosphere, comparison between measurements and simulations", Astrophysics, Space Science Transactions volume 8 (2011) pages 1–5.

Sloan T and Wolfendale A W 2008, "Testing the proposed causal link between cosmic rays and cloud cover", Environmental Research Letters vol. 3 page 024001.

Sloan T and Wolfendale A W 2011, The contribution of cosmic rays to global warming", Journal of Atmospheric and Solar-Terrestrial Physics, vol. 73 pages 2352–2355.

Svensmark H and Friis-Christenson E (1997), "Variation of cosmic ray flux and global cloud coverage – a missing link in solar climate relationships", Journal of Atmospheric and Solar-Terrestrial Physics Vol. 59 pages 1225–1231.

Svensmark H (2007), "Cosmoclimatology: a new theory emerges" News Rev. Astron. Geo. Vol. 48 page 18.

Temperley 1953, "Properties of Matter", University Tutorial Press 1953.

Voiculescu M, Usoskin IG, Mursala K (2006),"Different responses of clouds at the solar input", Geophysics Research Letters Vol. 33 page L21802.

Exercises

1. Assuming smooth flow compute the terminal velocity in air of a water droplet of radius 10μm (viscosity of air is 18 10^{-5} N s m^2, gravitational acceleration g=10 m/s^2, density of water=1000 kg/m^3). Compute the Reynolds number for this droplet and state whether the flow is smooth or turbulent. Calculate the terminal velocity and Reynolds number under the same assumptions for a raindrop of radius 1 mm. Show that the flow is turbulent in this case and comment on the accuracy of the terminal velocity which you calculate for this drop.
2. Assuming that water vapour behaves as an ideal gas, compute the value of α in the Kelvin equation (equation A2) expressed as $e^{\frac{\alpha}{r}}$. For an aerosol particle consisting of ammonium sulphate of mass 2 10^{-19} kg compute the value of b in the Kohler equation. Plot the Kohler curve for this aerosol particle. (Answers α=0.0012μm, b=2.0 10^{-5}μm^3.)
3. Show that the peak value of the Kohler curve occurs at radius r_{cr} which is the solution to the equation

$$\alpha {r_{cr}}^3 - 3br_{cr} - \alpha b = 0$$

How could you solve this equation? Solve the equation using your proposed method for the values of α and b given in the solution to problem 2. Calculate the value of S_{crit} at this peak value. (The values of r_{cr} and S_{crit} should agree with the values in your plot from problem 2).

4. It can be shown that the growth of a water droplet with time, *t*, follows the relationship

$$r\frac{dr}{dt} = \frac{S-1}{F_k+F_D}$$

Where *r* is the radius of the droplet, *S* is the degree of supersaturation of the surroundings F_K and F_D, and are terms depending on the thermal conductivity and diffusion coefficient of water vapour in the surrounding air, respectively. Show that the radius of a droplet will increase as the square root of time. A certain droplet in a region of supersaturated air takes 1 hour to grow to a radius of 4μm. Plot a graph to show the droplet radius as a function of time.

5. A perfectly clean U tube is filled with water (density ρ=1000kg/m^3) of surface tension σ=73 10^{-3} N/m with angle of contact of zero. One arm has radius r_1 and the other has radius r_2. Show that when the water settles to its equilibrium level the difference in height of the meniscus levels will be given by

$$h = \frac{2\sigma}{\rho g}\left(\frac{1}{r_2} - \frac{1}{r_1}\right)$$

Calculate the height difference when r_1=2 mm and r_2=1 mm. Why is it necessary to have the U tube scrupulously clean for this to be a meaningful calculation?

6. Estimate the radius of a droplet of water at which the surface energy due to surface tension is equal to the latent heat needed to evaporate the droplet. The following reason why small droplets have difficulty in growing is sometimes given; the surface energy in a small droplet is larger than the latent heat needed to evaporate it. Hence a small droplet evaporates due to its stored surface energy. Explain why this statement is not true. (Latent heat of vaporisation of water is 226 10^4 J/kg, surface tension of water vapour is 73 10^{-3} N/m, density of water is 1000 kg/m^3).

7. A soap bubble is blown at the end of a narrow tube. When the bubble reaches radius *R* the pressure is released and it is allowed to contract. Show that the radius, *r*, of the soap bubble will vary with time, *t*, as

$$R^4 - r^4 = \frac{4b}{\pi}\sigma t$$

where the volume per second of air flowing down the tube varies as *b* times the pressure difference between the ends of the tube and σ is the surface tension of the soap solution.

5 ENERGY CIRCULATION AND MONITORING

Introduction

The solar energy absorbed by the Earth is circulated by the flow of winds in the atmosphere and by ocean currents. Most of the energy is absorbed in the oceans because they are so much more massive than the atmosphere. However, the circulation in the ocean is slower since ocean currents move more slowly than winds i.e. air currents. This Chapter discusses the circulation of this energy since it is very important from the point of view of the climate. The monitoring of the state of the atmosphere and oceans particularly since the advent of satellites allows us to understand how increasing greenhouse gases affect other aspects of the oceans as well as surface warming.

5.1 THE SEASONS

The Earth's seasons are caused by the tilt of the Earth's axis at an angle of 23.5 degrees relative to the orbit plane. In its yearly orbit around the Sun in July the Northern Hemisphere points towards the Sun while in January it is the Southern Hemisphere's turn. This is illustrated in figure 5.1 which shows that in July the days are longer and there is greater insolation in the Northern Hemisphere while in the Southern hemisphere this occurs in January.

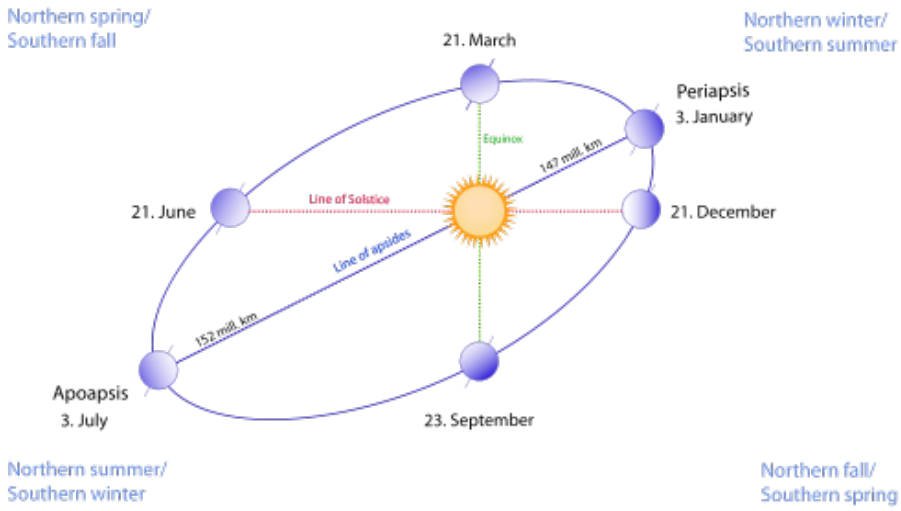

Figure 5.1 The orbit of the Earth showing how the tilt of the Earth's axis causes January summer in the Southern Hemisphere and the July summer in the Northern Hemisphere. Note that the diagram is not to scale and the ellipticity of the orbit is exaggerated. (Copied under the GNU Free Documentation License and available under the Creative Commons Attribution and Share-Alike License).

The orbit of the Earth is not constant but changes over time scales of order 20000–100000 years. It is such changes which are thought to cause periods of ice ages on the Earth (see Chapter 9).

5.2 ENERGY CIRCULATION

The differences in energy falling on different parts of the globe due to seasonal changes in insolation are reduced by the circulation of energy by means of either ocean currents or winds in the atmosphere. The difference between the energy falling at the Equator and the Poles is similarly reduced by this circulation.

The energy flux, F, falling on the Earth's surface at a position where the angle between the normal to the Earth's surface and the direction of the Sun is θ is given by

$$F = S(1 - R)T \cos\theta \qquad 5.1$$

where S is the solar constant (the energy from the Sun falling on a plane of unit area perpendicular to the direction of the Sun per unit time at the Earth's orbit radius), R is the fraction of the energy reflected and T the fraction transmitted through the atmosphere. Hence much more energy falls on the Earth at the Equator where $\cos\theta \sim 1$ than at the Poles where $\cos\theta$ is much smaller.

Much of this energy is absorbed by the oceans and is then circulated quite slowly by ocean currents. Less of the energy is absorbed by the atmosphere where it is circulated more rapidly by winds. The forces causing the ocean and wind currents are pressure differences. These currents are affected by the motion of the Earth itself. The effects of such forces are too small to be noticeable on everyday objects. However, they have a large effect on air and ocean currents moving large distances. They are known as Coriolis Forces. These are not strictly forces but apparent accelerations as viewed by a stationary observer on the Earth's surface and are caused by the rotation of the Earth.

In this Chapter we will examine the prevailing winds and ocean currents so that we can begin to understand the circulation of the energy around the globe.

5.3 CORIOLIS ACCELERATION

To understand this qualitatively, suppose a bullet is fired at a distant target by a marksman standing at the North Pole. The bullet takes time to reach the distant target. By the time it reaches the target the target will have appeared to have moved relative to the marksman due to the rotation of the Earth. Hence the bullet could miss the target. To the marksman who is moving with the Earth the bullet appears to veer towards the West since the target has actually moved Eastwards due to the Earth's rotation. To the marksman the bullet appears to undergo a Westward acceleration since it veers from a straight line trajectory. This is known as the Coriolis Acceleration, named after the discoverer of the effect. It is actually an acceleration which can be thought of as an effective force and for this reason it is known as the Coriolis Force.

A similar effect is visible everywhere on Earth. A moving object disconnected from the Earth's surface will appear to veer from a linear trajectory to an observer moving with the Earth since the start point of the object is moving at a different speed from the end point of the trajectory. The Coriolis acceleration is given $-2\,\boldsymbol{\Omega} \times \boldsymbol{v}$ where $\boldsymbol{\Omega}$ is the angular velocity vector of rotation of the Earth (see endnote 2 page 202) and $\boldsymbol{v}$ is the velocity vector of the object. For a derivation of this see Goldstein, Poole and Safko (2001). The Coriolis force is equal to the mass times the Coriolis acceleration.

5.4 THE WIND DIRECTION

The force causing the air to flow arises from the pressure differences in the atmosphere. The atmospheric pressure typically varies between 950 mbar and 1050 mbar over distances of order 1000 km. Hence pressure gradients of order 0.1 mbar per km are common. Figure 5.2 illustrates the effect of the combined force from the pressure gradient and the Coriolis force. The initial force from the pressure gradient would cause a parcel of air to move perpendicular to the isobars (lines of constant pressure) i.e. along AB in figure 5.2. As the parcel gathers speed the Coriolis force acts at right angles to the motion causing the trajectory to veer as shown at point B in fig 5.2. As the speed increases so does the Coriolis Force until the parcel moves along a trajectory where the Coriolis Force matches the pressure force. This is the equilibrium trajectory with the wind direction parallel to the isobars. The Coriolis acceleration, ie the vector product $-2\boldsymbol{\Omega} \times \boldsymbol{v}$, has a different sign in the Southern than in the Northern Hemispheres. Hence the wind flows in a clockwise direction around a high pressure zone or anti-clockwise around a low pressure zone in the Northern Hemisphere and opposite to this in the Southern Hemisphere.

Ocean currents are similarly affected by the Coriolis acceleration.

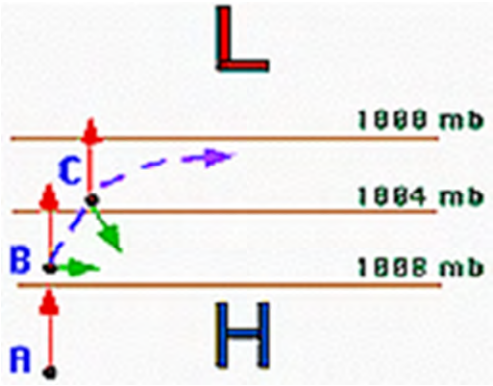

Figure 5.2 Illustrates how the effect of the Coriolis Force causes the wind to flow parallel to the isobars. The force from the pressure gradient is represented by the red arrows. The green arrows (perpendicular to the velocity vectors) represent the Coriolis force.

5.5 ATMOSPHERIC CIRCULATION

Figure 5.3 shows the directions of the prevailing winds on the Earth's surface.

Equation 5.1 shows that the solar energy falling on the Earth is greatest at the Equator of the Earth where $\cos\theta \sim 1$. The heating of the atmosphere is then greatest at the Equator and the heated air rises creating a low pressure zone which draws in colder air from higher latitudes where the air is heated less. To balance the cold air drawn in at the Earth's surface there is a returning current of warm air at high altitude near the tropopause (the layer of air next to the stratosphere). Thus heat is transported polewards by the atmosphere from the Equator.

The motion of these air flows is modified by the Coriolis force. For example in the Northern Hemisphere the Southward flow of air near the surface is turned towards the West and the Northward flow of air near the tropopause towards the East and vice versa in the Southern Hemisphere. The high altitude current eventually cools sufficiently to create high enough air density to sink. This occurs in the subtropics so that there is a circulatory motion known as a Hadley Cell (named after the discoverer George Hadley). This gives rise to the so-called Trade Winds in the subtropical zones of the Earth i.e. south-westerly (north westerly) air flow at the Earth's surface in the Northern (Southern) Hemisphere. The region between the Northern and Southern Hadley cells is known as the Doldrums where there is little air movement.

A similar mechanism occurs between latitudes 60 and 90 degrees giving rise to the so-called polar cell. The region in between these two cells gives a cell (the Ferrel Cell) in which the air moves in the opposite sense to that in the Hadley and Polar Cells. The detailed mechanisms of these three cells define the weather patterns in each zone and is of great interest to meteorologists. The three zones are illustrated in figure 5.3 where the surface winds are shown by the white arrows.

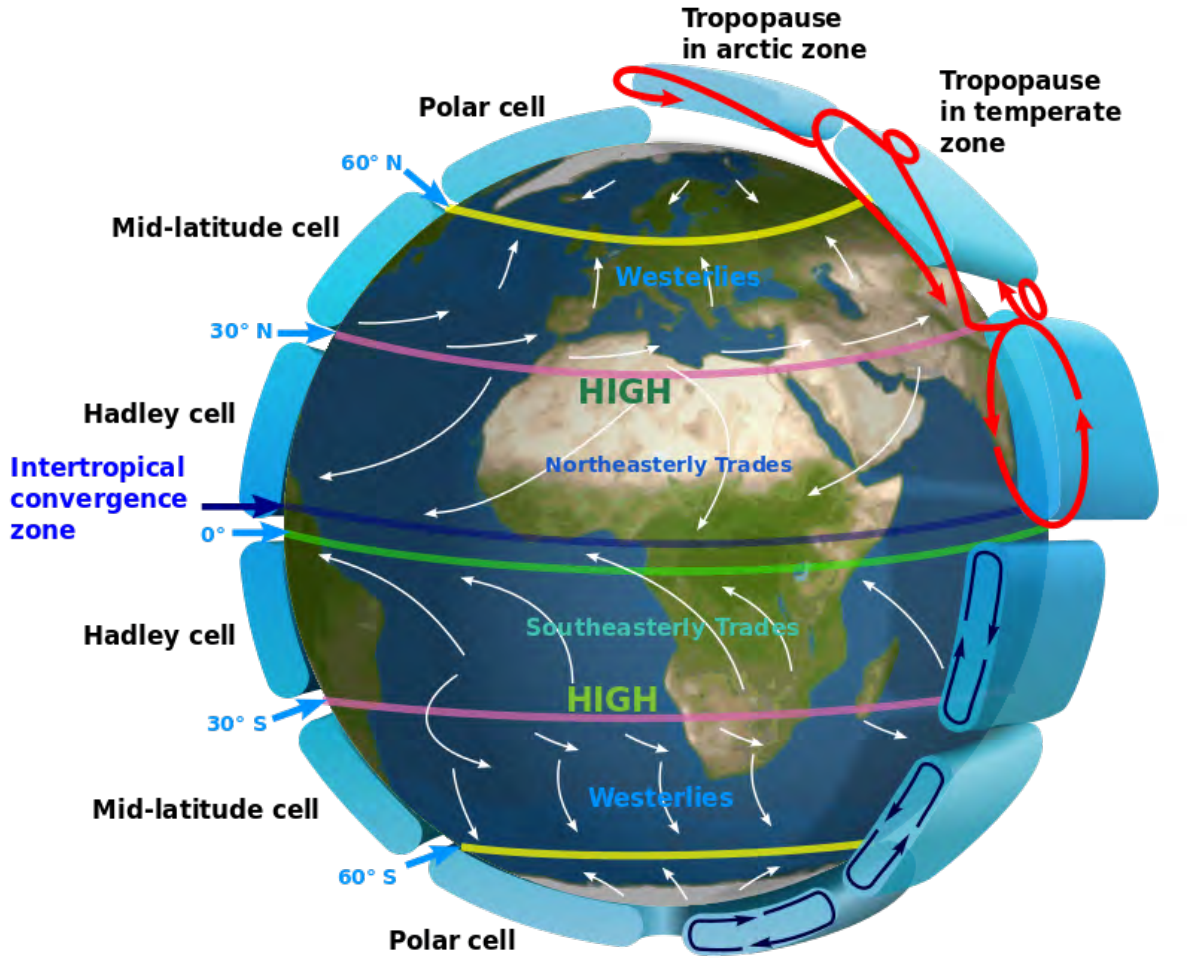

Figure 5.3 The prevailing surface air circulation in the atmosphere (white arrows) showing the Hadley Cell, Ferrel Cell (the Mid-latitude Cell) and the Polar cell. (Figure By Kaidor http://creativecommons.org/licenses/by-sa/3.0 avaialable under Creative Commons License.)

This pattern changes with the season. By Equator here we mean the point at which the sun is verically above. Hence this pattern migrates between the tropics on a seasonal basis due to the tilt of the Earth's axis. The fact that Western Europe sits roughly at the boundary between the Ferrel and Polar cells accounts for the rather changeable weather experienced there.

5.6 THE CIRCULATION OF THE OCEANS

5.6.1 THE CHEMISTRY OF SEA WATER

The presence of impurities changes the properties of sea water compared to pure water (the principal impurity is common salt NaCl). These impurities cause sea water to have higher density and lower freezing point than pure water. The freezing point, T_F of saline water of salinity, S, follows the relation

$$T_F = -0.057\, S$$

where the salinity $S = 1000s$ with s is the proportion by weight of impurity in the water.

Fortunately for life on Earth, pure water shows the remarkable property of having a maximum density at a temperature of 4°C. Ice then has a lower density than cold water and so floats. In consequence water freezes from the top rather than the bottom which is fortunate for water living organisms. The temperature of the maximum density, T_m, is lowered by the presence of impurities in the water, following the relation $T_m = 4.0 - 0.184S$.

The fraction of impurities in sea water is of order 3.5% by weight so that the salinity is $S = 35$. The impurities cause an increase in density of water from 1000 kg/m^3 for pure water to 1025 kg/m^3 for sea water. The density changes with temperature due to thermal expansion and depth due to the compressibilty of water. There are small but important variations in salinity and density from place to place in the ocean. Such variations cause salinity and density gradients which affect the ocean currents.

5.6.2 THE DEPTH PROFILE IN THE OCEAN

This is illustrated in figure 5.4. The upper layer of thickness of order 10 metres is the mixed layer. In this layer the surface heat absorbed from the Sun is mixed by wind and wave action so that the average temperature is approximately constant. Below the mixed layer comes the thermocline where the temperature changes most rapidly with depth. The salinity also changes slightly with depth. This layer is typically several hundred metres thick. The deep layer lies below the thermocline. In this layer the temperature and salinity are almost constant. However, the density changes with depth due to the compression forces from the overburden of water.

This picture changes with latitude as shown in figure 5.5. The depths of the mixed layer and thermocline decrease near the poles. The water here is cooled both by radiation and by winds so that the cooler water sinks at the poles. The result is a global circulation of water currents as shown in figure 5.6. This is known as the thermohaline circulation and is sometimes called the Ocean Conveyor belt. It is also sometimes refered to as the Meridional Overturning Circulation (MOC). The surface currents (red paths in figure 5.6) are driven by prevailing winds and sea water density gradients. They bring warm water to the poles which cools and sinks giving rise to returning deep water currents (blue paths). Some of this water upwells at middle latitudes and some contributes to the deep water current (fig. 5.5).

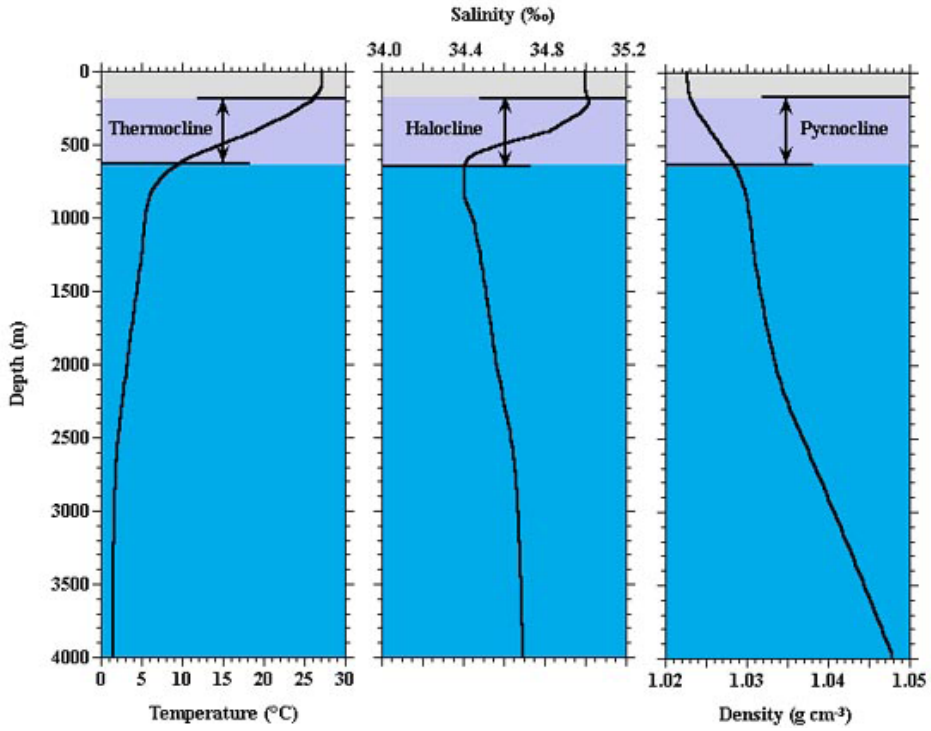

5.4 Typical variation of temperature, salinity and density with depth in the ocean (source http://ocp.ldeo.columbia.edu/open_house/whale_dir.shtml).

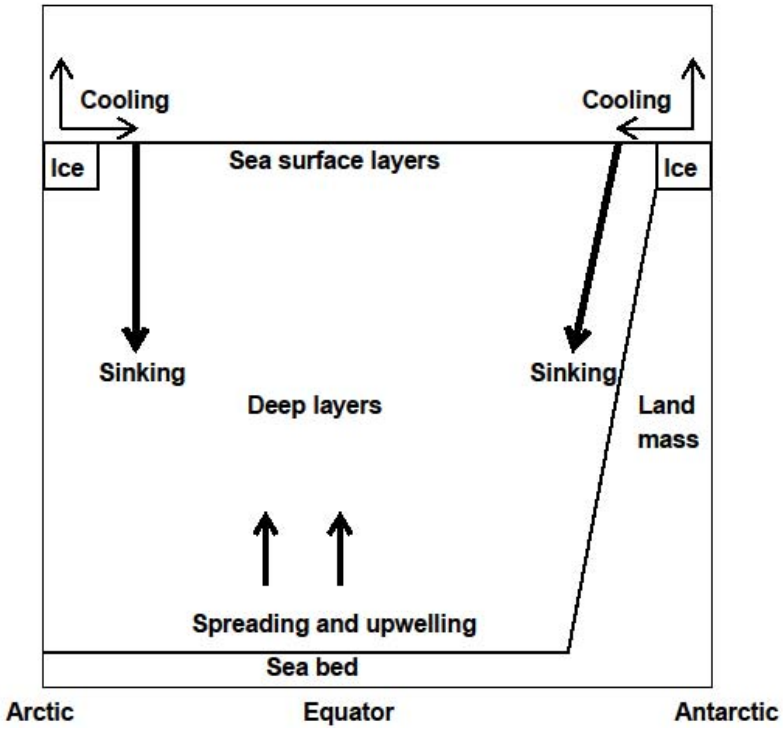

Figure 5.5 Section though the oceans from Arctic in the North to the Antarctic in the South where the ice is land based. The cooling of the waters at the poles is by wind and radiation. The cooled water then sinks and spreads out over the ocean bottom (see Taylor 2005).

5.6.3 THE PREVAILING OCEAN CURRENTS

The prevailing ocean currents as a result of the thermohaline circulation are illustrated in figure 5.6. By prevailing ocean currents we mean the general circulation ignoring all local effects which are superimposed on the general circulation. The local effects are usually more noticeable close to land. The Coriolis effect influences the water flow. For example, the effect on the prevailing current causes the ocean levels to differ across the width of the Atlantic by about 1 metre. It is thought that the prevailing current is slow taking of order centuries to complete a lap. The circulation is known as the thermohaline circulation since it is driven by temperature (thermo) and salinity (haline) gradients in the oceans.

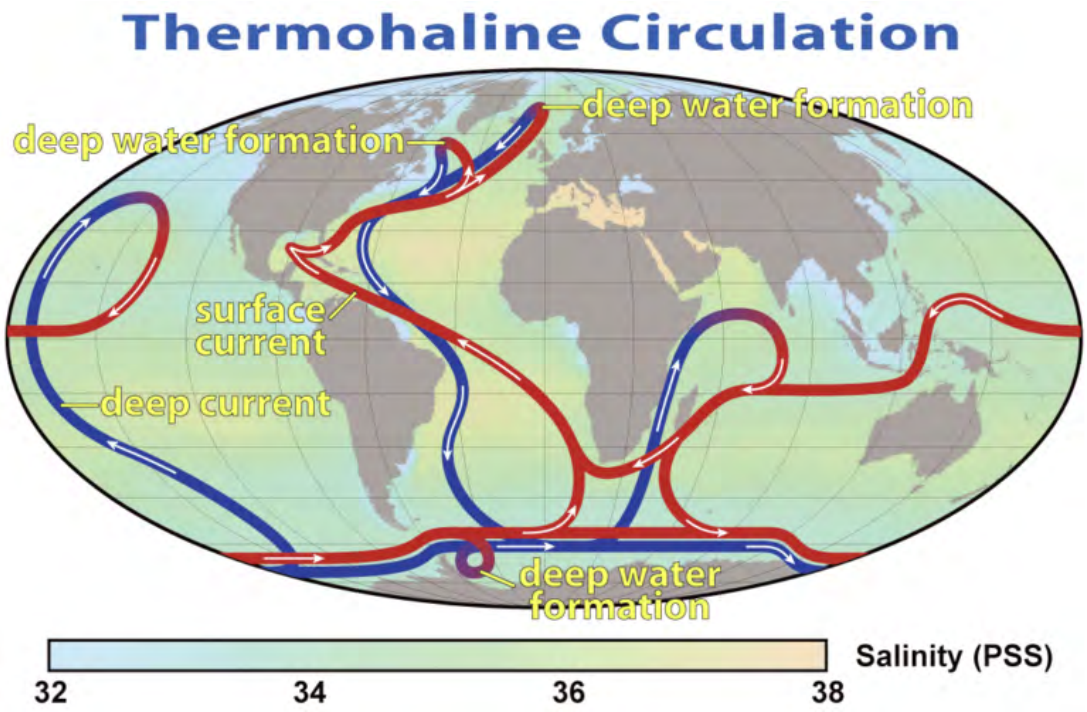

Figure 5.6 A summary of the path of the thermohaline circulation (source Robert Simmon, NASA). Blue paths represent deep-water currents and red paths the surface currents. Note that this is a simplified picture showing the prevailing currents but ignoring the ubiquitous local currents. (Figure avaialable under Creative Commons Share-Alike License).

5.7 MONITORING OF THE OCEANS AND ATMOSPHERE.

Monitoring of the oceans and atmosphere has been carried out for approximately 200 years. At first the measurement techniques were primitive. However, these have all improved substantially with time.

The Royal Navy's ships have regularly measured sea surface temperatures on their World-wide voyages. Up to the 1940s this was done by sampling the local ocean using a bucket over the side of the ship and measuring the temperature of the water by thermometer. This was changed to reading engine water intake temperatures in the 1940s. The atmosphere was similarly monitored by weather stations around the World set up for the purpose of weather forecasting.

In the 1970s the space programme began and many monitoring satellites have been placed in orbit around the Earth. Remote sensing became more sophisticated allowing more precise monitoring of both the atmosphere and ocean. Furthermore, at the beginning of the 21st century a series of 4000 buoys were deployed around the globe by the Argo Project. This allows many properties of the ocean to be monitored world-wide at depths down to 2000 metres. These include salinity, density and temperature profiles. The buoys are parked at a depth of 1000 metres and every 10 days or so they dive to a depth of 2000 metres and then move to the surface measuring all the time. On the surface their data are transmitted to the base station by satellite as well as their position by the GPS system. The total ocean heat content has been computed from the temperature profiles. The ocean currents at a depth of 1000 metres are monitored from the drift of the buoys.

Similar careful monitoring of the atmosphere has allowed the average global temperature to be measured initially from data from weather stations and more recently from satellites orbiting the Earth (see Chapter 8).

Some of the results of such monitoring of the climate are shown in figures 11.1 and 5.7. Fig 11.1 shows the atmospheric concentration of carbon dioxide since 1955. The rise is due to the burning of fossil fuels. This has been shown by isotope analysis of the ^{13}C (AR5 2013) and ^{14}C (Baxter and Walton 1970) in the air. The change with time of these isotopes is characteristic of production from old carbon such as is contained in fossil fuels rather than naturally recycled carbon dioxide. The dissolved concentration in seawater also increases and its acidity as measured by the ph value which decreases as the ocean becomes more acidic (since carbon dioxide is slightly acidic).

Figure 5.7 shows other aspects of global warming. These include the Northern hemisphere spring snow covering and area of summer ice coverage in the Arctic. Both of these have decreased due to melting as the Earth warms. The warming also leads to an increase in both the ocean heat content and a rise in the sea level.

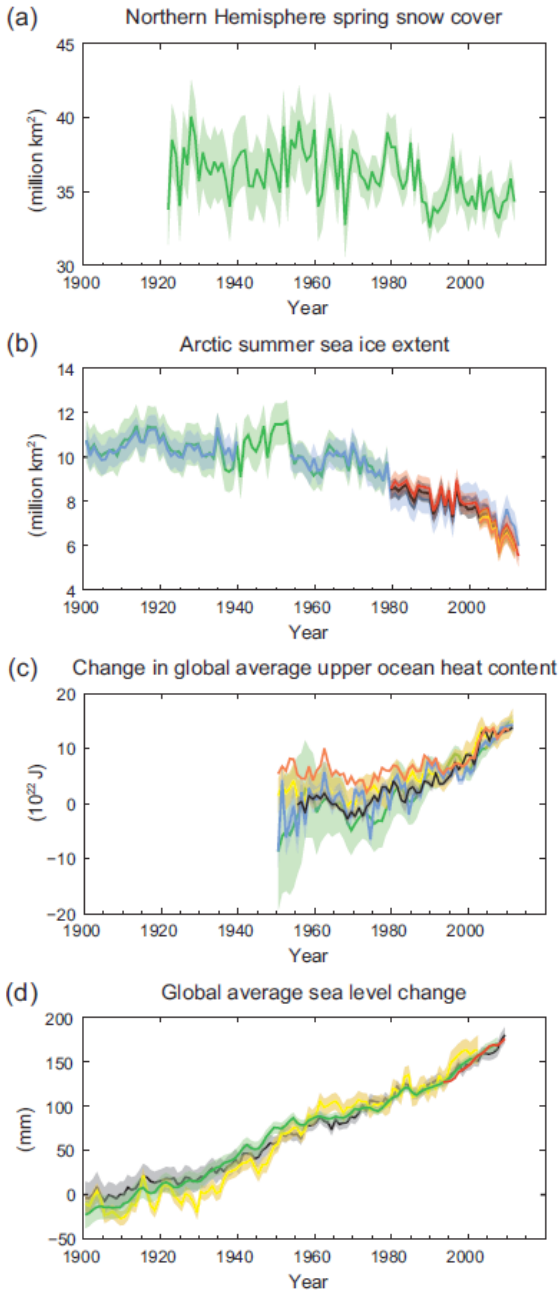

Figure 5.7 Multiple observed indicators of the changing global climate. The shaded bands show the measurement uncertainties (note the improved precision in later years): a) Extent of the Northern hemisphere March-April snow cover, b) Extent of the July-August-September (summer) Arctic sea ice, c) change in global mean upper ocean (0–700m) heat content relative to the mean of all data sets in 1970, d) global mean sea level relative to the 1900–1905 mean of the longest running data set and with all data sets aligned to the same value in 1993, the first year of satellite altimetry data. (Source figure SPM3 in the report of WG1 of the IPCC 5th Assessment Report (AR5 2013)).

5.8 THE RISING SEA LEVEL

The two main contributors to the rising sea level are thermal expansion as the ocean warms and run-off from into the oceans from melting glaciers and ice sheets as a result of global warming. This is illustrated in figure 5.8.

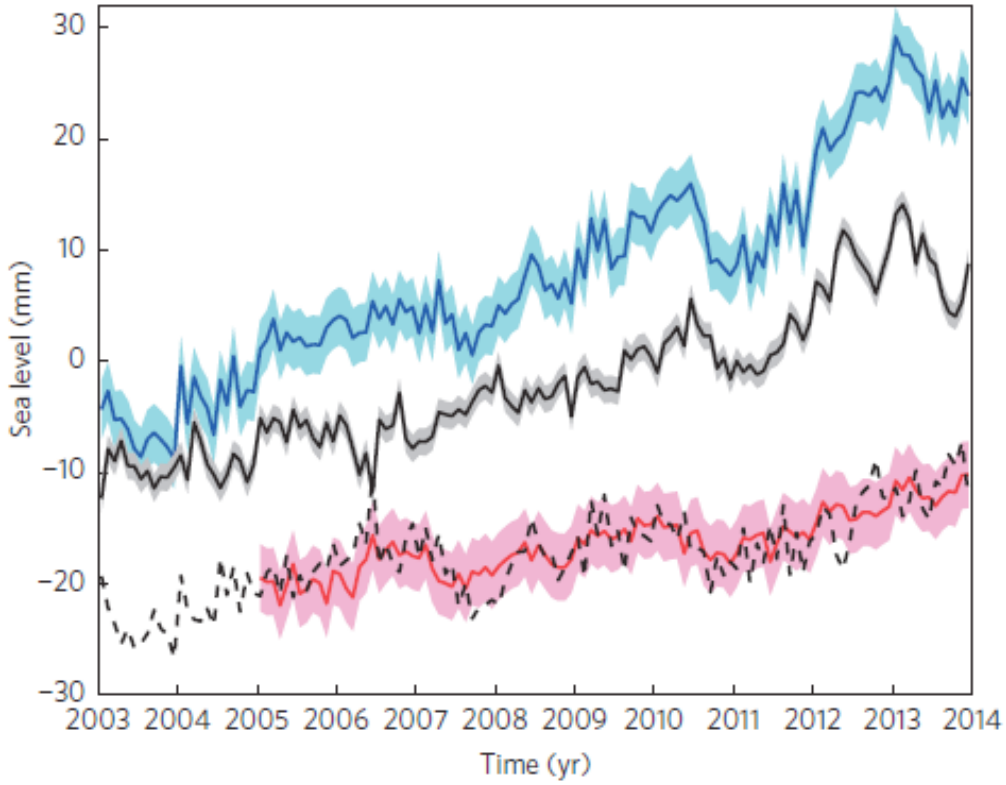

Fig 5.8 The total average sea level rise from satellite altimetry (blue curve). The rise in sea level from meaurements of the ocean mass evolution (black curve) from the GRACE project. The red curve shows the estimated contribution from thermal expansion in the upper 2000m of ocean depth from the ARGO buoy project. The dashed black curve shows the difference between the black and blue curves. The agreement between this and the red curve shows that most of the thermal expansion takes place in the upper 2000m of ocean with little expansion below this depth i.e. little of the excess heat due to global warming disappears below a depth of 2000m. The curves have been corrected for seasonal effects and are offset for clarity (source Llovel et al 2014).

The blue curve in figure 5.8 shows the measured rise in the average sea level rise from 2003 to 2014, as determined from satellite altimetry. The black curve shows the rise computed by the GRACE project which monitors the gravitational field of the Earth. From this the total ocean mass change due to melting ice sheets and glaciers can be computed. This is shown as the black curve in figure 5.8. The dashed black curve is the difference between the black and red curves and this is assumed to be the rise in the sea level due to the thermal expansion of the whole ocean as it warms. The red curve shows the thermal expansion for the layer of ocean above a depth of 2000 metres computed from the rise in the mean ocean temperature from the Argo project.

The fact that the thermal expansion from the whole ocean depth dashed black curve) agrees well with that from depths above 2000 metres (red curve) indicates that there is little warming of the ocean at depths below 2000 metres. From the measured rise due to thermal expansion the heat uptake by the ocean above 2000 metres depth was determined to be 0.72±0.10 W/m^2 (Llovel et al 2014). This is compatible with the difference between energy falling on the Earth and that radiated by the Earth, as measured by satellites (AR5 2013 and exercise 5). This shows that the difference is accounted for by the measured absorption in the oceans.

The Argo system has been used to show that there is substantial heat disappearing down to depths of 1500m (Chen and Tung 2014). They show that the ocean heat content down to such depths increased significantly between the years of 2000–2012. They hypothesised that the slow down in mean surface temperature during this period is due to a mechanism involving the fresh water from the melting of polar ice. They further hypothesised that this could be an oscillatory mechanism leading to alternate periods of slowing down and speeding up of the mean global temperature rise such as has been seen in the global temperature record in the past.

References

AR5 2013. Working Group 1 contribution to the Fifth Assessment Report of the IPCC.

Baxter M.S. and Walton A. 1970, 'A theoretical approach to the Suess effect', Proc. Roy. Soc. London A318 pp. 213–230.

Chen X. and Tung K.T., 2014, 'Varying planetary heat sink led to global-warming slowdown and acceleration', Science Vol. 345, pp. 897–903. Doi:10.1126/science.1254937.

Goldstein H., Poole C.P., Safko J.L., 2001, "Classical Mechanics", Addison-Wesley, Released by Pearson Education Ltd., Edinburgh. ISBN-13:978-0201657029.

Levinson D.H. and Lawrimore J.H. 2009 "State of the Climate in 2007", Edited by D.H. Levinson and J.H. Lawrimore in Bulletin of the American Meteorological Society, volume 89 Number 7 (Special supplement pages 1–179).

W. Llovel et al 2014, 'Deep-ocean contribution to sea level and energy budget not detectable over the past decade', Nature Climate Change, Vol ume 4 pp. 1031–1035. Doi 10.1038/NCLIMATE2387.

Taylor F.W. 2005, 'Elementary Climate Physics', First Edition, Oxford University Press.

Exercises.

1. Estimate the mass of the ocean. (The mean depth of the ocean is 3.8 km and it covers 71% of the surface of the Earth which has surface area 5.1 10^{14} m^2). The mean atmospheric pressure is 1.01 10^5 N/m^2 averaged over the Earth's surface. Estimate the mass of the atmosphere? By what factor is the total heat capacity of the atmosphere less than that of the ocean. (Specific heat capacities of sea water and air are 3900 and 993 J kg^{-1} K^{-1}, respectively).

2. Explain what is meant by the term Coriolis effect. A naval vessel in the Southern hemisphere at latitude 60 degrees fires a shell from a gun at a target 15 km away in a direction due North from the ship. It takes 50 seconds for the shell to reach its target. Unfortunately, the gun aimer by mistake calculates the correction for the Coriolis effect for the Northern hemisphere. Assuming that in all other respects his/her aim is perfect, calculate by how far the shell will miss its target. Why is it not necessary to correct for any Coriolis effect on the vertical component of velocity? (Neglect the effects of air resistance).
3. The 17^{th} and 18^{th} century slave trade was based on wind-driven sailing ships travelling southwards from Europe, picking up slaves in West Africa and taking them to North America. Explain how this was facilitated by the prevailing winds. Why would the Bay of Biscay and the Doldrums be looked on with disdain by the sailors of the time.
4. Figure 5.8 (red curve) shows that the average sea level rise attributable to thermal expansion from warming of the ocean at depths above 2000 metres was 10 cm between 2003 to 2014. What is the average temperature rise of the ocean above this depth? (Coefficient of volume expansion of water is $2.1\ 10^{-4}$).
5. Llovel et al 2014 found that the total energy being absorbed by the oceans is 0.72 W/m^2 (see figure 5.10). The IPCC (box 3.1 page 265 of the report by WG1 in the 5^{th} AR) report that between 1993 and 2010 the imbalance between the energy radiated from the Earth and the solar energy falling on it was 163±40 ZJ (1 ZJ=10^{21} J). The surface area of the Earth is $5.1\ 10^{14}$ m^2 and 71% of the Earth's surface is covered by ocean. Show that most of the observed energy imbalance reported by the IPCC is being stored as energy in the ocean.

6 ABSORPTION OF INFRA-RED RADIATION

In this chapter we explore the principal processes which lead to the absorption of electromagnetic radiation. We concentrate on those aspects which cause multi-atomic molecules to be strong absorbers in the infra-red region of the electromagnetic spectrum. The small traces of them in the atmosphere are therefore important for the climate. In contrast, the main constituents of the atmosphere which consist of simpler diatomic molecules such as nitrogen (N_2) and oxygen (O_2) are weak absorbers. This leads multi-atomic substances such as water vapour (H_2O), carbon dioxide (CO_2), nitrous oxides (NO_x) and methane (CH_4) to be strong greenhouse gases.

The physics underlying the absorption and emission of electromagnetic radiation is by excitation of the energy levels of the individual atoms and molecules. A description of the different classes of energy levels in atoms and molecules is therefore given. We explain how the closely spaced energy levels in molecules are broadened so that they overlap. In consequence, at atmospheric temperatures and pressures molecules exhibit band emission and absorption spectra.

The asymmetric multi-atomic molecules which make up greenhouse gases have large electric dipole moments allowing vibrational energy levels of the molecules to be excited by electromagnetic radiation. This accounts for the strong absorption in the infra-red region where the Earth thermally radiates most of its energy. In contrast, symmetric diatomic molecules of oxygen and nitrogen do not have electric dipole moments so that such levels are not excited.

6.1 ATOMIC SPECTRA

The spectrum of wavelengths emitted from excited atoms or molecules has been shown to be a series of monochromatic emissions with sharply peaked distributions of energy with wavelength. These became known as spectral lines since they appeared as sharp lines in early spectroscopes.

In the early 20th century such emission (and absorption) was shown to be due to the atoms having fixed and discrete energy levels as illustrated in figure 6.1. The explanation of such phenomena led to the development of quantum mechanics. Absorption occurs if the atom is raised to a higher energy level and emission as it relaxes back to a lower energy state. The wavelength at which absorption or emission occurs is set by the difference in the energy levels between which the transition occurs. Thus

$$h\nu = \frac{hc}{\lambda} = E_2 - E_1 \tag{6.1}$$

where h is Planck's constant, ν and λ are the frequency and wavelength of the emitted or absorbed radiation and E_2, E_1 are the two energy levels between which the transition occurs. The energies of photons emitted and absorbed by transitions between excited states in atoms are mainly in the visible and ultra-violet regions of the electromagnetic spectrum.

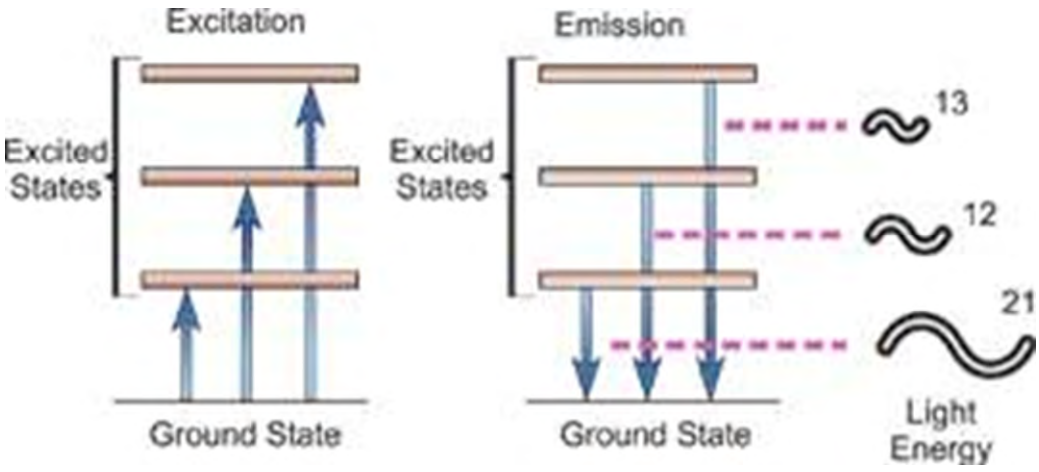

Figure 6.1 Shows the energy levels such as those in an atom. The left hand panel shows the situation where incoming radiation is absorbed by the atom raising the energy to one of its excited states. The right hand panel shows the emission of photons of radiation at energies corresponding to the differences between the energy levels. The absorption of photons (left hand panel) resonates when the incoming photons have energies corresponding to the differences between energy levels and the absorption becomes strongest in consequence.

6.2 MOLECULAR SPECTRA

In addition to the excited energy levels of the constituent atoms in molecules, there are other energy levels associated with the rotational and vibrational states of the molecules between which absorption and emission transitions can occur.

6.2.1 ROTATIONAL SPECTRA

Quantum mechanics shows that angular momentum is quantised with values $\sqrt{J(J+1)}\,h/2\pi$ where J is an integer, and h is Planck's constant. A semi-classical argument (see Appendix A6.1) shows that the difference between neighbouring rotational energy levels is

$$\Delta E = E_{J+1} - E_j = \frac{h^2}{8I}(J+1) \tag{6.2}$$

where I is the moment of inertia of the molecule.

The energies of the transitions from rotational spectra are in the far-infra red or very short wavelength radio region of the electromagnetic spectrum (see exercise 6.1). Consequently the emission and absorption of radiation by the excitation and de-excitation of rotational levels is in this part of the spectrum which has only minor relevance for climate science.

6.2.2 VIBRATIONAL ENERGY LEVELS

The atoms of a molecule are bound together by interatomic forces and they are able to vibrate about their equilibrium positions. The atoms can be pictured as bound in a potential well. We know from quantum mechanics that such bound systems lead to quantised energy levels. The energy difference between these levels leads to the absorption and emission of electromagnetic radiation energy in the infra-red region of the spectrum.

As we shall see the vibrational energy levels of greenhouse gases are in the region of the electromagnetic spectrum where the thermal radiation from the Earth is at a maximum. It is this fact which makes gases such as carbon dioxide, methane and water vapour important greenhouse gases.

However, to excite the vibrational energy levels by electromagnetic radiation the molecules must have a finite electric dipole moment. Molecules with electric dipole moments can be thought of as radio antennae. Electromagnetic radiation then stimulates the vibrational states allowing infra-red energy to be absorbed. De-excitation of excited vibrational levels leads to the emission of radiation.

Molecules of the significant greenhouse gases have large electric dipole moments. However, the molecules of the major components of the atmosphere (nitrogen, oxygen and argon) are symmetric diatomic molecules. Such symmetric systems have zero electric dipole moments as described in the next paragraph. Therefore their vibrational energy levels are not excited by electromagnetic radiation. In consequence the majority of the infra-red radiation thermally radiated by the Earth is absorbed by the greenhouse gases in the atmosphere with little absorbed by the nitrogen and oxygen molecules.

The fact that symmetric diatomic molecules such as nitrogen and oxygen have zero electric dipole moments is a result of the symmetry of electromagnetic interactions under the reversal to the time coordinate, a fundamental property of Nature. An electric dipole moment exists because one section of the molecule is electrically charged and the remaining section is charged with the opposite sign charge (with overall charge zero). If time is reversed these charges do not change sign. However, other properties of the molecule such as angular momentum change sign. As time is reversed the direction of the angular momentum changes relative to the charge distribution, implying a different kind of molecule. Hence time reversal symmetry ensures that the electric dipole moments of symmetric molecules is zero.

6.3 THE BROADENING OF SPECTRAL LINES

From equation 6.1 we might think that the emissions all occur at exactly the same frequency and wavelength. This is not the case since the energy levels in the atoms and molecules are broadened by several different effects. The main effects are the natural line width, temperature broadening by the Doppler effect if the atoms are in motion and pressure broadening caused by the proximity of other atoms in the material.

6.3.1 THE NATURAL LINE WIDTH

This effect can be understood from the Heisenberg uncertainty principle that $\Delta E\, \Delta t \sim h/2\pi$. An atom or molecule remains in an excited state for a finite time, Δt, known as the lifetime. Hence the energy level is broadened by an amount $\Delta E \sim h/(2\pi\, \Delta t)$. Such broadening of the energy levels means that the emitted or absorbed radiation has a distribution which is approximately Gaussian with width $\Delta\lambda$ i.e. the spectral line is not exactly monochromatic.

6.3.2 TEMPERATURE BROADENING

As the temperature of a gas changes the speed of the molecules changes since their kinetic energy is temperature dependent. Classically the kinetic energy, E, of an atom of mass m moving with mean speed at temperature T is given by

$$E = \frac{1}{2} m\, \bar{v}^2 = \frac{3}{2}\, kT \tag{6.3}$$

where k is Boltzmann's constant (Lue 2009).

If the atom moves towards the observer the frequency of an emitted spectral line increases and if away the frequency decreases due to the Doppler effect. It can be seen therefore that the random movement of the atoms in the gas causes a broadening of the spectral line. The frequency distribution of the spectral line is Gaussian with a standard deviation, Δf, due to this effect about the most probable value, f_0, which is given by

$$\frac{\Delta f}{f_0} = \sqrt{\frac{kT}{mc^2}} \tag{6.4}$$

where f_0 is the frequency at rest and c is the speed of light. This equation is derived below in Appendix A 6.2.

6.3.3 PRESSURE BROADENING OF SPECTRAL LINES.

From the point of view of climate science this is the most significant cause of spectral line broadening. As the pressure in a gas increases the collision frequency with other molecules increases and the proximity to other molecules decreases. A collision by an excited molecule with another molecule can stimulate it to de-excite, thus decreasing its lifetime in the excited state. By the Heisenberg uncertainty principle this causes a broadening of the energy level. Furthermore and more importantly, the decreasing mean distance between molecules as the pressure increases allows the electromagnetic fields of molecules to influence each other, causing shifts of the excitation energy levels. Both these effects lead to a broadening of the individual spectral lines.

The vibrational energy levels of molecules are numerous and closely spaced. The broadening described above increases roughly linearly with pressure. This means that at high enough pressure and temperature the spectral lines from transitions between them merge together and the absorption spectra appear as bands. This is shown in figure 2.8 (chapter 2) where the absorption in the atmosphere of electromagnetic radiation occurs in broad bands of wavelength and the individual vibrational lines are not resolved.

The effects are complicated and are usually modelled using a mixture of experimentally and theoretically derived parameters in such software packages as HITRAN and MODTRAN (Rothman et al 2012).

6.4 ABSORPTION OF RADIATION

6.4.1 THE BEER LAMBERT LAW

This law applies to the absorption of radiation which is destroyed as it passes through the material, for example x-rays. The x-ray photons are converted into electrons in the material by either the photo-electric effect or by Compton scattering and so are destroyed. If an x-ray beam passes through a slab of absorber of thickness dx the number of photons converted to electrons, *dR*, is proportional to the number of photons, R, in the beam passing through the slab and the thickness of the slab *dx* i.e.

$$dR = -kRdx \tag{6.5}$$

where k is the constant of proportionality and the negative sign indicates a decrease in the number of photons. Integrating on both sides

$$\int_{R_0}^{R} \frac{dR}{R} = \int_{0}^{x} -kdx \tag{6.6}$$

i.e. $$R = R_0 e^{-kx} \tag{6.7}$$

where R_0 is the initial intensity i.e. number of photons in the beam and R is the intensity at depth x in the slab. The quantity k is known as the absorption coefficient. This is the Beer-Lambert Law. It describes the familiar situation of an exponential change when a quantity changes by a fraction of itself e.g. as in the decay of radioactive isotopes.

The fraction of photons (i.e. the probability) reaching depth x is $\frac{R}{R_0} = e^{-kx}$. Hence the average depth of penetration by the photon beam is given by

$$\lambda = \int_0^\infty x e^{-kx}\, dx = \frac{1}{k} \qquad (6.8).$$

The quantity λ is known as the mean free path of the x-rays in the material and k is known as the absorption coefficient. The quantity λ is related to the cross section per interaction of a scattering centre (e.g. an atom) in the material, σ, by

$$\lambda = \frac{1}{n\sigma} \qquad (6.9)$$

where n is the number of scattering centres (e.g. atoms) per unit volume in the material.

6.4.2 ABSORBANCE AND TRANSMITTANCE AND OPTICAL THICKNESS

The transmittance of the slab of material is defined to be the fraction of the radiation which passes through the slab and is given by $T = e^{-\frac{x}{\lambda}}$ and the absorbance of the material is $1 - T$.

A material is said to be optically thin if the absorbance is small i.e. the transmittance is large. Conversely it is said to be optically thick if the absorbance is large and the transmittance is small.

6.4.3 ABSORPTION OF INFRA-RED RADIATION IN THE ATMOSPHERE

Consider infra-red radiation passing through a slab of atmosphere. Absorption takes place by the excitation of molecular energy levels. However, the slab will heat up as a result of this absorption of energy. This will result in the thermal emission of infra-red radiation from the slab which adds to the passing radiation. Hence the simple Beer-Lambert law must be modified to account for this extra energy release. An extra term is added to equation 6.5 to allow for the radiation from the slab. Equation 6.5 then becomes

$$dR = -kRdx + B(T)dx \qquad (6.10)$$

where *B(T)* represents the thermally radiated energy from the slab which has been heated to temperature *T*. This is related to the Planck formula described in chapter 2. Equation 6.10 is known as the radiative transfer equation.

Equation 6.10 is not readily solvable and a number of mathematical techniques using different assumptions and approximations have been employed to provide a solution to it (for a review see Kratz and Cess 1985). Figure 6.2 shows a comparison of three of the solutions known as models for the absorbance of water vapour as a function of concentration in air.

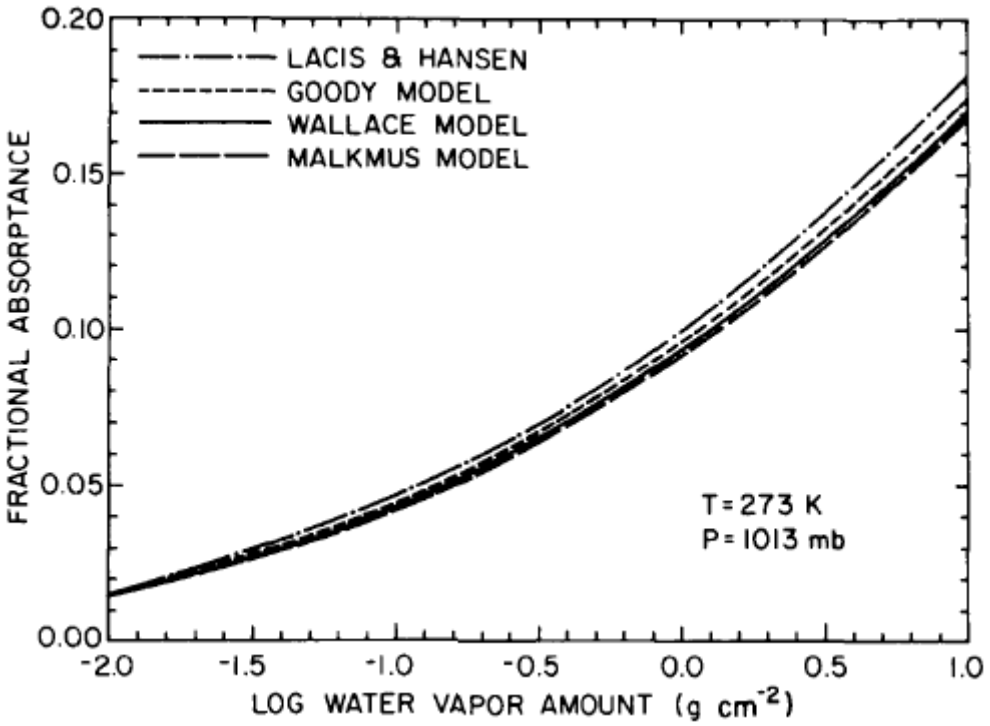

Figure 6.2 The absorbance of water vapour as a function of its concentration in the air as predicted from the solutions of the radiative transfer equation from Goody, Wallace and Malkmus. The Lacis and Hansen curve represents a parameterisation of some earlier work (see Kratz and Cess (1985) for the details.

Here the solution from the random band model of Goody is adopted to solve equation 6.10 (Goody and Yung 1985). This shows that the solution to equation 6.10 for the transmittance *T* of the slab of atmosphere of thickness *x* is given by

$$T = e^{-\frac{Sx}{\delta}(1+\frac{Sx}{\pi\alpha})^{-1/2}} \tag{6.11}$$

where the δ is the spacing between vibration lines of the molecular spectra, α is the width of each line and S is a constant known as the line strength. Care must be taken with the units in equation 6.11 which are usually expressed as follows. The thickness x is that of the air at a pressure of 1 atmosphere, the line spacing δ and line width α should be expressed as wave number i.e. the reciprocal of the wavelength. In the c.g.s. system of units x is in cm thickness at 1 atmosphere pressure, α and δ in cm^{-1} and S then has units $atmosphere^{-1}\ cm^{-2}$.

Note that for thin slabs when x is small, so that $\frac{Sx}{\pi\alpha} \ll 1$, equation 6.11 reduces to the Beer-Lambert formula in equation 6.7 with $k = S/\delta$. In contrast for thick slabs of atmosphere when $\frac{Sx}{\pi\alpha} \gg 1$ equation 6.11 approximates to

$$T = e^{-\frac{(S\pi\alpha x)^{1/2}}{\delta}} \qquad (6.12).$$

The thick slab formula in equation 6.12 is used in the next chapter, allowing for the variation with pressure of the line width α.

6.5 THE ABSORBANCE OF THE ATMOSPHERE

The total absorbance of the atmosphere as a function of the wavelength of the radiation is shown in figure 2.8 (see Chapter 2) for the greenhouse gases water vapour, carbon dioxide and ozone. The figure also shows the regions of the spectrum at which solar radiation falls on the Earth (mainly visible) and radiation emitted by the Earth (mainly infra-red). It can be seen that the atmosphere is almost opaque (100% absorbance) at infra-red wavelengths apart from the narrow band between wavelengths 8–12 μm which allows some transmission of energy from the surface to outer space.

6.6 CONCLUSIONS

In this chapter we have discussed the molecular science which makes the more complicated molecules such as carbon dioxide act as greenhouse gases. Strong absorption of infra-red radiation by such gases is demonstrated and the absorption is quantified. Equation 6.12 will be used in the next chapter to illustrate the first order process which explains why increasing greenhouse gas concentrations result in global warming.

APPENDIX A6.1 SEMI-CLASSICAL ARGUMENT TO JUSTIFY EQUATION 6.2

Classically, the kinetic energy of a rotating body is

$$\frac{1}{2}I\omega^2 = \frac{(I\omega)^2}{2I}.$$

Setting the classical angular momentum of the body to be equal to its quantised equivalent gives

$$I\omega = \sqrt{J(J+1)}h/2\pi$$

Where J is an integer. Hence the energy associated (E_J) with the rotation is given by

$$E_J = \frac{h^2}{8\pi^2 I}J(J+1) \qquad \text{A6.1}$$

Hence a transition from the energy level E_J to the level E_{J-1} will involve the emission of a quantum of energy $E_J - E_{J-1}$. Subtracting the two values in equation A6.1 gives the energy of the quantum emitted as in equation 6.2.

APPENDIX A6.2 DOPPLER BROADENING OF SPECTRAL LINES – PROOF OF EQUATION 6.4

Define the z axis as the axis from the gas sample to the observer. The observer viewing an atom moving with velocity component v_s along the z axis will observe a frequency, f, from an atom emitting at frequency f_0 given by

$$f = f_0(1 + \frac{v_z}{c})$$

due to the Doppler effect. From this we see that frequency and velocity are related by

$$v_z = c(f - f_0)/f_0 \text{ and } dv_z/df = c/f_0 \qquad \text{A.6.2}$$

Now the probability of the atom having velocity components v_x, v_y, v_zfollows the Maxwell Boltzmann distribution

$$P(v_x, v_y, v_z) = (\frac{m}{2kT})^{3/2} e^{-m(v_x^2+v_y^2+v_z^2)/2kT} dv_x dv_y dv_z \qquad \text{A6.3.}$$

Now only the z component contributes to the Doppler shift of the line. Integrating over v_x and v_y gives, (noting that these variables are Gaussians which integrate to unity)

$$P(v_z)dv_z = (\frac{m}{2kT})^{1/2} e^{-mv_z^2} dv_z \qquad \text{A6.4.}$$

$$\text{Now } P_f(f)df = P(v_z)\frac{dv_z}{df}\, df = (\frac{m}{2kT})^{1/2} e^{-\frac{mc^2}{2kT}(\frac{f-f_0}{f_0})^2} \frac{c}{f_0} df$$

This can be seen to be a Gaussian distribution in frequency with standard deviatio

$$\frac{\sigma}{f_0} = \frac{\Delta f}{f_0} = (\frac{kT}{mc^2})^{1/2}$$

as in equation 6.4.

References

Goody R.M. and Yung M. 1989, Atmospheric Radiation, Oxford University Press.

Lue L 2009 "Chemical Thermodynamics" published by Bookboon, ISBN 978-87-7681-497-7.

Kratz D.P. and Cess R.D. 1985, "Solar absorption by atmospheric water vapour: a comparison of radiation models", Tellus 37B pp. 53–63.

Peixoto J.P. and Oort A.H. 1992, "Physics of climate", American Institute of Physics, New York.

Rothman L.S. et al., 2012 "The HITRAN2012 molecular spectroscopic database", Journal of Quantitative Spectroscopiy and Radiative Trnasfer", Volume 130 (HITRAN2012 Special Issue) pp. 4–50.

Exercises

1. The oxygen molecule is shaped like a dumbbell with two oxygen atoms of mass 2.7 10^{-27} kg separated by a distance of 1.5 10^{-10} m. Assuming that the atoms are point masses show that a molecule excited to the second energy level would de-excite by emitting a photon of wavelength of order 2.7 mm, i.e. in the far infra-red region of the spectrum or short radio waves. Discuss the accuracy of this estimate.
2. Hydrogen atoms are raised into excited states in a hydrogen discharge tube. The wavelengths of the emitted spectral lines are found to follow the simple relation

$$\frac{1}{\lambda} = R_H\left(\frac{1}{n^2} - \frac{1}{m^2}\right)$$

λ with R_H = 1.097 107 m^{-1} and n and m integers. Calculate the wavelength of the lowest line with n=2. The lifetime in this excited state is found to be 10^{-8} seconds. Estimate the natural line width of the emitted spectra from this excited state.

3. If the temperature of the gas in problem 2 is 1000K compute the width of the spectral line due to temperature broadening.
4. What precautions would you take if you wish to measure the natural line width of a spectral line?
5. Why are the principal components of the atmosphere (oxygen and nitrogen) not strong absorbers of near infra-red radiation? Explain why carbon dioxide and water vapour absorb strongly in the region of the spectrum and so are greenhouse gases. Other trace gases in the atmosphere are the noble gas argon (Ar) and freon ($CC_{l2}F_2$) from some spray cans. Would you expect these to contribute to the greenhouse effect?
6. An apparatus is set up to measure the absorption of infra-red radiation from a broad band source in carbon dioxide at low pressure. A wavelength filter is used to measure the absorption due to the individual vibration lines. Each line is found to absorb a fraction f per centimetre of air equivalent at atmospheric pressure of the radiation from the source. A total of n absorption lines are observed to contribute to the absorption in the gas. Show that the line strength S (defined in equation 6.13) is given by $S = nf\delta$ where δ is the line spacing.

7 CLIMATE MODELS

7.1 INTRODUCTION

The climate is a multiple variable entity. In order to model it successfully all aspects of it must be understood. This is what the experts attempt to do in their models of the climate.

In this chapter we will describe the simple model alluded to in Chapter 1 which ignores all complexity in order to understand the physical basis underlying the reasons why increasing greenhouse gas levels cause warming of the planet. We will then go on to discuss briefly the more complicated models which are necessary for a more complete understanding of the Earth's climate.

7.2 WARMING OF THE EARTH'S SURFACE BY GREENHOUSE GASES.

We have seen in previous chapters that the Sun radiates electromagnetic energy, some of which is absorbed by the Earth. In consequence the Earth warms and radiates thermal energy itself. At the temperature at the surface of Earth this is mainly in the infra-red region of the spectrum. By the law of conservation of energy the Earth's temperature reaches an equilibrium value when the energy falling on it balances that radiated away.

The total solar energy falling on the surface of the Earth is $E_{in} = \pi R^2 S(1-A)$ where A~0.3 is the albedo fraction i.e. the fraction of the energy reflected from the Earth, mainly by clouds, R is the radius of the Earth and S=1366 W/m^2 is the solar constant. The latter is defined as the energy from the Sun falling on a plane of unit area in the sphere containing the Earth's orbit. The average solar energy falling on the Earth's surface is E_{in} divided by the area of the surface of the Earth, $4\pi R^2$. Hence, the mean solar energy falling on unit area of the Earth is given by $S(1-A)/4$.

In equilibrium the Earth must radiate away the same amount of energy as that which falls on it by the Law of Conservation of Energy (first law of thermodynamics). The Earth will warm to a temperature at which the heat radiated by thermal radiation is the same as that falling on it from the Sun. This temperature is known as the effective radiation temperature of the Earth, T_E. If the Earth were a perfect black body then this heat radiated per unit area would be σT_E^4, by Stefan's Law (see Chapter 2) so that the equilibrium condition would be

$$\frac{S(1-A)}{4} = \sigma T_E^4. \qquad (7.1)$$

From this we see that T_E = 255K (Stefan's constant = 5.7 10^{-8} W m^{-2} K^{-4}). This is known as the effective radiation temperature.

We saw in Chapter 6 that the atmosphere is a strong absorber in the infra-red region of the spectrum because of the greenhouse gases it contains. Hence by Kirchoff's Law it will be a strong emitter i.e. the atmosphere will act almost as a black body. As a result the Earth will radiate to space at an altitude where the pressure is low enough for the radiation not to be absorbed. At this altitude the temperature will be close to the value of T_E = 255K required to maintain energy balance.

Consider the hypothetical case of the Earth with an atmosphere which did not contain greenhouse gases. The atmosphere would be unable to absorb the infra-red radiation emitted from the surface. The surface temperature would be a little above T_E = 255K (-18°C). The finite emissivities of the materials at the surface of the Earth cause a small increase above 255K. In the most part these are high (i.e. > 0.9 e.g. water which covers 71% of the surface area of the planet has emissivity from 0.95–0.99). Hence the surface temperature would be a few degrees above T_E. It is clear that at such low temperatures liquid water on the Earth would freeze and the planet would be uninhabitable by life as we know it. This is even true if water vapour is allowed to be present in the atmosphere since carbon dioxide is the main absorber at higher altitudes where the water vapour is frozen out.

The presence of some carbon dioxide in the atmosphere allows the infra-red radiation to be absorbed so that the atmosphere acts like a blanket around the Earth which warms the surface to a level at which life can exist. We shall see that adding more carbon dioxide "thickens" the blanket and causes increased warming.

The warming effect of the greenhouse gases in the atmosphere can be understood as follows. The main constituents of the atmosphere, nitrogen and oxygen which consist of symmetric diatomic molecules, do not absorb electromagnetic energy in the infra-red region of the spectrum. However, infra-red radiation excites the vibrational states in the molecules of the greenhouse gases (carbon dioxide, methane and water vapour) so that they strongly absorb infra-red radiation (see Chapter 6). The infra-red energy absorbed by them allows the atmosphere to warm and in consequence radiate thermally in all directions. Some of this energy comes back to the surface of the Earth, causing warming there.

7.3 THE EFFECT OF INCREASING CARBON DIOXIDE LEVELS – A SIMPLE PICTURE

Since industrialisation the greenhouse gas concentrations in the atmosphere have increased markedly as shown in figure 7.1. The increase in carbon dioxide has been shown to be from the burning of fossil fuels from the isotope admixtures.

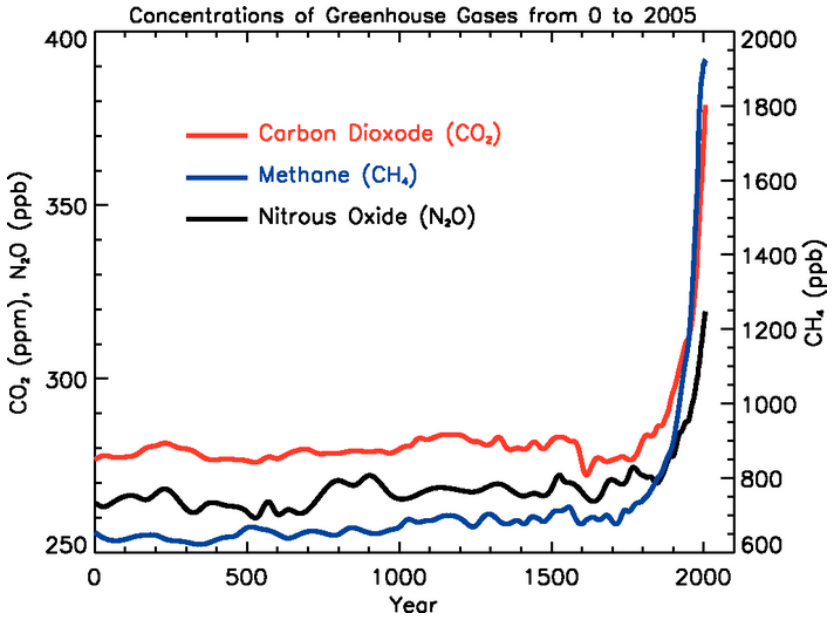

Figure 7.1 The variation of the greenhouse gas concentrations in the atmosphere over the last 2000 years in ppm for CO2 and parts per billion (ppb) for methane and nitrous oxides. The increase since industrialisation in the 19th century can be clearly seen (IPCC AR4 2007).

The atmosphere near the Earth's surface is strongly absorbent of the infra-red radiation radiated from the Earth's surface due to the presence of greenhouse gases and so it is warmed. As we saw in Chapter 3, at this level convection dominates the energy transfer from the Earth's surface to the upper atmosphere and the thermodynamics of the atmosphere cause the temperature to decrease almost linearly with altitude at the lapse rate, $dT/dz \sim 6$ K per km. The pressure decreases with altitude and in consequence the absorptivity for infra-red radiation decreases. At a high enough altitude the atmosphere becomes thin enough for the infra-red radiation heading away from the Earth's surface to escape into space without further absorption in the atmosphere above it. At such an altitude, to maintain thermal equilibrium, the temperature reaches the effective radiation temperature, T_E, so that energy balance is maintained. This is illustrated in figure 7.2 (left hand panel).

Greenhouse gases mix well in the air so that they diffuse quickly through the whole atmosphere. As greenhouse gas concentrations increase the altitude at which radiation can escape to space increases (see right hand panel of figure 7.2). This occurs when the air thickness between the layer and space is of order one mean free path, τ, of an infra-red photon, i.e. $\tau \sim 1$. Since the lapse rate is fixed by thermodynamics, if the altitude at which radiation to space increases, then the surface temperature must increase by simple geometry as illustrated in figure 7.3.

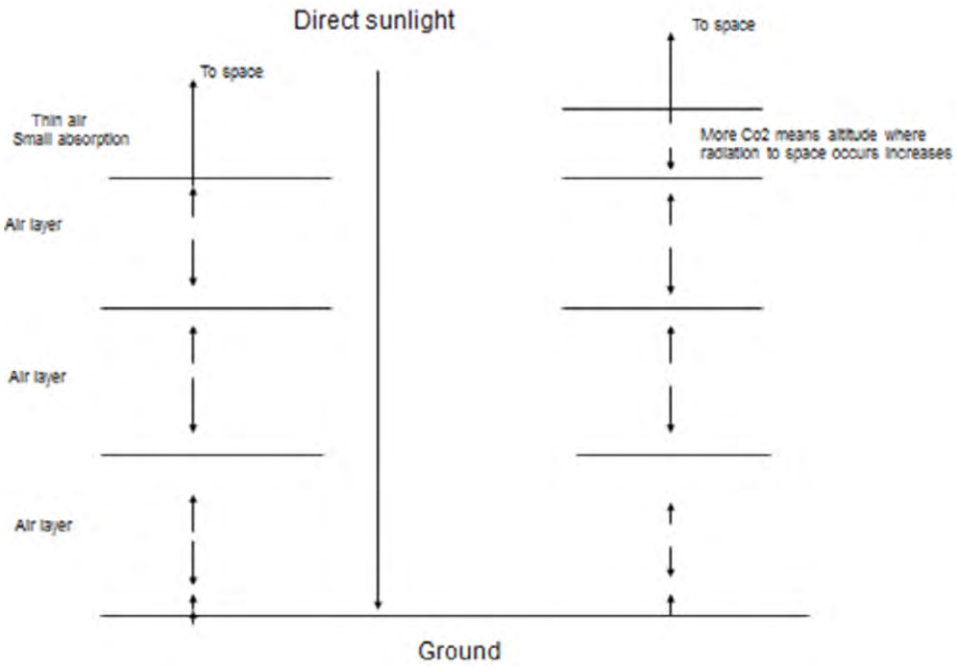

Figure 7.2 Left hand diagram shows the Earth's atmosphere divided into layers. The direct sunlight passes through the atmosphere to the Earth's surface and is almost unabsorbed since it is mainly in the visible region of the spectrum. The Earth's surface warms and thermally emits infra-red radiation which is then absorbed in an air layer, warming it. This layer radiates energy, some down and some up. The downward radiation warms the surface and the upward warms the layer above it. The next layer similarly warms, emitting radiation both up and down, some of which can warm the layer above and some the surface. This process occurs through successive layers until the air becomes thin so that the upward radiation is no longer absorbed but escapes to space. The right hand diagram shows what happens when the green-house gas concentration increases. In this case the atmosphere absorbs and reradiates infra-red energy up to higher altitudes. The fixed lapse rate then shows that the temperature at the Earth's surface must increase, as illustrated in fig. 7.3.

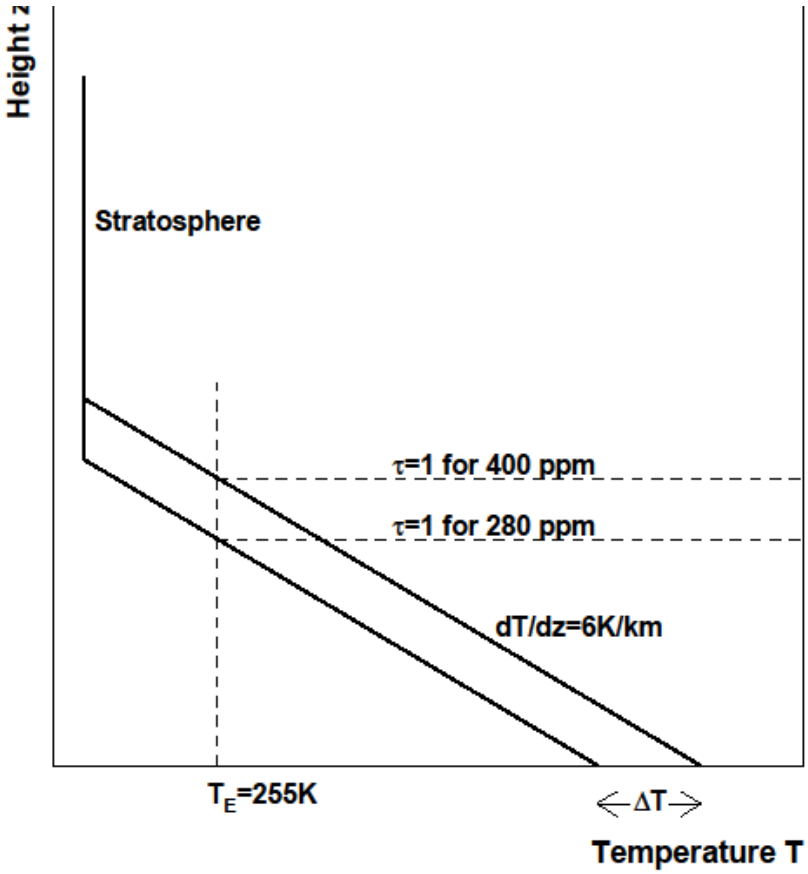

Figure 7.3 Shows the geometrical argument leading to warming at the surface as the height in the atmosphere at which radiation to space occurs (taken as $\tau = 1$). As this height increases due to the increasing greenhouse gas concentration from 280 ppm to 400 ppm the slanting line moves to the right since the slope (lapse rate, see Chapter 3) is fixed by thermodynamics i.e. the surface temperature increases by an amount ΔT.

Quantifying this picture and making several assumptions It is shown in Appendix A7 that as the greenhouse gas concentration increases from a_1 to a_2 the temperature increases by an amount

$$\Delta T = \frac{HL}{2} \ln\left(\frac{a_2}{a_1}\right) \tag{7.2}$$

Where H is the scale height of the atmosphere (approximately 6 km in the troposphere) and L is the lapse rate (approximately 6K/km in the troposphere).

Figure 7.4 shows a comparison of the temperature rise predicted by equation 7.2 compared to the measurements of the average global temperature (GISS 2014). Here we have taken the variation of carbon dioxide concentration with time from figure 7.1. The simple picture clearly overestimates the measurements. The discrepancy is discussed further below.

Conventionally, the climate sensitivity to carbon dioxide is defined as the increase in average global surface temperature when the carbon dioxide level doubles. The climate sensitivity predicted by equation 7.2 for $\frac{a_2}{a_1} = 2$ is 12.4 degrees. As we shall see below more complete models, which agree well with the measurements, predict a climate sensitivity of from 1.5 to 4.5 degrees (IPCC 2013), which is considerably less than that from equation 7.2. Again the discrepancy between the predictions of the simple picture and reality shows up.

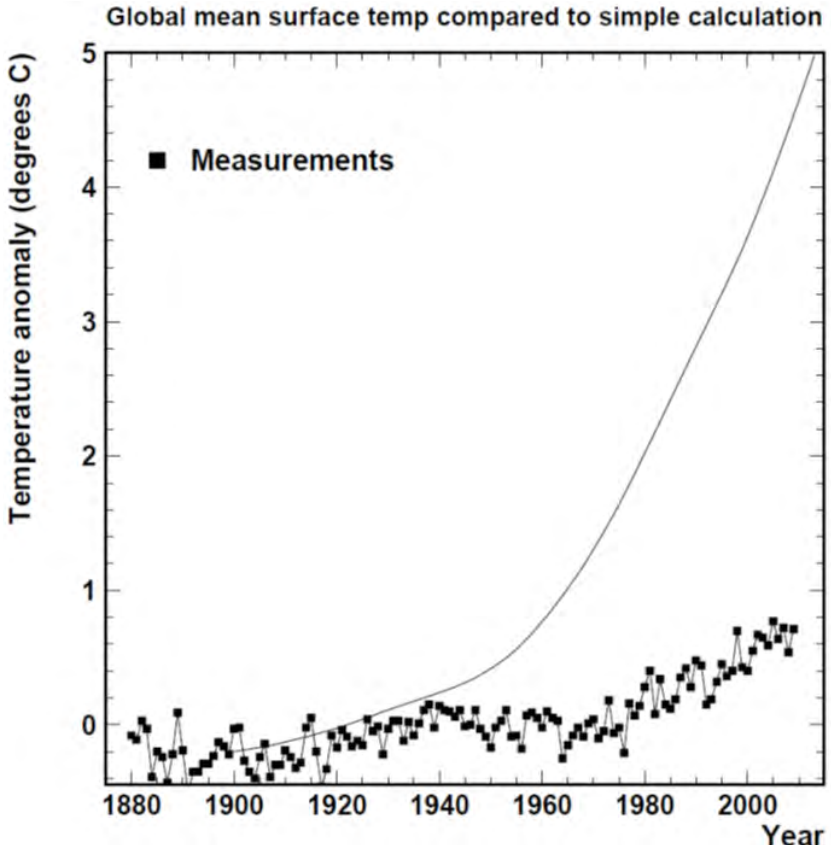

Figure 7.4 Comparison of the prediction of the simple model given in equation 7.2 (solid smooth curve) with the measured average global temperature rise (temperature data from GISS, Hansen et al 2010).

There are many approximations made in deriving the simple formula in equation 7.2 and this will explain some of the discrepancy. However, the major part of the discrepancy with measurements (and the more complete models) can be understood from the fact that the climate is very complicated. Many more effects are present in the real climate than those represented by the simple picture described above. All of these effects are ignored in deriving the results of the simple picture. However, the simple model described gives a pictorial representation of the lowest order process of global warming produced by the effect of increasing greenhouse gases such as carbon dioxide.

The simple picture also assumes an equilibrium situation with the energy falling on the Earth equal to that radiated away. This is not the case. The increasing greenhouse gas concentrations have disturbed the equilibrium so that there is more energy falling on the Earth than radiated away. The excess energy is absorbed in the upper 2000m depth of the ocean as measured by Llovel et al 2014. This is equal to the energy imbalance from satellite observations as reported in the IPPC 5th Assessment Report (IPCC1 2013) to within the 20% uncertainty on the measurement (see Chapter 5, exercise 5).

7.4 MORE COMPLETE MODELS OF THE CLIMATE

Models of the climate exist which attempt to simulate all its known features. They include the circulations in both the oceans and the atmosphere and so they are called General Circulation Models (GCMs). There are many in existence. They must also simulate the absorption of heat as well as the uptake of CO_2 in both the land and the oceans. The latter cause delaying effects due to the inertia in the system. They also include simulations of both the carbon and water cycles of the Earth.

In addition feedback mechanisms must be simulated. A negative feedback mechanism is a process in which the heating of the Earth induces a mechanism which causes cooling of the atmosphere. An example of a negative feedback comes from clouds. As the Earth's surface warms more water vapour evaporates into the atmosphere which causes more low clouds to form. This increases the Earth's albedo which reduces the heat uptake of the Earth, producing a cooling effect. A positive feedback is the opposite i.e. warming produces further warming. An example of a positive feedback mechanism is the replacement of melting of ice and snow as the Earth warms by either sand or water. Ice and snow are quite reflective of solar radiation but if they are replaced by sand or water, which are less reflective, more solar energy is absorbed by the Earth i.e. the warming causes further warming. This is a positive feedback mechanism.

GCMs attempt to model all known aspects of the climate including feedbacks and the effects of water vapour in order to try to understand the observations. These are often built upon computer programs which were originally designed for weather forecasting.

Figure 7.5 shows the results of the models compared to the measurements (thick black line). The upper panel includes all known forcings (including anthropogenic, i.e. man-made forcings). It can be seen that the models agree well with the measured temperatures. However, if anthropogenic forcings are excluded as in the lower panel the models disagree with the measurements.

The simple model described in section 7.5 illustrates the dynamic processes at work which explain why increasing greenhouse gas concentrations are expected to lead to global warming. The fact that the more complete models agree with the measurements is strong evidence that mankind is affecting the mean global surface temperature by producing increasing quantities of greenhouse gases.

7.5 RADIATIVE FORCING (RF)

The simple model described in sections 7.3 and 7.4 assumes the Earth's climate is in equilibrium in which the total energy flux falling on the Earth is the same as that radiated from it. However, when perturbations (or climate drivers as they are sometimes called) take place it takes time to achieve equilibrium. During this time the energy falling on Earth will be different from that radiated. The net energy flux (downward minus upward) is known as the radiative forcing. This is a concept developed by climatologists to quantify the effects of different climate perturbations. As such perturbations represent out of equilibrium situations they are difficult to compute except within the framework of climate models (GCMs). The usefulness of the concept arises because the warming effect of any perturbation, ΔT, is found to be proportional to the RF, ΔF, i.e.

$$\Delta T = \lambda \Delta F \tag{7.9}$$

where the constant λ is known as the climate sensitivity parameter which must be determined by a GCM. It is a number which varies between 0.3 and 1 K W^{-1} m^2 and is determined from the models. It can be defined for any level in the atmosphere. However, it is defined by the IPCC (IPCC 2013) as the change in net downward flux of energy (shortwave plus long wave in Wm^{-2}) at the tropopause or top of the atmosphere due to a change in the climate perturbation after allowing stratospheric temperatures to readjust to radiative equilibrium, while holding all other state variables (such as tropospheric temperatures, water vapour and cloud cover) fixed at the unperturbed levels. The perturbation is defined by the IPCC (IPCC 2013) as the difference between the condition in the year 1750 and that at the time considered. The forcings must be calculated within the framework of the climate models.

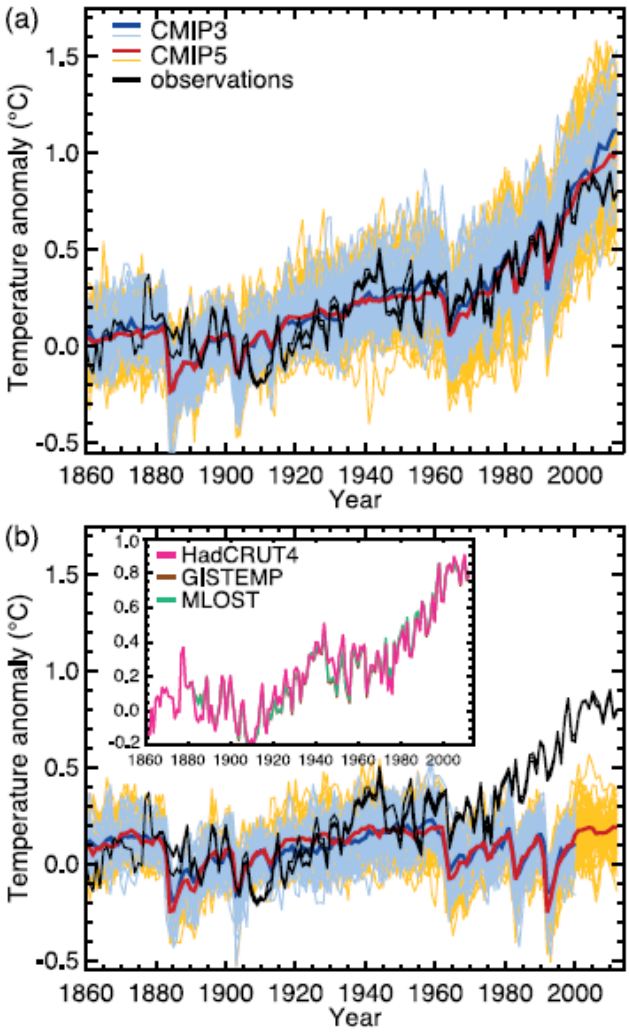

Figure 7.5 The results of the several runs of various models are overlayed and compared with the measurements (black curve). The yellow and blue bands show many runs of the models overlayed. CMIP3 and CMIP5 apply to the models at different assumptions on future greenhouse gas emissions. The red and blue curves show the averages of each set of models. The spread gives a measure of the uncertainty. The upper panel (a) includes anthropogenic and all known natural forcings. The lower panel (b) contains models with only natural forcings. The sharp dips correspond to known large volcanic eruptions. The inset in the lower panel shows a comparison of the different temperature measurements. (IPCC2 AR5).

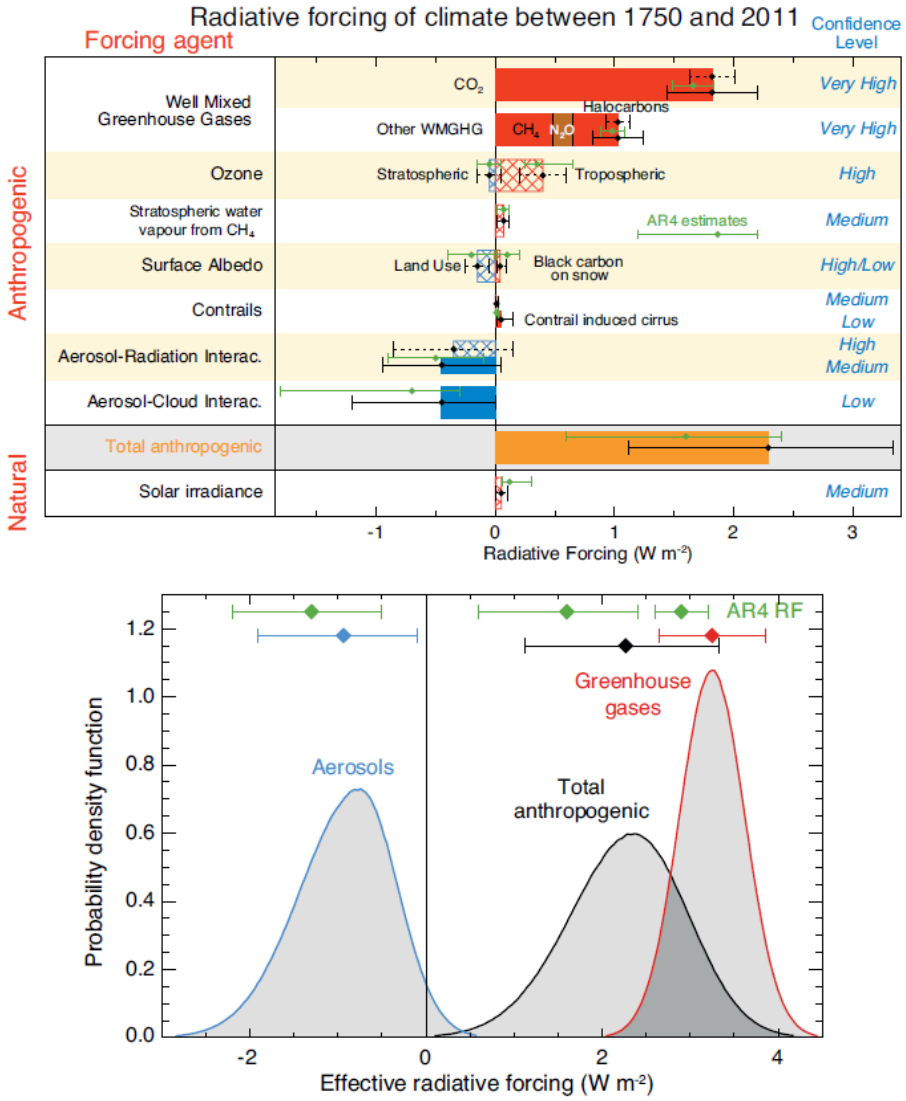

Figure 7.6 (Upper panel)The calculated radiative forcing from the various anthropogenic perturbations of the climate (IPCC3 2013). All other effects which result from these perturbations (e.g. water vapour) are computed as feedbacks from these drivers. (Lower panel) the probability distribution functions for the two major perturbations (greenhouse gases, red curve and aerosols, blue curve). The black curve gives the probability distribution function for all effects. The horizontal bars show the 90% confidence interval of the quantity i.e. its uncertainty.

Figure 7.6 shows the state of knowledge of the different anthropogenic radiative forcings for each process considered. The horizontal bars show the uncertainties (90% confidence interval). A similar figure to this one was shown in the 4th Assessment Report by the IPCC. Some of the measured value have changed slightly (not by more than the quoted uncertainty) and the uncertainties have decreased. Hence the conclusion that the 20th century global warming is man-made became significantly stronger between AR4 and AR5.

The most probable RF (RF at the peak) is 2.4 W/m^2. This represents the best estimate of the true RF which produces the observed warming. Integrating the probability distribution function in figure 7.6 from zero to 1.2 W/m^2 gives the probability for the anthropogenic forcing to be less than half the most probable or best estimated value. This probability is 5%. The IPCC conclude, therefore, that the probability for more than half the RF to be natural is 5% i.e. it is extremely likely that the 20th century global warming is man-made.

7.6 CONCLUSIONS

The lowest order process which causes increasing greenhouse gases to warm the Earth is the rising altitude due to this increase at which radiation of infra-red radiation to space takes place. Applying geometry to this picture predicts about a factor 4 more warming than observed. This permits a relatively simple explanation of the warming without the need for complicated climate models although of course simplified and inaccurate as a result. This explanation gives a physical reason which explains why increasing concentrations of greenhouse gases lead to global warming. To understand fully the observed warming all the other processes which are ignored in deriving this simple picture must be included in the climate models. Such models reproduce the observed warming well giving extremely strong evidence that the observed global warming in the 20th century is anthropogenic (man-made).

The probability that more than half the warming could come from natural sources is of order 5% allowing the IPCC to conclude that it is extremely likely (more than 95% probable) that the warming observed in the 20th century is produced by man-made greenhouse gases from the burning of fossil fuels.

APPENDIX A7 DERIVATION OF EQUATION 7.2

We saw in Chapter 6 that the transmittance of a thickness x of air is

$$T = \exp(-\frac{sx}{\delta}\left(1+\frac{sx}{\pi\alpha}\right)^{\frac{1}{2}}) = \exp(-\tau) \tag{7.3}$$

where $\tau = \frac{sx}{\delta}(1+\frac{sx}{\pi\alpha})^{1/2}$ which in the case of strong absorption $(\frac{sx}{\pi\alpha} \gg 1)$ approximates to $\tau \cong \frac{1}{\delta}(sx\pi\alpha)^{1/2}$ (see equation 6.12, Section 6.4.3). Here we have used the random band model with the line strength s (in units m^{-2} at a pressure of 1 atmosphere), x is the thickness of air traversed at a pressure of 1 atmosphere (i.e. in units m), δ is the line spacing in terms of wave number (i.e. in units m^{-1}) and α is the line width in terms of wave number (units m^{-1}).

The approximation is made that radiation to space begins at an altitude where the value of τ is of order unity i.e. of order unit mean free path for an infra-red photon to escape to space.

Suppose that at a particular time when the concentration of carbon dioxide is a_1 the thickness of atmosphere at which $\tau \sim 1$ is x_1. At the altitude at which this is the thickness of air to outer space, the line width will be a_1 (note that the line width is pressure dependent due to pressure broadening of the vibration lines). Suppose the concentration of carbon dioxide increases to a_2 so that the altitude at which $\tau \sim 1$ increases and the thickness of air to outer space becomes x_2. At the increased altitude the air pressure will decrease to a value at which the line width becomes α_2. To make $\tau = 1$ at each altitude

$$a_1 x_1 \alpha_1 = a_2 x_2 \alpha_2 \tag{7.4}.$$

The mass of a column of air of thickness x at 1 atmosphere pressure above an area dS is $\rho_A x\, dS$ where ρ_A is the density of air at 1 atmosphere pressure. However, the real atmosphere has variable density with altitude (see Chapter 2) so that the mass of air above an altitude is $\int_z^\infty \rho(z)dzdS$. The mass of real atmosphere above altitude z and that adjusted to a pressure of 1 atmosphere are the same so that

$$\rho_A x dS = \int_z^\infty \rho(z)dz\, dS \tag{7.5}.$$

We now make the following approximations.

1. The air behaves as an ideal gas so that for a mass m of air occupying volume V at pressure P and temperature T, $PV = \frac{m}{M}RT$ so that the density $\rho = \frac{m}{V} = \frac{MP}{RT}$, where M is the molar mass of air and R is the universal gas constant per mole.
2. The atmospheric pressure decreases exponentially with altitude, z, so that $P = P_0 e^{-z/H}$ where H is the scale height which is approximately 6 km (see Chapter 3). Here we are making the further approximation that the scale height is independent of altitude (see Chapter 3).
3. That the line width varies linearly with pressure, P, i.e. $\alpha = kP = kP_0 e^{-z/H}$ with k a constant.
4. We neglect the variation in temperature(in degrees K) with altitude.
5. We assume that absorption of infra-red radiation is complete up to the altitude at which $\tau = 1$and it is zero at altitudes above this. In practice there will be a more gradual change in the absorption.
6. The wavelength dependence of the absorption height is ignored.
7. We assume a constant lapse rate over the whole Earth.

With these approximations and cancelling the factors dS equation 7.5 becomes

$$\text{i.e.} \quad \begin{aligned} \rho_A x &= \int_z^\infty \frac{MP_0}{RT} e^{-z/H}\, dz \\ x &= \frac{MP_0 H}{\rho_A RT} e^{-z/H} \end{aligned} \tag{7.6}$$

where z is the altitude at which x is the thickness of air at 1 atmosphere pressure at which radiation to space begins $(\tau = 1)$. Adding subscripts 1 and 2 for situations with atmospheric concentrations a_1 and a_2 of carbon dioxide for which τ is unity in each case, equation 7.3 becomes

$$a_2 e^{-2z_2/H} = a_1 e^{-2z_1/H} \tag{7.7}.$$

Here various factors have cancelled. From this it follows that the change in altitude at which radiation to space begins when the concentration of carbon dioxide increases from a_1 to a_2 is given by

$$z_2 - z_1 = \Delta z = \frac{H}{2} \ln\left(\frac{a_2}{a_1}\right) \tag{7.8}.$$

The lapse rate $L = \frac{dT}{dz}$ is roughly constant at 6K per km (see Chapter 3) so that we can derive the change in temperature with concentration to be that given in equation 7.2 i.e.

$$\Delta T = L\,(z_2 - z_1) = \frac{HL}{2}\ln\left(\frac{a_2}{a_1}\right).$$

References

Hansen J., Ruedy R., Sato M. and Lo K. 2010 "Global surface temperature change" Reviews of Geophysics 48, RG4004, doi.10.1029/2010RG000345. Data available at http://data.giss.nasa.gov/gistemp/

IPCC AR4 (2007) Report of WG1 in 4th Assessment Report fig. 2, available at http://www.ippc.ch

IPCC 2013, The 5th Assessment Report (AR5) of the IPCC (available at the web site in reference IPCC AR4 2007).

IPPC1 2013, AR5 Box 3.1, page 265 in the report of WG1.

IPCC2 2013 AR5 Figure TS.9 In the report of WG1. IPCC 2013.

IPCC3 2013 AR5 Figure TS.6 in the report of WG1, IPCC 2103.

Llovel W., Willis J.K., Landerer F.W. and Fukumori I., 2014, "Deep-ocean contribution to sea level and energy budget not detectable over past decade", Nature Climate Change, Volume 4 pp. 1031–1035.

Exercises

1. What is meant by the term "the effective emitting temperature of the Earth"? Show that if the Earth acted as a perfect black body without greenhouse gases in the atmosphere the temperature at the surface would be the effective emitting temperature of 255 K. Assume that the Earth reflects a fraction 0.3 of the incident radiation (the albedo).
   (Mean surface temperature of the sun is 5780 K. Mass of the sun is 2 1030 kg. Radius of the Sun is 6.96 108 m. Mean distance of the Sun to the Earth is 150 109 m. Stefan's constant is 5.7 10^{-8} W m^{-2} K^{-4}).
2. Explain briefly how greenhouse gases allow warming of the Earth to a more comfortable temperature.
3. Calculate the effective radiation temperatures of the Earth if the albedo fraction is 0.25, 0.3 and 0.35. How would you expect the average surface temperature to change if the albedo fraction changed from 0.25 to 0.35? Sketch a graph to illustrate your result.
4. a) Plot a graph of temperature anomaly against time from the data given below. Calculate the predicted temperatures against time from the model given in section 7.4 and plot these as a curve to compare with the measurements.
   b) Recalculate your predictions assuming that pressure broadening in our model is proportional to $P^{1/2}$ (pressure P) rather than linear in P.
   c) Explain why you would expect the disagreements between these simple models and the data.
   Input data for question 4.

Year	1800	1850	1900	1950	2000
CO_2 concentration (ppm)	280	283	294	352	390
Temperature anomaly (deg C)	-0.4	-0.4	-0.3	0.0	0.4

5. The gravitational acceleration on Venus is roughly the same as on Earth and its effective radiation temperature is also similar. Its atmosphere is mainly carbon dioxide which has approximately the same heat capacity as air. The surface temperature on Venus is observed to be 735 K and the surface atmospheric pressure is 100 bar. Use the simple picture described section 7.4 to explain why the stratosphere on Venus begins at an altitude which is 6 times higher than that on Earth.
6. Suppose the Earth's atmosphere did not contain any greenhouse gases. What value of the average emissivity of the Earth's surface would be necessary for the average surface temperature to be roughly at today's value of 288K. Look up the emissivities of various materials and discuss if this emissivity is realistic.
7. The average heat energy from the interior appearing at the Earth's surface is 0.1 W/m^2. It is thought that most of this energy comes from the decay of very long half-life radioisotopes. Suppose that the Sun ceases to shine, show that the effective radiation temperature would eventually reach 36 K. What would be the temperature at the Earth's surface in this case?

8 MEASUREMENT OF THE AVERAGE GLOBAL TEMPERATURE

Monitoring the climate has required special statistical techniques to be developed in order to arrive at global averages. Central to this is the measurement of the average global temperature. In this chapter the different ways of measuring the average global temperature which have been adopted are described together with the uncertainties in the procedures. Since the assessment of such uncertainties involves statistical procedures a primer on basic statistics is given in the Appendix to the chapter.

8.1 INTRODUCTION

The realisation that global average temperature measurements can be made from sample stations separated by relatively large distances came when it was demonstrated that the temperatures in weather stations separated by less than 1000km were correlated (Hansen and Lebedeff 1987). This led to the discovery of the 20th century global warming and the formation of the United Nations Framework Convention on Climate Change (for a history see Weart 2015). In this chapter we describe the techniques and methods used to make these measurements.

Measurements of global temperature cover a considerable range of time (see Chapter 9 for historical measurements). Such measurements need to combine sources of multiple measurements covering a wide area of the Globe. There are two reasons for this. Firstly combining many measurements gives greater accuracy from the central limit theorem of statistics. This theorem tells us that if we have n measurements of a quantity with an uncertainty σ, the uncertainty on the average is $\sigma/\sqrt{n}$ i.e. the result becomes more precise with the increasing number of contributing measurements providing that all biases can be removed from each. The second reason is that the measurement in a single location only provides information about that particular location. Hence multiple samples from widely spaced locations on the Earth are needed to determine a global average temperature.

The mercury and alcohol in glass thermometer was invented in the 17th century but it was not until the 19th century that longer term temperature records became generally available. Before this time assessment of temperature must be made with less accurate values from proxies such as tree ring thicknesses, pollen distributions or analysis of marine and fresh water sediments. From the 19th century onwards stations began to be set up to monitor the weather. In addition, the Royal Navy used its ships to monitor the sea surface temperatures around the globe. Late in the 20th century it became possible to monitor the Earth's temperature from satellite measurements of its thermal radiation.

The procedure to determine the long term temperature is as follows. For a position $\boldsymbol{x}$ on the globe the temperature at time t, $T(\boldsymbol{x},t)$, is given by

$$T(\boldsymbol{x},t) = \theta(t) + C(x) + W(\boldsymbol{x},t) \tag{8.1}$$

where $\theta(t)$ is the mean temperature at that time, $C(x)$ is a term to represent the climate at that particular location and $W(x,t)$ is the temperature fluctuation due to the weather at time t. The latter two terms should average to zero over the surface of the Earth and over time. Hence, to achieve a measure of the global temperature data must exist for a long enough time range for the weather term to average to zero. In addition the data must cover a wide enough distribution over the globe to differentiate global from local changes. Finally when $\theta(t)$ has been obtained at a particular location the temperature anomaly is determined. This is the difference between $\theta(t)$ at the location and the average over a particular time period (usually around 1980). The anomaly is taken to eliminate uncertainties in the absolute scale of a station and to eliminate the local climate term $C(x)$. This allows comparison of the anomalies between different locations and global average changes to be determined.

8.2 DETERMINATION OF THE AVERAGE TEMPERATURES FROM MEASUREMENTS ON THE EARTH'S SURFACE

Much of the data on the Earth's temperature comes from readings at weather stations of which there are many thousands spread over the globe. These stations usually have measured the temperatures to an accuracy of a fraction of a degree. Such accuracy is not usually important for weather monitoring when day-by-day fluctuations are much greater. However, for long term climate monitoring such accuracy is necessary and to obtain a measure of $\theta(t)$ to high precision care must be taken to avoid inaccuracies as discussed below.

Several groups exist which have determined the time series of the average global temperatures from Earth-bound weather stations and ocean data from ship-borne measurements. The most commonly quoted time series are from the National Oceanic and Atmospheric Administration (NOAA) in the USA, the Goddard Institute for Space Studies (GISS) in the USA, the Berkeley Earth Project in the USA and from the Meteorological Office Academic Partnership at the Hadley Centre in the UK, responsible for the so-called Hadcrut series.

Generally the procedure adopted by each group is firstly to subject the data to quality control (for example to remove a few duplicate records which find their way into the data base). Each group divides the Globe into small grids which are usually 5 degree by 5 degree squares. Further quality control is then applied. For example, the Hadley centre (Brohan et al 2006) remove stations when the anomaly from the station differs by more than 5 times the error from the mean of the remaining stations in a grid. This leads to the loss of a few stations which are assumed to be producing erroneous results. The average global temperature anomaly in each grid square is then deduced from the stations within it interpolated to the centre of the grid square. The results are then averaged to determine the average anomaly within the square. For the grid squares without weather stations or ship-borne sea measurements, interpolation from outside the square is necessary in order to cover the whole globe. Each group has its own method of interpolation. Special techniques are necessary to merge the ocean surface data and the land data.

The groups use different data bases for the temperature measurements from the weather stations. For example, the groups in the USA use the data base of the Global Historical Climatology Network Monthly dataset (GHCN) while the UK group uses the World Meteorological Organisation (WMO) data base. Similar data bases have been compiled for sea surface temperatures. These have been compiled from measurements taken from moving ships by the Royal Navy as well as data from moored and drifting buoy observations. These data bases use the available network of weather stations and sea surface data. Hence much of the data is common between the two. However, the analyses of the data by each group are independent with different procedures adopted. In addition different selections are used for quality control and different procedures for interpolating into regions with either sparse or no coverage.

The number of land based weather stations grew from less than 1000 in 1900 to several thousand by the end of the 20th century. There was a particular rapid growth in the number of weather stations in the 1950s due to the establishment of measurement stations in Antarctica. The weather station data are rather randomly scattered across the globe, with some areas well populated and others more sparsely populated. Different methods of interpolation to the centres of the grid squares for the chosen grid pattern are used by each group. The HadCrut group adopt the Climate Anomaly method (Jones and Moburg 2003). Another method which has been used is the Reference Station Method (Hansen and Lebedeff 1987) and the First Difference Method (Petersen et al., 1998). The latter paper made a direct comparison between these three methods showing similar results for each. A further method known as Kriging was adopted by the Berkeley Earth project (Rohde et al 2013). The method was developed by Krige for gold exploration in South Africa using data from sample ground boreholes (Krige 1951). It is a powerful technique particularly in regions where there is sparse coverage by weather stations.

The data from each weather station must be inspected for steps due to calibration changes or changes of routine. Corrections for such steps are applied sometimes as adjustments to the data themselves (e.g. Brohan et al, the Goddard Institute for Space Studies or GISS data) and sometimes by other methods (e.g. the Berkeley Earth project).

Many changes lead to such steps in the average temperature for a station. For example if the weather station is relocated and its altitude is changed the average temperature will change (roughly by the lapse rate of 6 degrees C per km of altitude, see Chapter 3). Thus if the station is moved to a location which is 100 metres greater in altitude the average temperature will change by approximately 0.6 degrees and this must be corrected for. Another change in routine occurs if readings at the station were taken once per day and the time of day of the reading changes. This will lead to a small shift in temperature due to daily average temperature variations. Such a change is unimportant for weather monitoring but it must be corrected for in climate monitoring. Another type of correction occurs if the thermometer is replaced by one with a slightly different zero setting. Such small shifts at a measuring point require corrections to be applied. For example, an analysis of the records from 1218 weather stations in the US Historical Climatology Network found on average each record has one spurious shift in mean level of greater than 0.5 degree C for every 15–20 year period of the record (Menne et al 2009). Such changes are often not logged and the unlogged changes must be inferred by detecting steps in the average temperature for each station. The process has become known as homogenisation.

An interesting example of the production of a step arises from the ship-borne sea surface temperature measurements by the Royal Navy. In the 19th century these were made by sampling the sea surface water using a wooden bucket over the ship's side. The buckets issued to the ships were changed to canvas ones which allowed a small seepage of water through the side. This cooled by evaporation resulting in a lowering of the temperature of the sample in the bucket. Laboratory experiments measured the cooling to be 0.4 degrees C on average. Hence all the temperatures from Royal Navy ships after the change of bucket issue needed to be adjusted upwards. This correction became unnecessary after the 1940s when engine intake temperatures were recorded rather those from buckets dangled over the side of the ship.

Figure 8.1 (solid black line) shows the distribution of detected steps in the HadCrut analysis. Due to the fluctuations in the data larger steps (adjustments) are likely to be found but smaller ones are missed. The dip at small adjustment level is due to missed small steps. An uncertainty on the average temperature for each station must be deduced due to the missed adjustments. This is achieved in the HadCrut analysis as follows. The solid black line is assumed to belong to a Gaussian distribution and the one which reproduces the observed distribution at high adjustment level is chosen (dashed black line in figure 8.1). The difference between this Gaussian curve (dashed line) and the solid line is taken to be the distribution of the missed adjustments. This is observed to be Gaussian shaped with a standard deviation of 0.4 degrees C which is taken to be the calibration uncertainty for each station. The calibration uncertainty should then be random from station to station. Hence the overall calibration uncertainty is reduced when data from many stations in a grid square are combined.

As with all scientific measurements, large amounts of work go into determining the uncertainties on the measurements. The statistical uncertainty on the temperature in any grid is determined from the scatter of the measurements about the mean. The other uncertainties due to interpolation, calibration etc. are determined separately by a variety of methods. Similar analyses are performed for both land based and sea surface temperature data. As an example figure 8.2 shows the mean global temperature (HadCrut3) with the different uncertainties added in different colours (Brohan et al 2006). The red shaded band shows the 95% confidence level range of the annual measurement uncertainties. These include the statistical and homogenisation uncertainties as well as those from the uncertainty of the base year average (1961-1990). It also includes an uncertainty due to the finite size sample in each grid known as the sampling uncertainty. The green shaded band shows the 95% confidence level when these errors are combined with the uncertainty due to incomplete coverage. This is assessed by looking at the difference between the results with complete coverage in a region and that when many stations are excluded. Finally an uncertainty is included for bias effects due, for example, to corrections for encroaching urbanisation to stations (known as the urban heat island effect) or to thermometer exposure changes. The blue curve shows the effect of including these. The uncertainties from the different measurements should be independent of each other so they are added in quadrature.

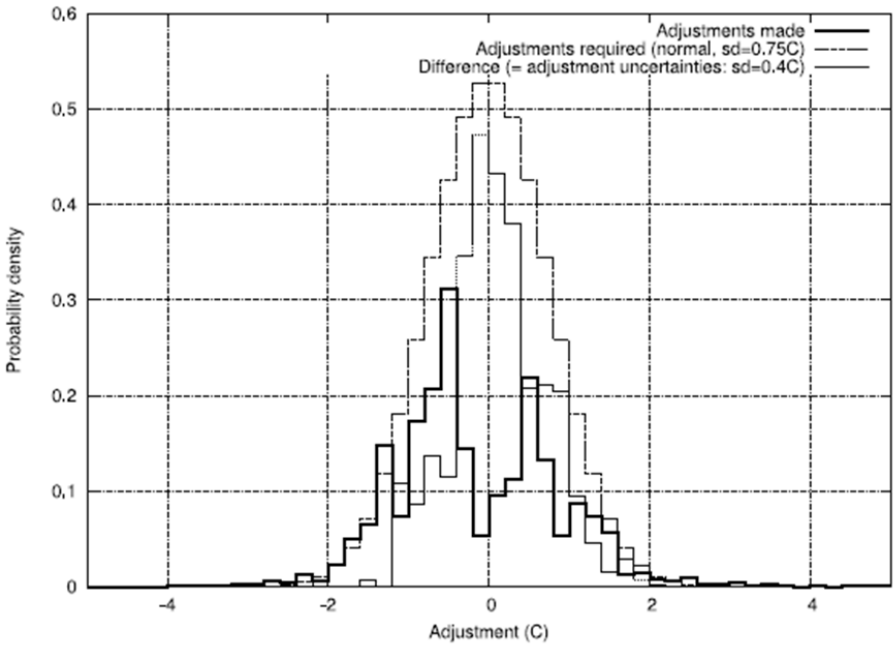

Figure 8.1 The solid black line shows the distribution of detected steps (or adjustments for changes in routine or calibration) made in the HadCrut analysis. The dashed and dotted lines are described in the text. (Source Brohan et al 2006).

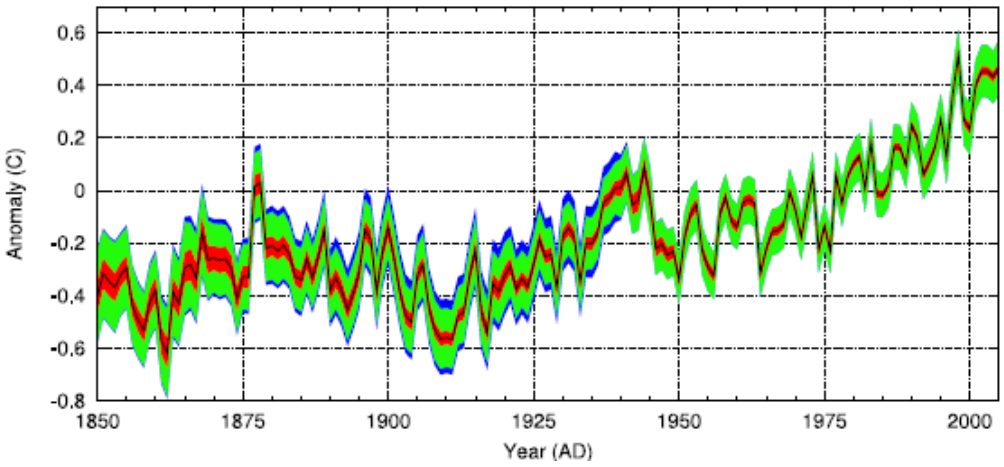

Figure 8.2 The HadCrut3 measurement of the global average annual temperature anomalies relative the base years defined as the 1961–1990 average (Brohan et al 2006). The black central line is the best estimate. The red, green and blue bands represents the uncertainties from the different sources combined together (see text). These uncertainties represent the 95% confidence level intervals.

8.3 MEASUREMENTS FROM SPACE

The temperatures in the atmosphere can be inferred from the measurements of the outgoing thermal radiation from the Earth as measured by orbiting satellites. The thermal electromagnetic radiation from the Earth is detected at several frequencies in the millimetre microwave radio band in the range from 50 to 60 GHz.

This frequency range corresponds to the band where the rotational lines of oxygen molecules in the air are excited (see Chapter 6). Oxygen is a strongly paramagnetic substance since the molecule contains two unpaired electrons in the triplet ground state. Hence oxygen molecules have a strong magnetic moment. This allows the higher rotational molecular states to be readily excited by the magnetic component of the thermal electromagnetic radiation. In contrast nitrogen molecules have a much smaller magnetic moment so that nitrogen molecules are excited much less. The different rotational levels, principally of oxygen, are resonantly excited by the outgoing thermal radiation and re-emit the radiation at the same frequency. This is detected by the satellite as a series of line spectra as well as the off-resonant frequencies. Because of self-absorption in the atmosphere the most strongly excited lines produce re-emitted radiation which emanates from high in the atmosphere. In contrast, the off-resonant radiation and weaker excited lines, for which the atmospheric self-absorption is smaller, come from lower down in the atmosphere. Further information is obtainable from the angular dependence of the detected radiation since the amount of specular radiation detected from reflection at the Earth's surface of down-welling thermal radiation depends on the angle at which the satellite observes.

Data have been obtained to date from two projects: the Microwave Sounding Unit (MSU) from 1978 to the early 2000s with four frequency channels and the Advanced Microwave Sounding Unit (AMSU) from 1998 to the present (2015) with 14 frequency channels. For the frequency of each channel, the probability of detecting in the channel a photon of that frequency emanating from a certain depth in the atmosphere is computed. This allows a weight function to be deduced for each channel which is this probability as a function of depth.

The data from the different channels are then taken and using the weight functions for each it is possible to deduce by an unfolding procedure the intensity of thermal radiation as a function of atmospheric depth. Comparing this with the known thermal radiation spectrum allows the temperature to be determined at each altitude albeit with rather coarse vertical resolution.

The procedures and corrections are very different from those for surface based determinations of the temperatures. The data are taken from a series of different satellites and so calibration and homogeneity corrections are necessary. However, these will be very different from those in the surface based measurements.

The global coverage of the satellite data is excellent and the land/sea differences are smaller, the main difference arising from the surface emissivity of land relative to ocean. However, the procedure to determine the temperatures is more convoluted (Mears and Wentz 2009). The temperature is determined at various altitudes. Here we are concerned with that in the lower troposphere (TLT) which may be used as a proxy for the surface temperature. Measurements are also available for the middle troposphere (TMT) and the stratosphere (TST).

Two groups have derived temperatures from the available satellite data: the Remote Sensing Systems (Mears and Wentz 2009) and the University of Alabama at Huntsville group (Spenser and Christy 2011).

8.4 COMPARISON OF SATELLITE AND SURFACE MEASUREMENTS OF THE GLOBAL AVERAGE TEMPERATURE

Figure 8.3 shows the data from two groups using the surface data (HadCrut and GISS) and the two groups using satellite data allowing comparisons to be made. The curves represent temperature anomalies but are displaced from each other for clarity.

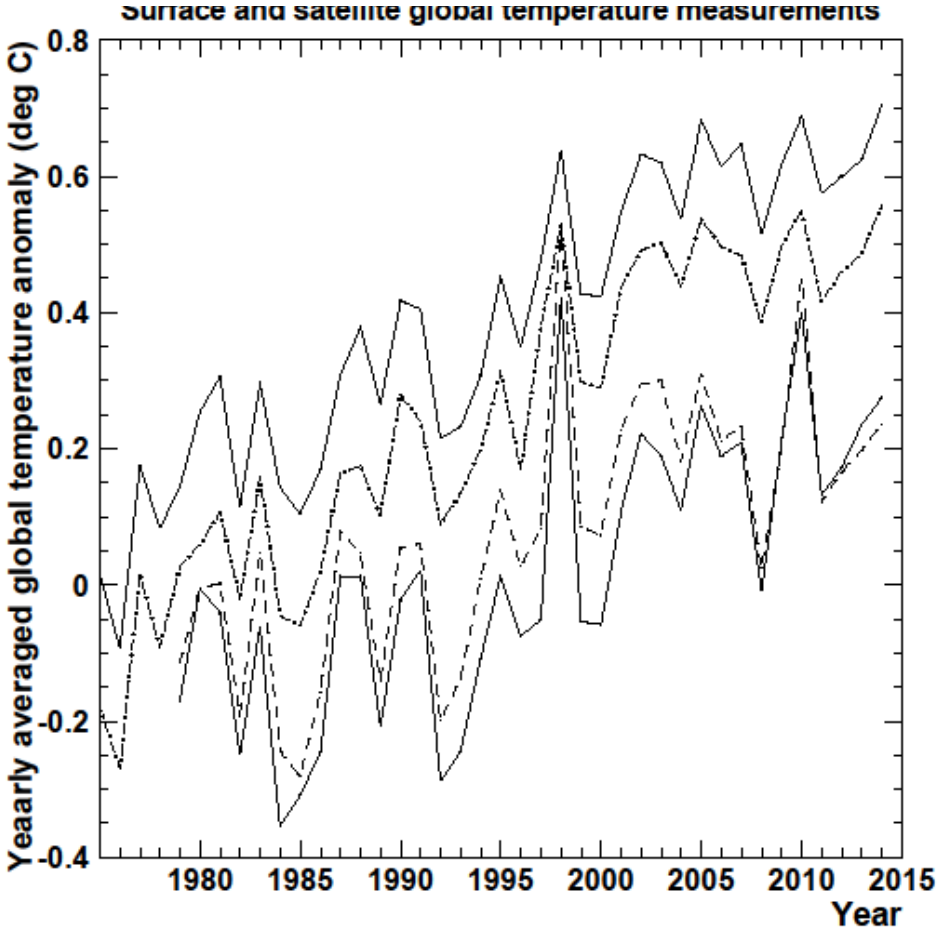

Fig 8.3 Satellite measurements of the yearly mean global temperature anomaly (vertical axis) UAH (lower solid curve, Spenser and Christy 2011) and RSS (dashed curve, Mears and Wentz 2009) groups compared to the surface-based measurements from GISS (upper solid curve, Hansen et al. 2010) and Hadcrut4 (dash-dotted curve, Morice et al 2012). Here the yearly means have been displaced from each other for clarity. These displacements are not significant since the absolute values depend on the comparison year. The average for each year is plotted and the points are joined by lines.

Figure 8.3 shows that there is reasonable overall agreement between the data sets with small differences due to the uncertainties in the measurements (typical uncertainties are shown on figures 8.2). As a comparison the gradients, dT/dt, of linear fits to the data have been determined from the large spike in 1998 to 2015. This spike is caused by the El Niño Southern Oscillations (ENSO), a known natural oscillation of the climate.

To determine both the gradients and the uncertainties the yearly averaged measurements for each data set were taken. This avoids fluctuations due to seasonal variations. These data were fitted by linear regression lines. The uncertainty on each measurement was taken to be the average deviation of the points from the regression line. This allowed the uncertainty on the gradient to be determined from the deviation of the measured value of χ^2 of the fit from the minimum value. The best fit values to the data from 1999 to 2015 are shown in Table 1 together with the measured uncertainty.

Table 1

Data set	UAH	RSS	GISS	HadCrut4
Slope (degrees C/year)	0.014±.008	0.004±.008	0.009±.008	0.006±.008

Here the quoted uncertainties represent the 90% confidence level interval in which the true value could lie about the best fit value given the uncertainties in the data. There is good agreement between the slopes within the measurement uncertainty. Therefore the differences between the slopes are not significant.

The average slope of all four data sets is 0.0084±.0050 degrees/year and the value of χ^2 to this mean for all four data sets is 2.85 for 3 degrees of freedom. The probability of obtaining a worse value than this is 50%. This shows that the fluctuations in the slopes are all compatible with those to be expected from the uncertainties in the measurements about the regression line. Hence there is no significant disagreement between the measurements.

The procedure was repeated for different start dates. Figure 8.4 shows the measured slopes as a function of the start date together with a vertical line to show the spread in values allowed by the uncertainty on each measurement determined as described above. It can be seen that the slopes all agree with each other within this measurement uncertainty at all start dates. The slopes of the RSS data are slightly smaller and even negative for later start dates. However, all the data are compatible with the other data sets within the measurement uncertainty. The slopes increase slightly as the start increases from 1998 to 1999. This is due to the tail of the El-Ninõ event which increased the temperatures at early times causing an artificial decrease in the slope. For later start dates the slopes all decrease together uniformly due to the influence of the 21st century hiatus in the mean global surface temperature.

The adjustments made for calibration and homogenisation are very different between the satellite and surface-data based reconstructions. The agreement between the different reconstructions indicates that such adjustments have been made reliably.

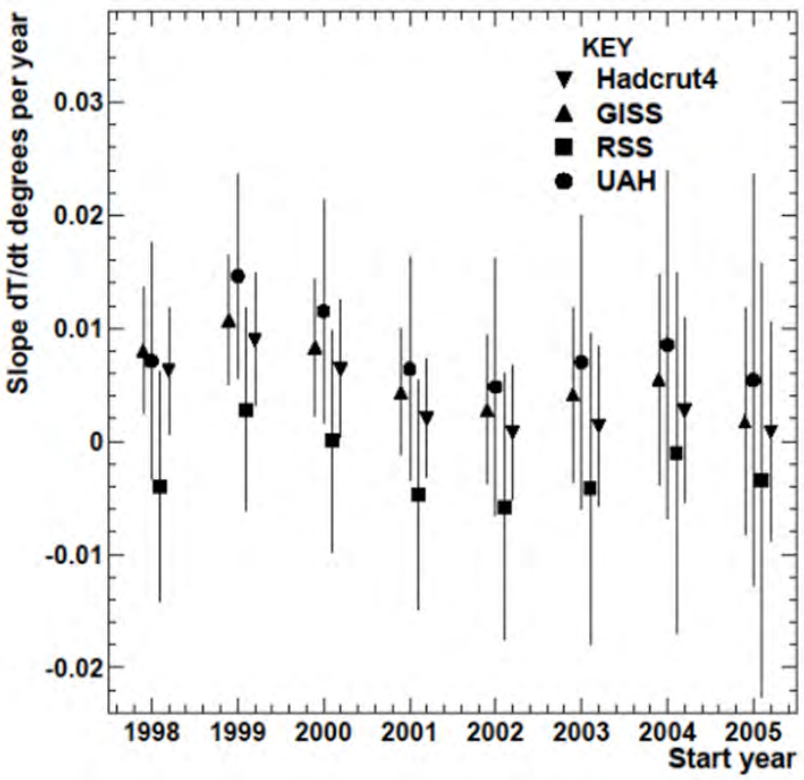

Figure 8.4. The slopes of the linear fits to the data in figure 8.4. These are the slopes of the regression lines (dT/dt) determined from the start date on the abscissa (x axis) through to the end date of 2015. The vertical bars show the 90% confidence range of the uncertainty within which the true value can lie given the uncertainties in the data.

APPENDIX A8 BASIC STATISTICS

Since the measurement of average global temperatures involves statistical analysis of large data sets we give here the necessary basic statistics in most cases without proof. Proofs can be found in books devoted to statistics. Enough information is given to help with the understanding of the statistical methods in dealing with large numbers of samples.

A8.1 Means of several measurements

If multiple measurements of a quantity, x, are made, each with equal accuracy, the distribution of the values of x will have a probability distribution function which is approximately Gaussian shaped i.e. the probability, $P(x)$, of obtaining a value of x between x and $x+dx$ is given by

$$P(x)dx = \frac{1}{\sqrt{2\pi}\sigma} e^{-\frac{(x-x_m)^2}{2\sigma^2}} dx \qquad 8.2$$

where x_m is the most probable value and σ is the standard deviation of the population. The standard deviation is a measure of the width of the probability distribution. In making a measurement the most probable value, x_m, will be the true value of the variable to be measured and σ gives an estimate of the uncertainty on a single measurement of x.

Integration of equation 8.2.shows that the probability of the measured value of x falling within the range $-\sigma < (x - x_m) < \sigma$ is 68%, or in the range $-1.64\sigma < (x - x_m) < 1.64\sigma$ is 90%, or in the range $-1.96\sigma < (x - x_m) < 1.96\sigma$ is 95%. The uncertainty in a single measurement x is sometimes taken as the standard deviation σ. Therefore, to determine the uncertainty in the measurement the standard deviation of the population to which x belongs has to be determined. Sometimes confidence intervals are quoted. Thus 1.64σ (*or* 1.96σ) gives the 90% (or 95%) confidence interval i.e. the range about the measured vale, x, in which the true value lies with 90% (or 95%) probability.

The root mean square (RMS) value of x gives the value of σ since

$$\int_{-\infty}^{\infty}(x - x_m)^2 P(x)dx = \sigma^2 \qquad 8.3$$

where x_m is the mean value of the population.

If there are N measurements of x then σ can be determined from the RMS value of the set of the N measurements. In principle $\sigma^2 = \sum_1^N (x - x_m)^2/N$ where x_m is the mean of the set. However, a less biased estimate for small samples is $\sigma^2 = \sum_1^N (x - x_m)^2/(N-1)$. Hence the standard deviation can be estimated in this way if several measurements of the same quantity, each with equal precision, are available. If only a single measurement is possible the value of σ must be assessed from the quality of the individual measurements which enter into the determination of x.

If several measurements of x (x_1, x_2,…..x_N) are available each with different uncertainties (σ_1, σ_2,….σ_N) then the best estimate of the truth is the weighted average given by

$$x_m = \frac{\sum_{i=1}^N x_i^2/\sigma_i^2}{\sum_{i=1}^N 1/\sigma_i^2} \qquad 8.4$$

and the uncertainty is given by $u^2 = {}^1/_{\sum_1^N 1/\sigma_i^2}$. It follows from this that if all the measurements have the same values of σ then $x_m = \sum_1^N x_i/N$ and the uncertainty is $u = \sigma/\sqrt{N}$. It then becomes clear that multiple unbiased measurements decrease the uncertainty in a result.

A8.2 The uncertainty on a quantity which depends on several measured quantities

The uncertainty on a function of more than one variable requires the correlation between the variables to be known. Suppose we have a function $f(x_1, x_2 \ldots x_n)$ where the are measured quantities each with uncertainty u_i then the uncertainty in f, u_f, is given by

$$u_f^2 = \sum_{i=1}^n \left(\frac{\partial f}{\partial x_i}\, u_i\right)^2 + \sum_{i,j=1,i\neq j}^n 2\left(\frac{\partial f}{\partial x_i}\frac{\partial f}{\partial x_j} r_{ij} u_i u_j\right) \qquad 8.5$$

where r_{ij} are the correlation coefficients between the i^{th} and j^{th} and measurements. This correlation coefficient, which is a measure of the covariance, is defined by

$$r_{ij}^2 = \frac{(\sum_{k=1}^N (x_i^k - \langle x_i \rangle)(y_j^k - \langle y_j \rangle))^2}{\sum_{k=1}^N (x_i^k - \langle x_i \rangle)^2 \sum_{k=1}^N (y_j^k - \langle y_j \rangle)^2} \qquad 8.6$$

where N is the total number of samples which have means $\langle x_i \rangle$ and $\langle y_j \rangle$ and Equation 8.6 shows that if the uncertainties are uncorrelated ($r_{ij} = 0$) then the uncertainties from each source add in quadrature.

Equation 8.6 is most easily understood from a function with 2 variables. By the chain rule of differentiation the change in f due to small changes in x_1, x_2 is

$$\delta f = \frac{\partial f}{\partial x_1}\delta x_1 + \frac{\partial f}{\partial x_2}\delta x_2 \qquad 8.7$$

To obtain the mean square deviation $(<\delta f^2>)$ which is taken to be the one standard deviation uncertainty in f,u_f, we square both sides of equation 8.7 and take the average so that

$$u_f^2 =<\delta f^2>= <(\frac{\partial f}{\partial x_1}\delta x_1)^2 + 2\frac{\partial f}{\partial x_1}\frac{\partial f}{\partial x_2}\delta x_1\delta x_2 + \left(\frac{\partial f}{\partial x_2}\delta x_2\right)^2 > \quad 8.8$$

$$= \frac{\partial f}{\partial x_1} <\delta {x_1}^2> +2\frac{\partial f}{\partial x_1}\frac{\partial f}{\partial x_2} <\delta x_1\delta x_2> + \frac{\partial f}{\partial x_2} <\delta {x_2}^2>$$

$$= (\frac{\partial f}{\partial x_1}u_1)^2 + 2\frac{\partial f}{\partial u_1}\frac{\partial f}{\partial u_2}r_{12}u_1u_2 + (\frac{\partial f}{\partial u_2}u_2)^2$$

The cross term follows from the definition of correlation coefficient in equation 8.6. Here u_1 and u_2 are the one standard deviation uncertainties of the populations of which x_1 and x_2 are measurements.

Note that if only single measurements of the set of quantities, *x,* are available the uncertainties and correlations have to be determined from an assessment of the data quality. This is often a difficult procedure.

A.8.3 Accuracies involving the counting of discrete events

The previous sections of this appendix have described the treatment of uncertainties of continuous measured variables. Here we consider uncertainties in counting discrete events e.g. in the decays of a radioactive isotope where each decay is a discrete event. Consider a test where *n* events is sampled and the outcome is either yes or no at each trial and the probability of a yes is *p*. The probability of obtaining yes k times follows the binomial distribution

$$P(k) = \binom{n}{k}p^k(1-p)^{n-k} \quad 8.9$$

where $\binom{n}{k} = \frac{n!}{k!(n-k)!}$ are the binomial coefficients. The root mean square deviation of such a distribution is $\sqrt{np(1-p)}$. This can be treated as the 1 standard deviation uncertainty in such a population.

In the event that *n* is large and *p* is small the probability follows the Poisson Distribution.

$$P(k) = \frac{e^{-m}m^k}{k!} \quad 8.10$$

where m is the mean value of k after many trials. For m greater than of order 5 the Poisson distribution is approximately Gaussian shaped with standard deviation $\sqrt{m}$. Hence if k events are counted from a large population the 1 standard deviation uncertainty is of order $\sqrt{k}$.

A8.3 Testing the significance of a result

The uncertainty in a measurement helps define its significance. For example suppose a quantity x is measured with uncertainty u, written $x \pm u$, and a hypothesis predicts that μ is the expected value of the quantity. The question arises as to whether the measurement, x, is significantly different from the predicted value, μ. The significance of the difference is usually judged by forming the statistical quantity $(x-\mu/u)$ i.e. the difference between the measured and expected values in uncertainty units.

Measured quantities usually behave roughly as Gaussian distributions and the quoted uncertainty, u, is often its standard deviation. The probability of obtaining a value with a greater deviation than x-μ can be computed. This is $\int_{x-\mu}^{\infty} \frac{1}{u\sqrt{2\pi}} \frac{e^{-(x-\mu)^2}}{2u^2}\, dx$ for positive differences or the integral evaluated from $-\infty$ to x-μ for negative differences. Standard tables of these integrals are available. If x belonged to the population with value μ the fraction of readings which would have differences greater than 1, 2 or 3 standard deviations is 32%, 5% or 0.3%, respectively. The difference is usually accepted as not significant if it is less than 2 standard deviations (5% probability of obtaining a bigger difference) allowing the argument that the values of x and μ could be compatible with each other. Greater differences than 2 standard deviations are usually taken as significant so that it can be argued that the values of x and μ are different from each other i.e. the measurement disproves the hypothesis which predicted the value μ.

NB the choice of the number of standard deviations at which significance is defined is subjective and depends on the measurement technique. For example in the discovery of the Higgs Boson at CERN the cut was made at 5 standard deviations. The reason to be so large is that many separate measurements are made before finding the result. The cut was increased to 5 standard deviations to guard against the possibility of the observed result being a statistical fluctuation in one of the many plots.

A similar technique, known as the χ^2 test, is used in the case of several measurements, $x_i \pm u_i$, and predictions μ_i. For example, the values of μ_i could be taken from a theoretical curve which the data are testing. In this test the value of

$$\chi^2 = \sum_{i=1}^{N} \left(\frac{x_i - \mu_i}{u_i}\right)^2 \qquad 8.11$$

is computed, where N is the number of measurements. If the u_i are the 1 standard deviation uncertainties it can be shown that χ^2 follows the probability distribution function

$$P(\chi^2) = \frac{e^{\left(\frac{k}{2}-1\right)} e^{-\frac{\chi^2}{2}}}{2^{\frac{k}{2}} \Gamma\left(\frac{k}{2}\right)} \qquad 8.12$$

where k is the number of degrees of freedom. The value of k will normally be the number of data points, N. However, if the theoretical curve has n parameters in determining it, $k = N - n$. Integrating this probability function ($\int_{\chi^2}^{\infty} P(\chi^2) d\chi^2$) allows the probability to obtain a worse value of χ^2 than that observed to be determined. These values are tabulated for different values of k e.g. see http://sites.stat.psu.edu/~mga/401/tables/Chi-square-table.pdf. A small probability of obtaining a worse value of χ^2 indicates either that the values of the μ_i are a poor representation of the measurements, x_i, or the measurements represent a large statistical fluctuation from the norm. A qualitative judgement then has to be made to decide which of these two is the case. As a rule of thumb if the probability of obtaining a worse value of χ^2 is 5% or less the usual decision is that the measurements disagree with the theory μ_i, disproving the hypothesis that the measurements x_i belong to the same population as the theoretical values μ_i. Conversely, higher values of the probability would be considered to be within normal statistical fluctuations so that the data provide experimental support for the theory.

A8.4 Testing if two variables x and y are linearly correlated in a data set (x_i, y_i)

The correlation coefficient, r, defined in equation 8.6, allows a statistical test to be made to determine if two variables are linearly correlated. If r is consistent with zero one would conclude that there is no correlation. It can be shown that the probability distribution of r roughly follows a Gaussian shape with standard deviation from the N measurements of $u = \frac{1}{\sqrt{N-2}}\sqrt{1-r^2}$. Hence, the ratio u/r gives the number of standard deviations from zero of the result. The probability that the observed correlation coefficient could come from the two variables if they were actually uncorrelated can then be determined. The probability is approximately 16%, 2.5% or 0.15% if the ratio is 1, 2 or 3, respectively. Note that these probabilities are ½ of those quoted in the integrals of the Gaussian above since one is only looking on the side of the distribution towards zero. The probability is approximately 5% if $u/r = 1.64$.

The probability can be deduced more exactly by forming the ratio

$$t = \frac{r}{u} = r\sqrt{\frac{N-2}{1-r^2}} \qquad 8.13$$

which gives a statistic, known as the Student's t test. The probability of obtaining a zero correlation coefficient (i.e. no correlation) from the set of N measurements can be looked up in standard tables (see https://www.easycalculation.com/statistics/t-distribution-critical-value-table.php). Again a value judgement has to be made in interpreting this probability. Usually if the probability is greater than 5% the correlation is accepted as a statistical fluctuation (otherwise the correlation is treated as real).

To determine the best fit line to the set of data (x_i, y_i) the minimum square deviation of the points from the line $y = mx + c$ is found i.e. the values of slope, m, and intercept, c, are chosen which minimise the quantity $\alpha^2 = \sum_{i=1}^{n}(y_i - (mx_i + c))^2$. Setting the differential coefficients of α^2 with respect to m and c to zero and solving the resulting two simultaneous equations gives

$$m = \frac{N[xy]-[x][y]}{N[xx]-[x][x]} \text{ and } c = \frac{[y][xx]-[x][xy]}{N[xx]-[x][x]} \qquad 8.14.$$

The uncertainties, σ_m and σ_c are obtained from the scatter of the points about the fitted line and these are

$$\frac{\sigma_m^2}{N} = \frac{\sigma_c^2}{[xx]} = \frac{\alpha^2}{(N-2)\Delta} \qquad 8.15$$

where $\Delta = N[xx] - [x]^2$.

Here we use the notation $[x] = \sum_1^N x_i$, $[xy] = \sum_1^N x_i y_i$,$[xx] = \sum_1^N x_i x_i = \sum_1^N x_i^2$ etc. (For further details see Topping 1972).

References

Brohan P., Kennedy J.J., Harris I., Tett S.F.B. and Jones P.D. 2006 "Uncertainty estimates in regional and global observed temperature changes: A new data set from 1850" Journal of Geophysical Research Vol 111 D12106 doi:10.1029/2005JD006548.

Hansen J.E. and Lebedeff S. 1987 "Global trends of measured surface air temperature", J. Geophysical Research Vol. 92 (D11), pages 13345–13372.

Hansen J., Ruedy R., Sato M. and Lo K. 2010 "Global surface temperature change" Reviews of Geophysics 48, RG4004, doi.10.1029/2010RG000345. Data available at http://data.giss.nasa.gov/gistemp/

Jones P.D. and Moberg A. 2003, "Hemispheric and Large Scale Surface Air Temperature Variations: an extensive revision and update to 2001", Journal of Climate volume 16 pp. 203–223.

Karl T., Arguez A., Huang B., Lawrimore J.H., McMahon J., Menne M.J., Peterson T.C., Vose R.S., Zhang H.M. 2015 "Possible artifacts of data biases in the recent global surface warming hiatus" Science.aaa6532/001 (available at sciencemag.org/content/early/recent).

Krige D.G. 1951, "A Statistical approach to some mine valuations and allied problems at the Witwatersrand", Master's thesis of the Univ. of Witwatersrand.

Mears C.A. and Wentz F.J. 2009, "Construction of the RSS V3.2 Lower-Tropospheric Temperature Dataset from the MSU and AMSU Microwave sounders", Journal of Atmospheric and Oceanic Technology Vol. 26 pp. 1493–1509 (The RSS data are available at http://images.remss.com/msu/msu_time_series.html).

Menne M.J., Williams C.N. and Vose R.S. 2009, "The US Historical Climatology Network Monthly Temperature Data, Version 2", Bulletin of the American Meteorology Soc vol. 90, pages 993–1007.

Morice C.P., Kennedy J.J., Raynor N.A. and Jones P.D. 2012 "Quantifying uncertainties in global and regional temperature change using an ensemble of observational estimates: the HADCRUT 4 data set" Journal of Geophysical Research 117, D08101, doi:10.1029/2010JD015220. Data available from http://www.metoffice.gov.uk/hadobs/hadcrut4/.

Petersen T.C., Karl T.P., Jamason P.F., Knight R. and Easterling D.R. 1998,"The first difference method: Maximizing station density for the calculation of long-term global temperature change", Journal of Geophysical Research vol. 103 pp. 25967–25974.

Rohde R. et al. 2013, "Berkeley Earth Temperature Averaging Process", Geoinformatics and Geostatistics: an overview 1:2 doi:10.4172/gigs.1000103).

Spenser R.W. and Christy J.R. 2011 "Climate data record program", NOAA Report CDRP-ATBD-0108, Sept 2011 data available at http://www1.ncdc.noaa.gov/pub/data/sds/cdr/CDRs/Mean_Layer_Temperatures_UAH/AlgorithmDescription.pdf.

Topping J. 1972, "Errors of observation and their treatment", published by Chapman and Hall, London and New York ISBN 0 412 21040 1.

Weart S. 2015 "Climate change impacts: The growth of understanding" Physics Today vol. 68(9) 46 available at http://scitation.aip.org.ezproxy.lancs.ac.uk/content/aip/magazine/physicstoday/article/68/9/10.1063/PT.3.2914. This article gives a history of the growth in understanding that increasing greenhouse gases lead to global warming.

Exercises

1. A climate change denier uses the fact that that the RSS data give a negative slope after 1999 to claim that global warming has stopped. Write him a letter using figure 9.5 to explain to him/her why the argument is wrong.
2. The probability distribution for the anthropogenic radiative forcing responsible for global warming is shown on the graph below (source IPCC AR4).

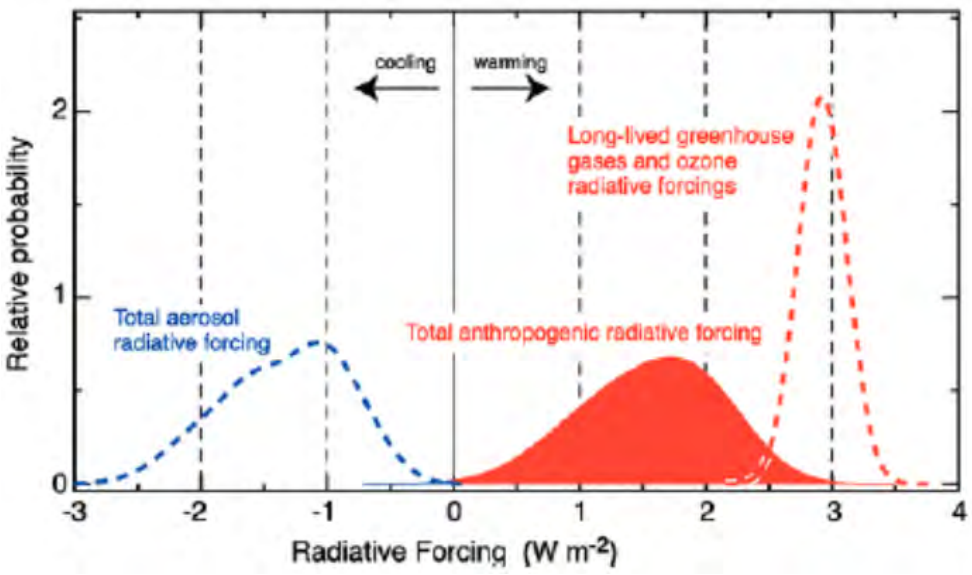

Estimate from the curve the probability that a) half the warming could be natural, b) one quarter could be natural.

3. Explain briefly the difference between the methods of measurement of the average global temperature using surface and space-based measurements. Highlight the advantages and disadvantages of each.
4. The velocity of light, c, is measured in four separate months by four groups of students in the same year using the same apparatus. The results were 299784, 299786, 299771 and 299776 km/sec. Show that the best fit line to these data gives $c = -3.9\,T + 299785.1$ km/s per month. One of the students asserts that the velocity of light varies with time. Why is his/her conclusion too strong? (Hint, either compute the correlation coefficient and its uncertainty or the uncertainty on the slope, see the Appendix).

9 HISTORY OF THE EARTH AND ITS CLIMATE

It is instructive to trace the history of the Earth and its climate. This allows a perspective on the claim by doubters of man-made climate change that the climate has always changed and the 20th century global warming was just another such change. In this chapter the large scale pre-historic changes to the Earth and its climate are described and contrasted with their relative stability since the last ice age ended some 12000 years ago. During this period of stability mankind and civilisations have flourished.

In this chapter the current picture of the history of the Earth and its climate are described. Mankind is a comparative newcomer into this picture and the picture of his/her evolution is still developing as different skeletal remains are found. It is thought that the first hominids appeared around six million years (Ma) (see endnote 3 page 202) ago and these finally evolved into the current species, homo-sapiens, around 200000 years ago (Lockwood 2007).

9.1 INTRODUCTION

The Earth and its climate have undergone many changes during its 4.6 billion year (Ga) life-time. This history has been mapped mainly from geology and palaeontology. The procedure has been a difficult one and there are significant uncertainties in the story. The following is a brief summary of the history as it is thought to have occurred.

9.2 FORMATION OF THE SOLAR SYSTEM

It is thought that the Universe began with a big bang 13.5 Ga ago with the material (elementary particles) at the so called Planck temperature of 10^{32}K. The Universe then expanded and cooled as the available energy became distributed throughout a larger volume. As the temperature cooled the collisions between objects became less violent allowing successive phase changes to take place such as the formation of nuclei at age about 100 seconds. At this time the temperature became low enough to allow the protons and neutrons to stick together when they collide to form light nuclei without subsequent collisions destroying them. After a time of about 300000 years the Universe became cool enough for electrons to stick to nuclei to form atoms. By that time the temperature had reached an average of 3000K and the mean collision energy would not be violent enough to dislodge the electrons. The Universe continued to expand and cool so that after a period of about 1 billion years the temperature had cooled to about 15K. At this temperature gravity would be a force which was strong enough to allow galaxies to form. These are masses of material held together by the gravitational force. The material is mainly hydrogen gas and helium but with other materials. Stars formed in the galaxies out of the hydrogen and with them planetary systems such as in the Solar System.

When the hydrogen gas is formed at the core of the star the pressure and temperature is such as to ignite nuclear fusion reactions in which protons fuse together to form helium (see Chapter 2 section 2.4). As the star progresses through its life-time the fusion can involve even heavier elements. Larger stars tend to be shorter lived, since they burn up their fuel more rapidly at the higher pressure at their core. This burning becomes endothermic for nuclei with atomic number greater than 26 (iron) where the average binding energy per nucleon in nuclei peaks. In consequence fusion processes halt when all the material has been burnt up to iron. Heavier nuclei are only formed during the violent collisions produced in the explosion at the death of heavy stars known as a super-nova.

Figure 9.1 shows an artist's impression of our galaxy, The Milky Way, as it is today. The brightness in the picture is proportional to the material density in the Galaxy. The bright spiral arms are thought to be the main regions where stars are born. These rotate around the Galactic centre. The solar system orbits the centre taking about 200 Ma to complete one revolution which is different from the rotation speed of the spiral arms. The difference between the rotation speeds of the spiral arms and the solar system is known as the pattern speed.

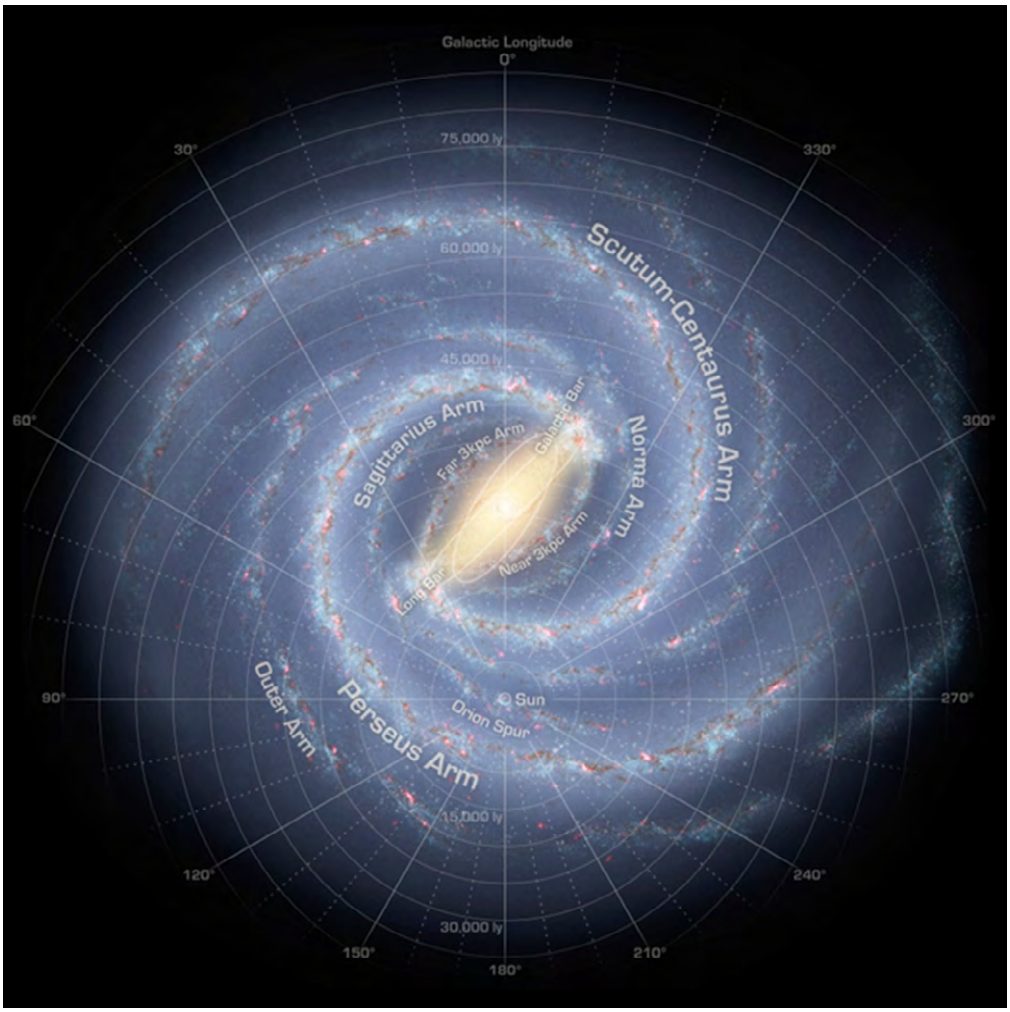

Figure 9.1 An artist's impression of the our galaxy, The Milky Way. The bright spiral arms are areas of greater density and are thought to be the main star forming regions (Image credit NASA/Adler/U. Chicago/Wesleyan/JPL-Caltech).

It is thought that the solar system formed 4.6 Ga ago from the Galactic material, possibly triggered by a shock wave from a nearby super-nova explosion. The evidence for this is that we find materials of higher atomic number than iron on the Earth. The Sun was born by accretion of hydrogen from the swirling cloud of material and plasma, sometimes known as the Solar nebula. The hydrogen came together until it reached a density and temperature which was sufficient to ignite the thermonuclear fusion reactions at its core.

The Earth and the so called terrestrial planets (Mercury, Venus, Earth and Mars) were born from the dust and heavier materials flung out at the birth of the Sun. These planets were then formed from the in-falling dust and debris. This in-fall would have heated the nascent planets into a molten state which would have shown extreme volcanic activity. In this molten state the heavier materials (mostly iron) sank to the bottom and the lighter materials (mainly silicates) floated to the surface. Hence the cores of the planets mainly consist of iron. In the early years after their birth there would have been frequent collisions with other objects within the solar nebula. The Earth's Moon is thought to have been formed in one such violent collision soon after the birth of the Earth. It is thought that this collision caused the Earth's axis to tilt and the Earth to rotate rapidly (once per day) about its axis.

The heavy outer planets Jupiter and Saturn are thought to be gas giants i.e. stars which failed to ignite. Many stars are observed to be double stars.

9.3 THE EARLY EARTH

The history of the Earth is summarised in figure 9.2. The primordial atmosphere of the terrestrial planets would have consisted of mainly hydrogen and some hydrides such as ammonia and water vapour. Subsequently, outgassing from the volcanic activity would have added large amounts of carbon dioxide (as in the current atmospheres of Mars and Venus) so that this quickly became the principal component. The period following the formation of the Earth up to 4 Ga ago is known as the Hadean Eon (after Hades, the God of the Underworld of Greek mythology). The naming of the different eons, eras and periods are given in the International Stratigraphic Chart available at http://www.stratigraphy.org/index.php/ics-chart-timescale.

By the end of the Hadean Eon the Earth had settled down. Its crust would have solidified quite quickly within a million years or so of its formation (see exercise 2). A significant event towards the end of the period was the late heavy bombardment between 3.8–4.1 Ga ago when a large number of meteoroids appear to have bombarded the inner planets. These were responsible for the craters which pockmark the Moon and Mercury. The oldest crystals (of zircon) found on Earth date from this time and they show evidence of the presence of liquid water. Presumably the atmospheric pressure (mainly CO_2) would have been great enough to prevent the water from evaporating in the hot conditions of the time. There is also evidence of tectonic plate activity at this time leading to subduction of liquid water and atmospheric gases. The oldest surviving rocks also date from just after the end of the Hadean Eon. However, the vast majority of rocks date from much later than this showing that the Earth has been in geological turmoil since its formation.

The next period in the Earth's history is the Archean Eon starting at the end of the Late Heavy Bombardment 3.8 Ga before present. Tectonic activity had begun and it is thought to have been more rapid than in later times so that material in the Earth's crust was recycled rapidly. Hence rocks from this period are somewhat rare. It is thought that by the end of the Archean Eon (2.5 Ga ago) plate tectonic activity was similar to that of today and the atmospheric temperature had become temperate. The Archean Eon gave way to the Proterozoic Eon 2.5 Ga ago during which multicellular life forms emerged.

The origin of water in the oceans is largely unknown. One source could have come from collisions with comets during the bombardments of the Hadean Eon but this is thought to be less than 10% of the Earth's water. Meteorites from the asteroid belt could also have contributed. Another source is water molecules acquired during the period of accretion when the Earth was forming. As the planet cooled during the Archean Eon clouds were able to form and rain to fall. This allowed the formation of the oceans.

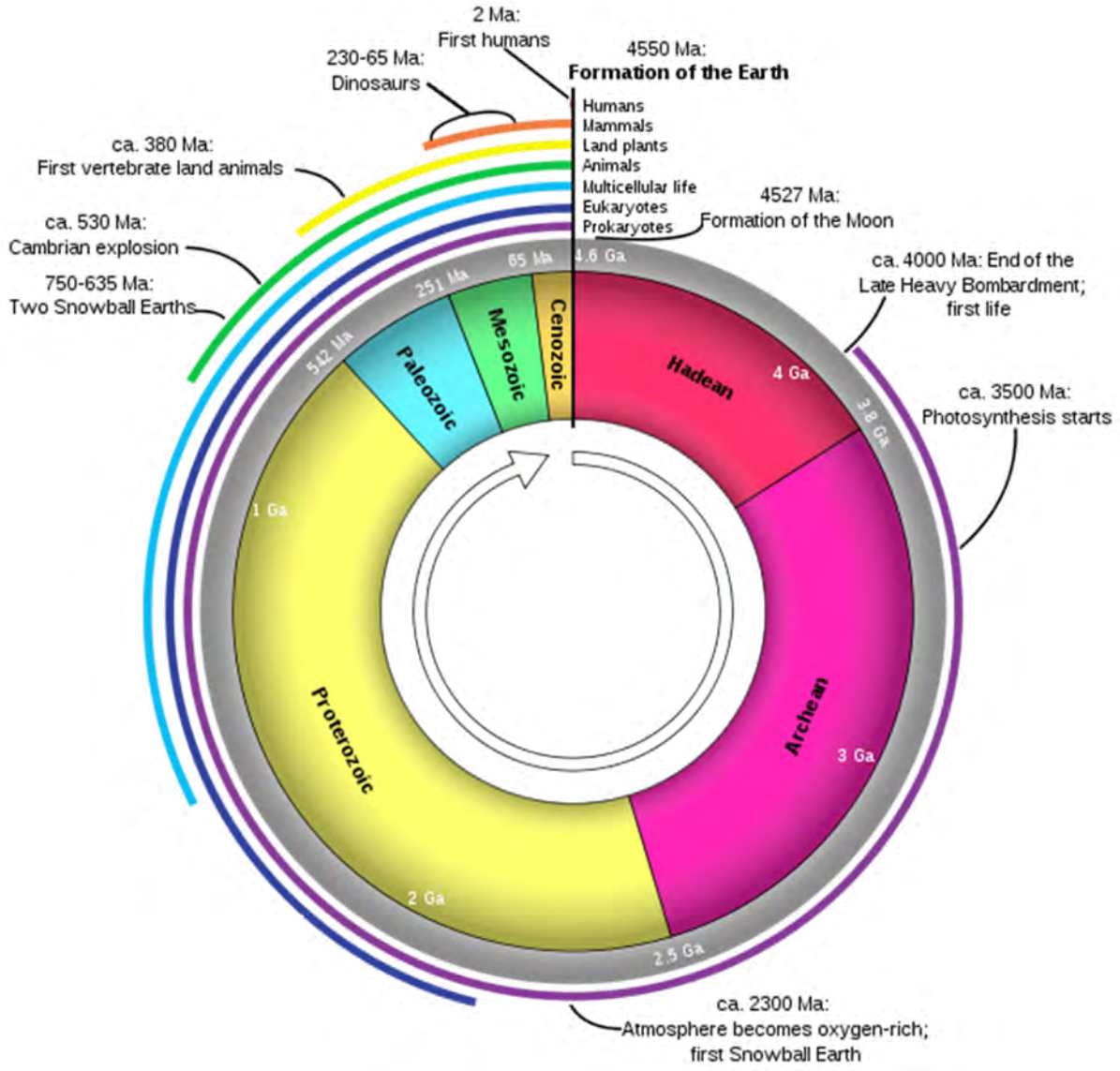

Figure 9.2 The geological clock – a summary of the history of the Earth. Time is represented as the angle measured clockwise from the topmost point. The different geological eons (Hadean, Archean and Proterozoic) and the Eras of the Phanerozoic Eon (Paleozoic, Mesozoic and Cenozoic) are named and are shown in different colours. (Ga=Gigayear = 10^9 years, Ma=Million years =10^6 years) (Source https://commons.wikimedia.org/wiki/File:Geologic_Clock_with_events_and_periods.svg).

The first life is thought to have appeared during the late Hadean Eon around 4 Ga ago. It appeared on Earth in the form of single cell bacteria (prokaryotes). Other single cell bacteria (such as cyanobacteria) evolved. These were able to fix carbon and nitrogen and produce oxygen by photosynthesis. The population of the Earth by such bacteria was to be so successful that the oxygen concentration became large enough to be significant. Oxygen is very chemically active and it began to kill off the bacteria by oxidation processes. The presence of oxygen in significant concentrations was therefore anathema to the carbon dioxide loving bacteria. In consequence it led a mass extinction of this life-form by about 2.3 Ga ago, the first known mass extinction of life on the Earth. This is sometimes known as the oxygen catastrophe. In addition the oxygen reacted with the atmospheric methane, a strong greenhouse gas, greatly reducing the latter's concentration. This is thought by some geologists to have triggered a "snowball Earth" condition i.e. a long glacial period during which the entire planet became ice-covered. Figure 9.3 shows estimates of the oxygen concentration in the atmosphere against time.

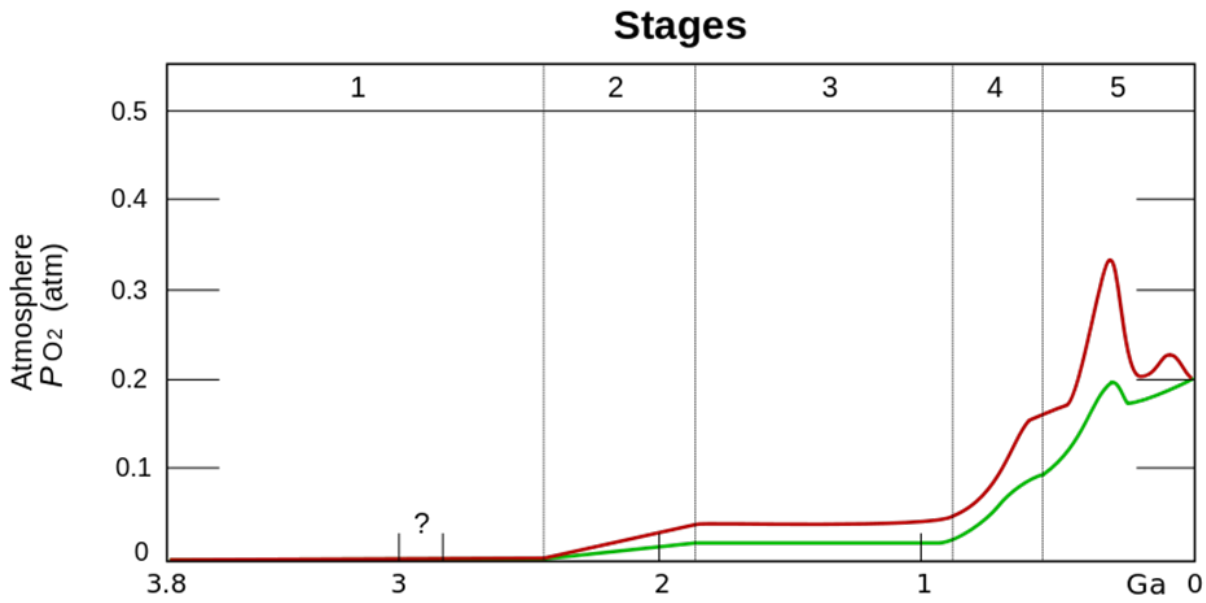

Figure 9.3 Estimates of the oxygen fraction of the atmosphere against time (1 Ga= 10^9 years). The red and green curves represent the range of the estimates. Stage 1 roughly represents the Hadean Eon, stage 2 the Archean, stage 3 the Proterozoic and Paleozoic, stage 4 the Mesozoic and stage 5 the Cenozoic Eons (Holland 2006, published under the Creative Commons Share Alike).

The origin of life on the planet 4 Ga ago is unknown. One theory (due to Hoyle and Wickramasinghe 1981) is that it was extra-terrestrial in origin, being brought to Earth by meteorites and comets at the time of the late heavy bombardment. Another theory is that life began in the soup of volcanic gases aided by spark discharges such as those in thunderstorms. Indeed the production of amino acids and RNA from spark discharges in gases was demonstrated in laboratory experiments (Miller and Urey 1959). It was suggested (Erlykin and Wolfendale 2010) that such violent storms could have been triggered by a near-Earth supernova explosion. A further possibility is that life originated in sources of volcanic activity such as in the region of the black smokers found today at mid-ocean ridges (Lane 2009).

Single cell bacteria such as prokaryotes continued to inhabit the Earth until approximately 2.5 Ga ago when multicellular organisms appeared. Multicellular organisms would eventually evolve into animal life by roughly 700 Ma ago. This marked the onset of the Phanerozoic Eon which finally arrived approximately 550 Ma ago.

During these eons continental drift due to plate tectonic activity caused the land masses of the Earth to pass through a series of super continents. The configuration of these bore no resemblance to today's continents. Eventually the supercontinent Pangea formed out of which today's continents evolved.

9.4 THE PHANEROZOIC EON STARTING ABOUT 540 MILLION YEARS AGO

The first animal life appearing some 700 Ma ago consisted mainly of oceanic creatures. However, the oxygen level in the atmosphere increased allowing the ozone layer around the Earth to form, protecting the land area from the fierce short wave ultra-violet light from the Sun. This allowed the land animals to evolve starting roughly 300 Ma ago.

Plate tectonic activity continued during all this time. Around 300 Ma ago the land mass was contained in the single continent, Pangea. This, under the influence of plate tectonics, split into the continents we see today. These drifted apart until the map of today's World eventually is recognizable (see figure 9.4, Dacey 2012). The first vertebrate animals appeared on Pangea around 380 Ma ago. These would evolve into mammalian life roughly 230 Ma ago.

The first humanoid creatures appeared around 6 Ma ago evolving eventually into our species (homo sapiens) a mere 200000 years ago (Lockwood 2007).

The sequence of continental drift from Pangea to the present World is summarised in figure 9.4.

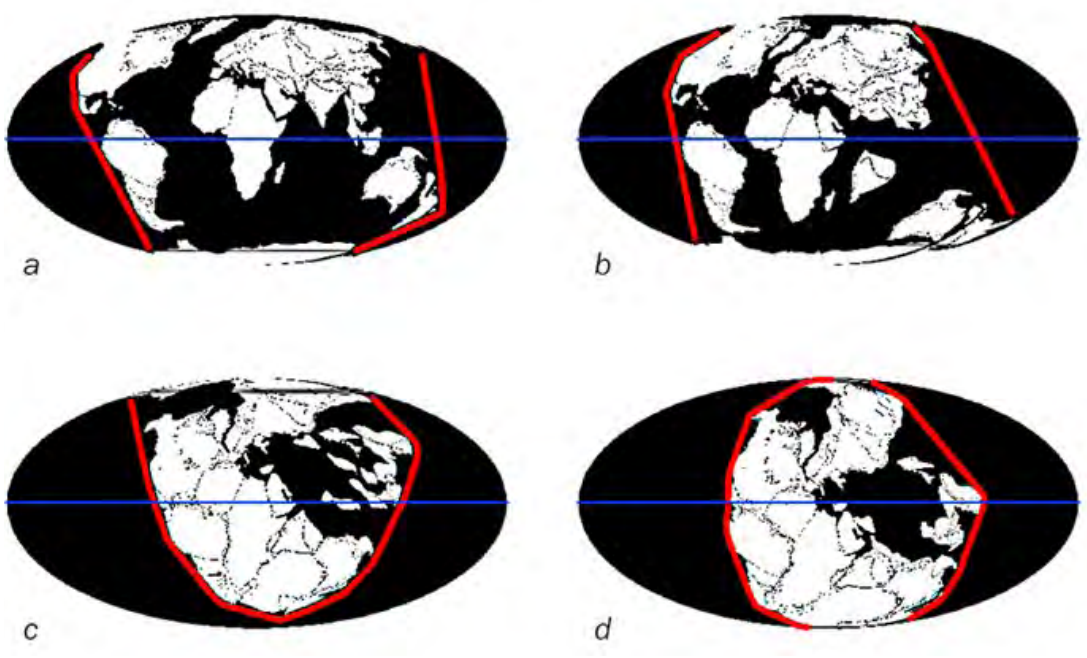

Figure 9.4 Evolution of today's Continents from the supercontinent Pangea over the last 260 Ma; a) as at present, b) 65 Ma ago c) 200 Ma ago and d) 260 Ma ago (Petrelis et al 2011) (For an instructive animated movie illustrating this evolution see C.R. Scotese https://www.youtube.com/watch?v=grMwSUBZZis).

The last 500 Ma or so are much better understood than the early Earth because of the more frequent occurrence of identifiable rocks and presence of fossils from the animals which emerged after the Cambrian explosion of life. It is this explosion of life which marks the beginning of the Phanerozoic Eon. During this time the CO_2 level in the atmosphere is thought to have fallen reaching today's level about 1 Ma ago. This is illustrated in figures 9.5 and 9.6 which show estimates of the temperatures and CO_2 throughout this period.

It is clear that the climate went through many different changes during this period with some periods when the Earth was completely ice-bound (snowball Earths). The cause of this is largely unknown. The Earth is thought to have recovered from these because of volcanic activity and dark algae in the snow allowing sunlight to be absorbed.

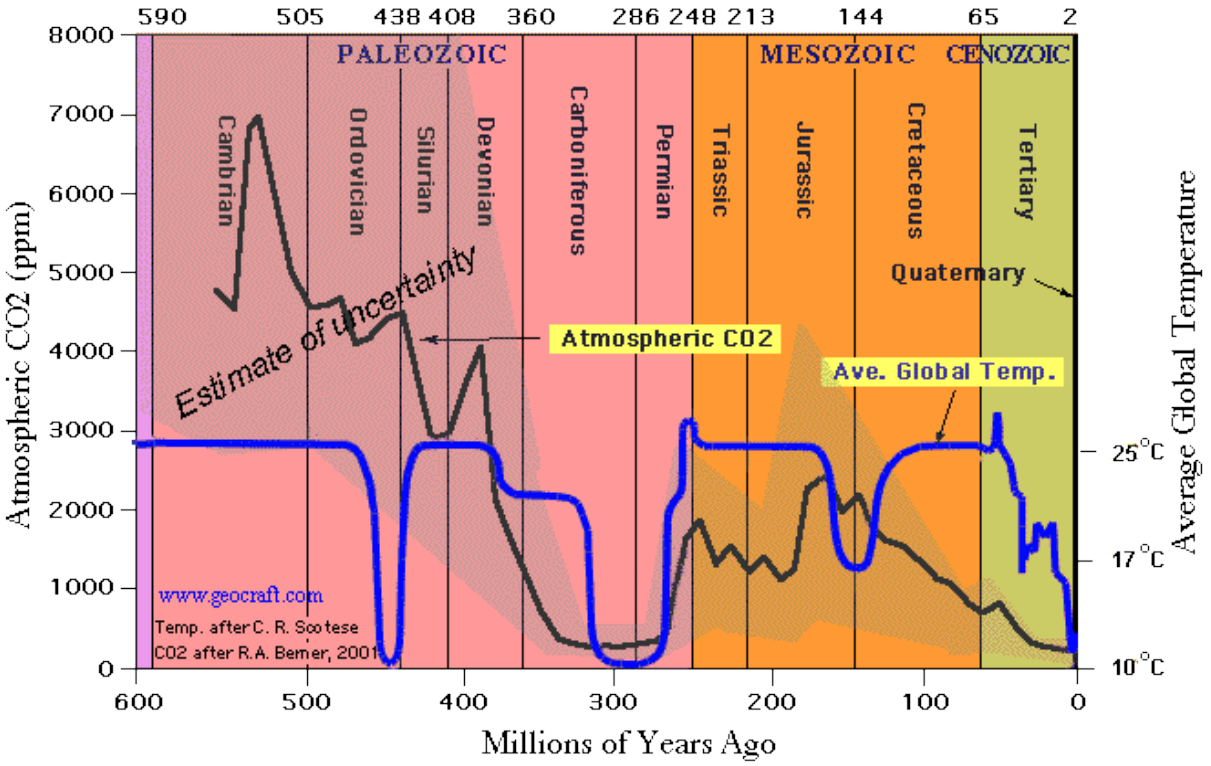

Figure 9.5. The CO_2 concentration of the atmosphere during the Phanerozoic Eon plotted against time (black curve, the lightly shaded area about the curve shows the uncertainty) as derived from the geological record. The blue curve shows an estimate of the mean surface temperature of the Earth. The 3 Eras are in upper case while the geological periods are in lower case letters. Note that the boundary ages have been slightly modified in recent years. (CO_2 from Berner and Kothavala 2001, temperatures from C.R. Scotese et al 1994).

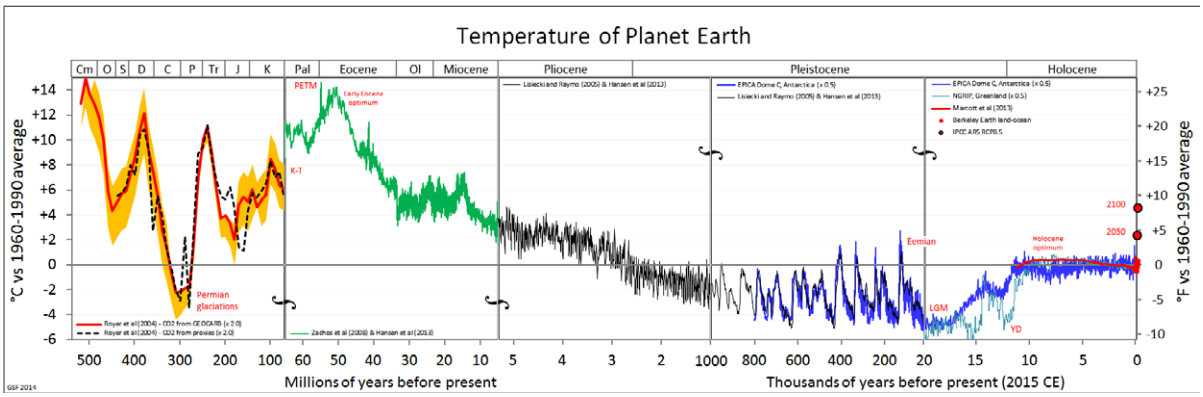

Figure 9.6 shows estimates of the global temperatures against time for the last 500 million years. The data back to 3 Ma ago come from coring techniques and are more certain than the earlier data (Author Glen Fergus, https://en.wikipedia.org/wiki/Geologic_temperature_record. available under Creative Commons Share Alike License).

9.5 THE LAST SEVERAL MILLION YEARS

The most recent geological era, the Cenozoic era, dates from 65 Ma ago. The general trend of the global temperature during this era has been cooling (see figure 9.6) with interruptions from ice ages during the last 1 Ma. The falling temperatures allowed the development of the ice sheets. The first Southern hemisphere ice sheets grew on Antarctica around 34 Ma ago. These are thought to have arisen from a variety of circumstances such as the falling level of CO_2 in the atmosphere (figure 9.5), isolation of the Antarctic continent due to continental drift and the uplift of its mountains. The first Northern hemisphere ice sheets appeared around 8 Ma ago with full development during the last 2.5 Ma, known as the Quaternary Period. This Period is associated with glacial-interglacial cycles which match the variations of the level of CO_2 in the atmosphere within the range 180–380 ppm. The upper level has now been exceeded due to the burning of fossil fuels (Lowe and Walker 2015).

The use of isotope ratios in sediments and in ice cores gives a good record of the climatic conditions during the Cenozoic Era and the Quaternary Period, better than was possible at earlier times. The ^{2}H and ^{18}O isotopes have proved extremely useful for the study of the climate of the Earth during this era. These isotopes are present in traces of 150 ppm (see endnote 4 page 202) and 2000 ppm, respectively, in water compared to the dominant isotopes ^{1}H and ^{16}O. The rates of evaporation and condensation for molecules of water containing the trace isotopes are slower than those containing the dominant isotopes since they have slightly heavier nuclei. Furthermore these rates are temperature dependent. Hence measurement of these isotope concentrations provides a proxy for temperature at the time a sample was laid down.

9.5.1 ICE CORES

As a result of the temperature dependence of the condensation process, during colder times, precipitation in the Earth's polar regions contains slightly more ^{18}O and ^{2}H than in warmer times. The trace elements are then locked in the polar regions by successive snowfalls and can be recovered at present times by taking core samples. The depth in the core gives the time at which the snow was deposited. Ice cores in the Antarctic have been taken down almost to the bedrock (depth 3.2 km) and the deepest (EPICA) covers a time range of 800000 years. Unfortunately, in the Northern hemisphere the Arctic is ocean and the only land mass which preserves the ice is Greenland. Cores have been taken here but the 3 km depth covers a shorter time than in the Antarctic.

Figure 9.7 shows an ice core illustrating the stratification.

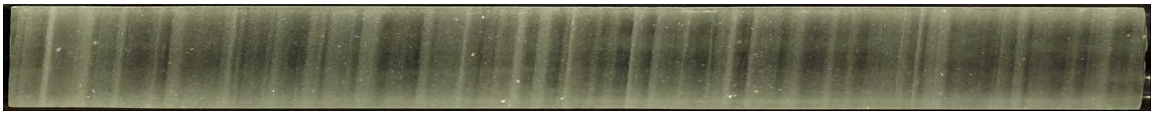

Figure 9.7 A section of the GISP2 ice core at depth 1837 metres showing the yearly stratification from snowfalls. This stratification disappears at greater depths due to the great pressure which causes the flow of ice. At these depths the age has to be estimated using a variety of techniques (GISP = Greenland Ice Sheet Project, photograph in the public domain, provided by the US Geological Survey).

Once the ice core has been retrieved it is carefully cut into sections which are preserved and transported to a laboratory where precise measurement of the isotope concentrations are made by mass spectrometry. The temperature dependence has been studied in laboratory experiments so that the concentration of the isotopes in the ice cores can be used as a proxy for the surface temperature measurements at the time. In this way temperature against time can be determined.

The results from two ice cores taken in the Antarctic known as Vostok (Petit et al 1999) and EPICA (Augustin et al 2004) are shown in figure 9.8. The changes in ^{2}H and ^{18}O concentrations labelled δD and $\delta^{18}O$ as a function of time before the present (right hand side) are shown. Note that increasing δD and $\delta^{18}O$ is vertically downward corresponding to decreasing temperature with lowest temperatures roughly 10°C cooler in the depths of an ice age than in the warmer periods. The cold periods correspond to ice ages and the warmer periods are known as interglaciations.

As well as the concentrations of ^{18}O and ^{2}H isotopes, the concentration of CO_2 and dust were measured. However, there will be some diffusion of gaseous isotopes such as CO_2 which causes some uncertainty in the age of a sampled gas.

The increased dust concentrations at the end of each ice age is thought to be caused by the reduced sea level revealing large sandy areas which fuel dust production during storms. At the height of the ice ages the sea level was approximately 120 metres lower than today due to much of the water being locked up in ice.

Figure 9.9 shows a comparison of the temperature as measured from the GISP2 ice core taken in Greenland in the Arctic and the Vostok ice core taken in the Antarctic. The Arctic data are limited in time range due to the more rapid transfer of ice out of the ice sheet. The temperature swing in the Arctic during the last ice age is roughly double that in the Antarctic and seems to be less smooth with short spikes of warmth occurring from time to time. Note the stability in the temperatures after the ice age ended about 12000 years ago. Hence in the ice ages the average global temperature was 10–20°C lower than today.

At the height of the last ice age (18–20000 years ago) approximately 30% of the Earth's land surface was ice-covered, including much of northern Eurasia and North America. The Earth emerged from this ice age by about 10000 years ago although ice sheets in Scandinavia and North America lingered on after this date.

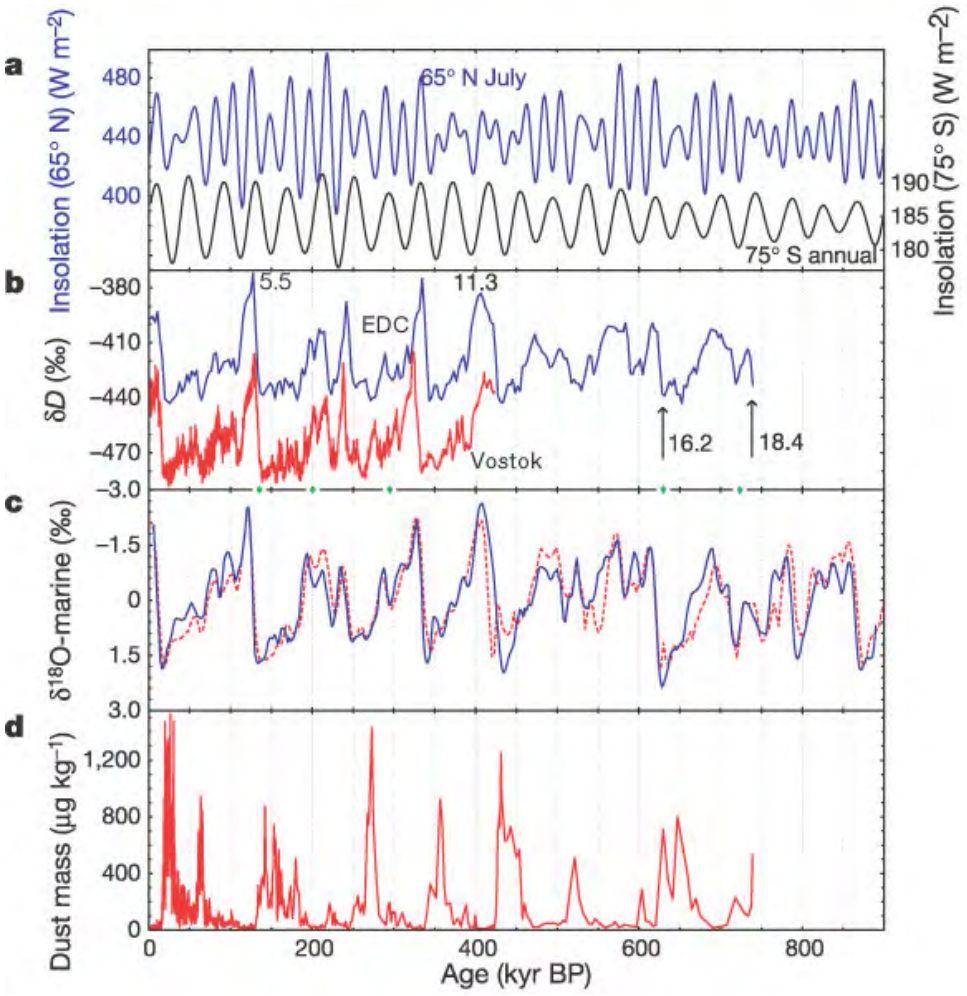

Figure 9.8 The change in concentrations of the trace isotopes $\delta^{18}O$ and δD as a function of time (recovered from the depth in the core) (EPICA, Augustin et al 2004, and Vostok, Petit et al 1999). The upper panel shows the calculated insolation (solar energy input to the Earth) against time at latitude 65 degrees North and 75 degrees South computed from the Milankovich cycles (see below). The red curve in the lower panel shows the variation in the dust content in the core with time.

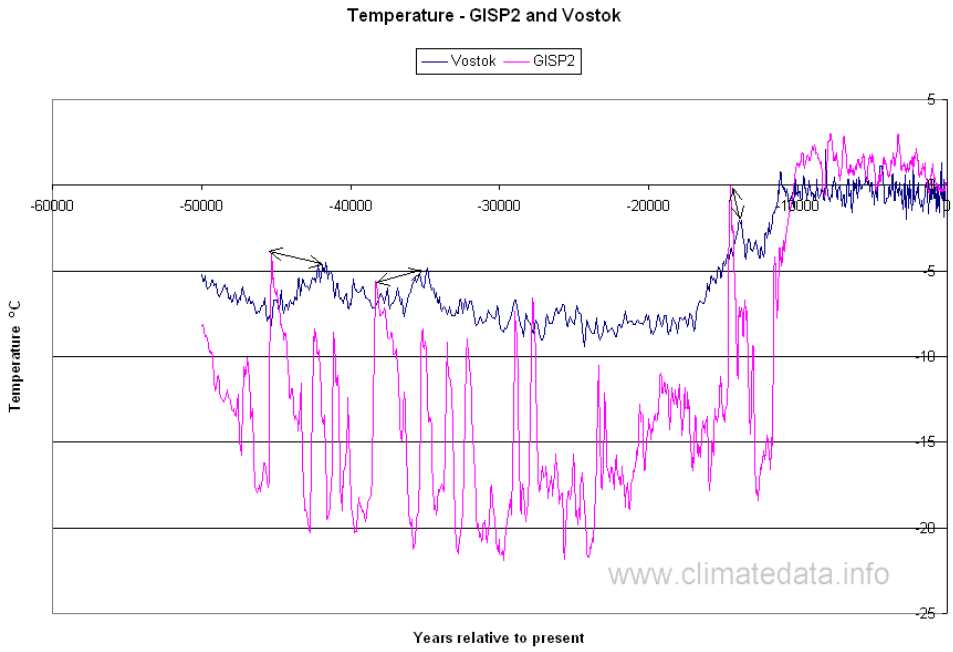

Figure 9.9 Comparison of the temperature variation in the last ice age in the Arctic (red, GISP2) and Antarctic (blue, Vostok) (Figure from www.climatedata/info/proxies/ice-cores/ data available from NOAA at https://www.ncdc.noaa.gov/paleo/study/2450, see Blunier and Brook 2001).

9.5.2 THE ICE AGES

During the last million years or so the climate seems to have oscillated between an ice age state and an interglacial state (see figure 9.8) with interglacials occurring approximately every hundred thousand years (Lowe and Walker 2015). This is thought to have been produced by small changes in the Earth's orbit known as Milankovitch cycles (for a history see Lee J. 2012). The three features of the Earth's orbit which are thought to influence the ice ages are shown in figure 9.10. These features cause changes to the solar energy falling on the Earth (known as insolation).

The first feature is the ellipticity of the Earth's orbit around the Sun which is not perfectly circular. It currently has ellipticity $e = 0.017$ where ellipticity, more usually termed eccentricity, is defined as $e = (r_a - r_b)/(r_a + r_b)$. Here r_a and r_b are the orbit radii at apogee (maximum radius) and perigee (minimum radius), respectively. The eccentricity varies with time as shown in figure 9.11. The second feature is the tilt angle of the Earth's axis to the plane of the orbit, known as the obliquity of the ecliptic. This is currently at an angle of $23.5°$ but varies from $21.5°$ to $24.5°$ with a period of 41000 years. The third feature is the precession of the Earth's axis which shows periodicities of between 19000–24000 years. The upper panel of figure 9.8 shows how the solar insolation varies at two different latitudes under the influence of these features.

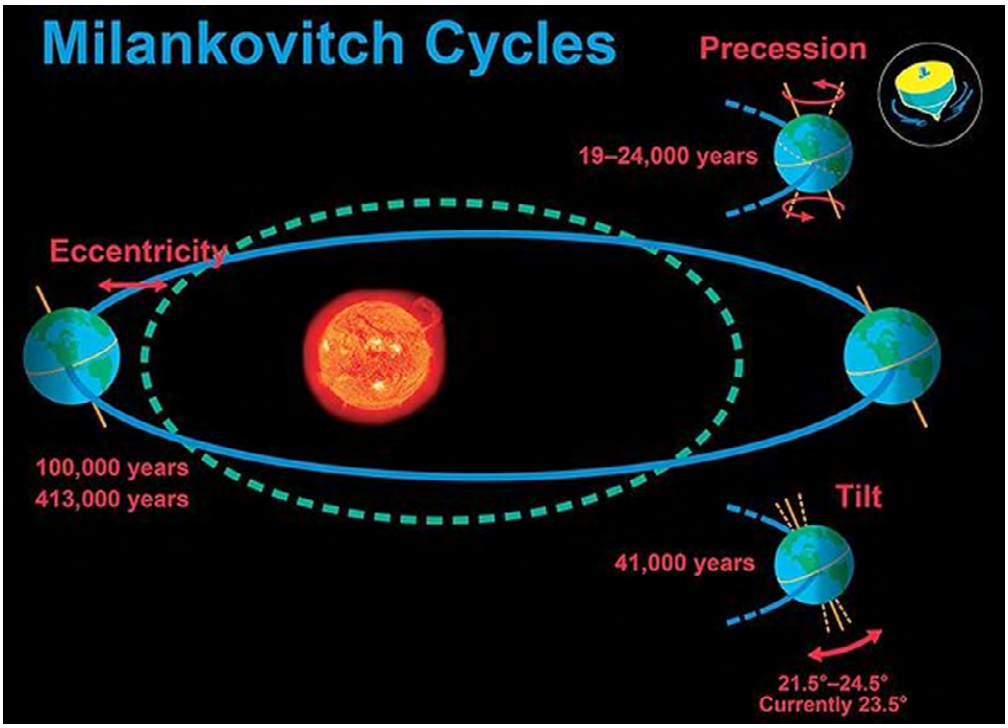

Figure 9.10 The features of the Earth's orbit which affect the climate. These are the ellipticity, the precession and the tilt angle of the Earth's axis which each vary roughly harmonically with the periods shown in the figure (Image available under the Creative Commons Share-Alike License).

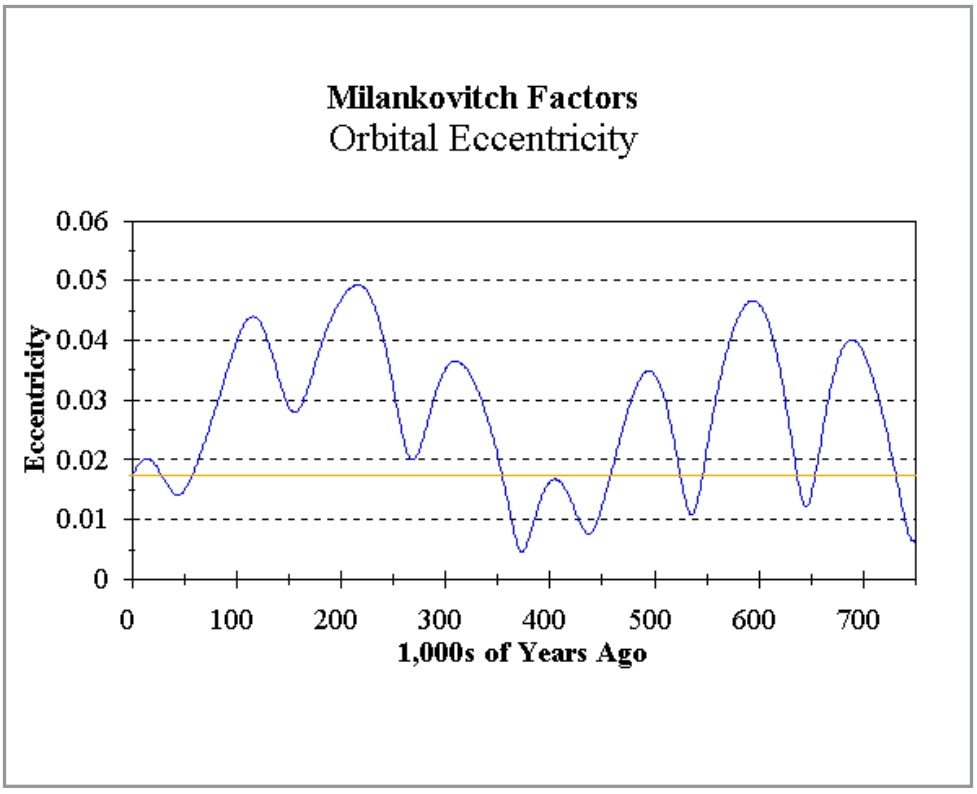

Figure 9.11 Graph showing the variation of the eccentricity of the Earth's orbit as a function of time (source source of data Berger and Loutre 1991and graph available from http://www.museum.state.il.us/exhibits/ice_ages/eccentricity_graph.html). The yellow line shows the current eccentricity.

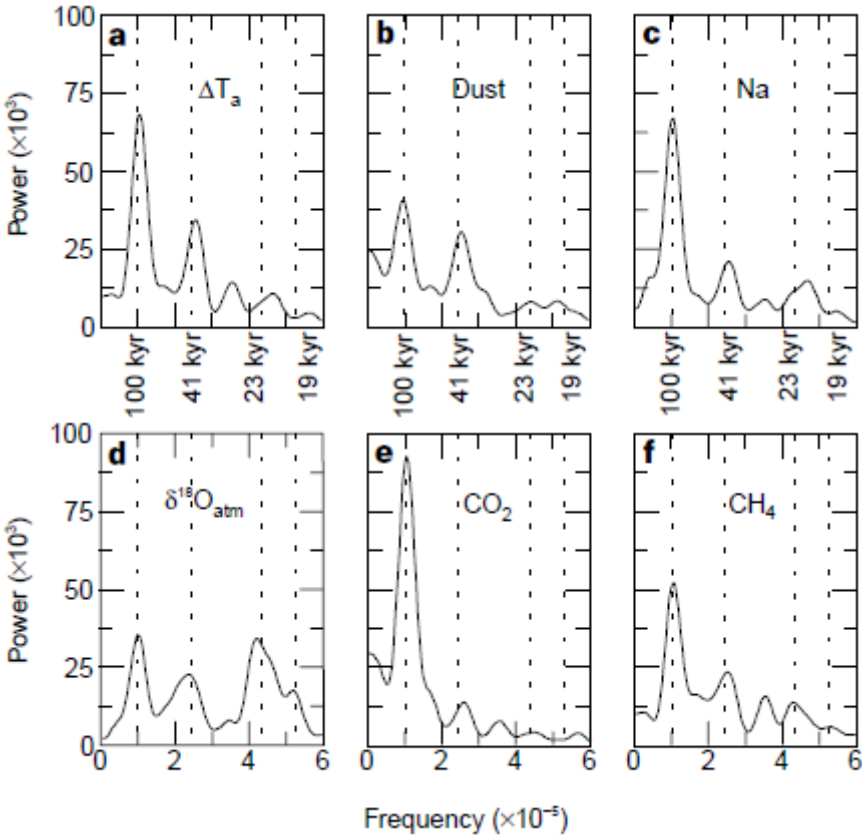

Figure 9.12 Periodograms obtained from a Fourier analysis of the Vostok Antarctic ice cores (Petit et al 1999). The peaks at periods of 100kyr and 41kyr correspond to those expected from the periodicities in the ellipticities and tilt angles. The fainter peaks around periods of order 20 kyr (1kyr=1000 years) are to be expected from the precession periodicity. What is thought to happen is that to enter an inter-glacial period the summer melting is greater than the winter freezing so that gradually over an order of ten thousand years the ice recedes to the polar region. The process proceeds in reverse at the onset of an ice age. Precisely why some peaks in the insolation (see figure 9.14) create an inter-glacial and others do not is unknown. One suggestion is that on some of the peaks the fresh water from melting ice causes a slow-down of the ocean currents leading to an increase in tropical warming. This brings a large release of CO2 as the tropical ocean warms.

The evidence that these features play a significant role in the formation of ice ages comes from a Fourier analysis (see Appendix A9) of the temperature data shown in figures 9.8. These show the periodicities of the Milankovitch cycles, see figure 9.12.

It is thought that small changes in insolation cause the ice to creep towards the Equator of the Earth gradually year by year until we have an ice age. However, it is not clear what features of the change in insolation (fig 9.8 top panel) cause such a change (lower panels of figure 9.8). As a result it is difficult to predict when the next ice age will occur. This would be possible if we had a good understanding of the cause of the observed ice ages. Perhaps the fact that the ice ages were not so intense before 1 Ma ago (see below) could be explained by the stimulation of the Milankovitch cycles by the gravitational interaction with our larger neighbouring planets, Jupiter and Saturn. A full and convincing explanation of the cause of ice ages awaits an inspired idea.

9.5.3 SEDIMENT CORES

The trace elements ^{18}O and ^{2}H are absorbed from the water and locked during calcification in the shells of benthic foraminifera (bottom-living sea creatures) or in those of surface-living plankton. When these creatures die their shells form part of the sediment on the ocean or lake bottom. The trace elements calcify into the shells during the creatures' life time at a rate which is temperature dependent and so analysis of the shells allows the temperature history to be traced. The sediment layers build up with time storing the history which can be recovered at present times by taking core samples. The position in the core again gives the date of a sample and the trace element concentration the temperature at the time of the sample. Again the trace element concentrations are measured precisely using modern mass spectrometry techniques.

Figure 9.13 shows the results of 57 deep sediment cores analysed by Lisieck1 and Raymo 2005. The ice ages, readily discernible in the ice core data during the last million years, seem to die out at earlier times and the temperature increases by of order 10 degrees C by 4 million years ago.

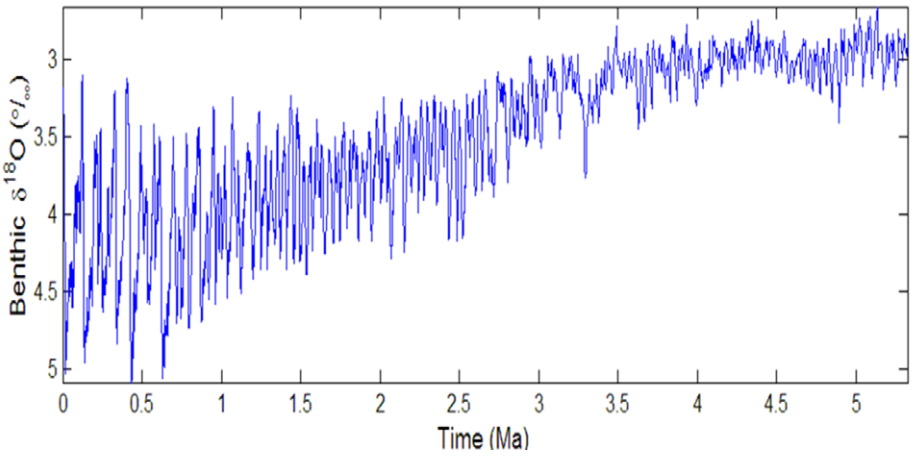

Figure 9.13 Temperature as a function of time over the last 5 million years. The oscillations which characterise the ice ages seemed to die out at ages greater than 1 million years (Lisiecki and Raymo 2005, figure by kind permission of L. Lisiecki).

Further information on the Quaternary Period comes from the terrestrial record of landforms and sediments. Moraines and glaciofluvial deposits are ordered chronologically and dated by radiometric techniques. A recent development has been the application of cosmogenic radionuclide dating of rocks. This allows the determination of the age of a bedrock surface or glacial erratic rock since it was first exposed to cosmic rays. However, the terrestrial record is generally incomplete as successive ice sheet expansions tend to destroy evidence of earlier glacials and interglacials (Hambrey and Harland 1981).

9.5.4 TEMPERATURE DURING THE LAST 12000 YEARS SINCE THE LAST ICE AGE

Figure 1.1 shows the average temperatures during the last 2000 years in both Northern and Southern hemispheres as well as the global average. The data show a small cool period around 1600 which has become known as the "Little Ice Age". The mean temperatures at that time were about 1°C lower than today. Around 1000 years ago the mean temperature was of order 0.7°C lower than today. This has become known as the "Medieval Warm Period".

A recent study of sediment cores (Marcott et al 2013) extends these temperature reconstructions to the end of the last ice age 12000 years ago (the graph is available at http://cdn.theatlantic.com/static/mt/assets/science/marcott-B-CD.jpg). This reconstruction is compatible with those in figure 1.1 for the last 2000 years. It goes on to show that the mean global temperature increased by roughly 0.7°C going further back in time from 2000 to 6000 years. This shows that the mean temperature in Old Testament biblical times 6000 years ago was similar to that we measure today. Going further back in time, the temperature then remained roughly constant until the descent into the last ice age 12000 years ago. Thus in the time since the last ice age we have had a relatively stable climate with mean temperature changes of from 0 *to* 1°C lower than today's temperature.

This stable climate has allowed mankind to develop from being a hunter-gatherer to the civilisations of the modern World.

9.6 CONCLUSION

We have seen that the Earth has been through many periods when the climate was very different from that of today. Since the end of the last ice age 12000 years ago the climate has been rather stable. This has allowed mankind to flourish, to develop from a stone age existence into today's civilisations and with them their towns and cities and all the culture that comes with this. It remains to be seen if our modern civilisation will be able to cope with the changes predicted if the burning of large quantities of fossil fuels is to continue with its attendant expected global warming.

In 2015 the Paris Agreement was reached by the Governments of the World. This is an agreement within the United Nations Framework Convention on Climate Change (UNFCCC) to limit greenhouse gas emissions so that the resulting global warming would be kept to below 1.5°C. This is less than the 2°C beyond which climatologists believe that the climate change resulting from global warming will be dangerous. Continued unlimited burning of fossil fuels is expected to lead to average temperature increases of from 3 to 5°C by the year 2100.

APPENDIX A9.1 FOURIER ANALYSIS

The Fourier theorem states that any continuous periodic function, $f(t)$, can be expressed as a the sum of a series of cosine and sine terms as follows

$$f(t) = \sum_{n=0}^{\infty} c_n \, e^{in\omega_n t} \tag{A9.1}$$

where $e^{-inw_n t} = \cos n\omega_n t + i \sin nw_n t$ and the c_n are complex coefficients containing the phase and amplitude information for the angular frequency ω_n and the n are integers. The summation runs from $n = 0$ to ∞. To avoid complications with the term corresponding to n=0 it is usual to subtract the average of the data set from every value. The values of the coefficients c_n are obtained by multiplying both sides of equation A9.1 by $e^{-inw_n t}$ and integrating i.e.

$$\int_0^T f(t) \, e^{-in\omega_n t} \, dt = \lim_{T\to\infty} T \, c_n. \tag{A9.2}$$

Here we are using the fact that $\int_0^{\infty} e^{-in\omega_n t} \, e^{im\omega_m t} dt = \lim_{T\to\infty} T \, \delta_{mn}$ where δ_{mn} is the Kronecker delta function and T is the time over which the integral is computed. In practice data sets never cover infinite times and the computed Fourier coefficients, c_n, are approximations.

Suppose the function is defined in the range $0 < t < T$, we can calculate the approximate Fourier coefficients by making the assumption that the function is either zero outside the defined range or it is periodic. We change the variables in the exponents to $2\pi t/T$ in equation A9.1 which then becomes

$$f(t) = \Sigma_{n=1}^{\infty} c_n e^{in\omega_n 2\pi t/T}. \quad \text{(A9.3)}$$

And the coefficients as defined in equation A10.2 become

$$c_n = \frac{1}{T}\int_0^T f(t)\, e^{-in\omega_n 2\pi t/T} dt. \quad \text{(A9.4)}$$

We define the Fourier transform of the function *f(t)* as $g(\omega)$ as

$$g(\omega) = \int_0^{\infty} f(t)\, e^{-i\omega t} dt \quad \text{(A9.5)}$$

If we define $\omega = n\omega_n 2\pi/T$ we see that $Tc_n = g(\omega_n)$. Here to cover the range to infinity we integrate outside the defined range where we have defined *f(t)* to be zero, i.e.

$$f(t) = T\Sigma_{n=1}^{\infty} g(\omega_n) e^{i\omega_n t}.$$

Hence, the Fourier transform can be used to reconstruct the function from the Fourier coefficients in both amplitude and phase. The square of Fourier coefficient represents the power at that frequency.

Some practical points should be noted. To minimise spurious peaks it is advisable to compute the Fourier transform over an integer number of periods of the frequency ω. This avoids spurious contributions to the integrals from fractions of periods. In noisy data it is advisable to take as wide a time range as possible to average the noise. In binned data if some bins are missing they should be filled by a guess e.g. the previous value or an average value.

In any Fourier analysis random peaks appear in noisy data such as in climate analyses. The significance of a peak should be judged by the probability that the peak will be generated randomly by the noise. This can be deduced as follows.

We assume that the real and imaginary parts of the noise follow Gaussian distributions with standard deviations σ. Hence the probability to obtain a peak with amplitudes *R* and *I* in the real and imaginary parts is

$$P(R)dR = \frac{1}{\sigma(\sqrt{2\pi})} e^{-\frac{R^2}{2\sigma^2}} dR \quad \text{and} \quad P(I) = \frac{1}{\sigma(\sqrt{2\pi})} e^{-\frac{I^2}{2\sigma^2}} dI$$

Hence the probability to obtain the values R and I is the product of these

$$P(R,I) = \frac{1}{2\pi\sigma^2} e^{-\frac{R^2+I^2}{2\sigma^2}} dRdI$$

Now $R^2 + I^2 = A^2$ where is the total amplitude of the peak and $dRdI = Ad\theta\, dA$ where θ is the phase angle. The latter becomes $2\pi AdA$ when integrated over the phase θ. Hence the probability to produce and peak of amplitude A is

$$P(A)dA = \frac{A}{\sigma^2} e^{-\frac{A^2}{2\sigma^2}} dA.$$

The statistical significance of a peak can then be judged from the probability to obtain a peak larger than the one observed. This is given by

$$P(A' > A) = \int_A^\infty \frac{A}{\sigma^2} e^{-\frac{A^2}{2\sigma^2}} dA = e^{-\frac{A^2}{2\sigma^2}} \quad \text{(A9.6)}$$

Conventionally the 95% confidence range on any measurement is quoted. The value of A for which $P(A' > A) = 0.05$ is sometimes used to define the statistical significance of a Fourierpeak. However, in any Fourier analysis if N frequencies are sampled then there will be $0.05N$ peaks which appear randomly and appear to have 95% confidence level significance. Hence, care must be applied in judging the statistical significance of any Fourier peak.

References

Augustin L. et al 2004, EPICA Collaboration, "Eight glacial cycles from an Antarctic ice core", Nature 429, pp. 623–628.

Berger A. and Loutre M.F. 1991, "Insolation values for the climate of the last 10 million years" Quaternary Science Review volume 10, pp. 297–317.

Berner R.A. and Kothavala Z., 2001 "GEOCARB III a revised model of atmospheric CO2 over Phanerozoic time", American Journal of Science volume 301 (2), pp. 182–304.

Blunier T. and Brook E.J. 2001, "Timing of millennial scale climate change in Antarctica and Greenland during the last glacial period", Science volume 291 pp. 109–112.

Dacey J. 2011 "Continents may reflect conditions in the Earth's core", Physics World, Oct 2011, published by the Institute of Physics.

Erlykin A. and Wolfendale A.W. 2010, "Long term variability of cosmic rays and possible relevance to the development of life on Earth", Surveys in Geophysics, volume 31 page 383, also available at arxiv.org/pdf/1003.0082.

Hambrey M.J. and Harland W.B. 1981 in "The Evolving Earth" published by The British Museum (Natural History), Cambridge University Press, edited by L.R.M. Cocks, ISBN 0 521 28229 2.

Holland H.D. 2006 "The oxygenation of the atmosphere and the oceans", Philosophical Transactions of the Royal Society B volume 361 pages 903-915. Doi:10.1098/rstb.2006.1838.

Hoyle F. and Wickramasinghe N.C. (1981) "Evolution from Space" (Simon and Schuster Inc. N.Y. and J. Dent and Son, London).

Lane N. 2009, "Life Ascending" Profile Books, London. ISBN 978 1 86197 848 6.

Lee, J. (2012), Milankovitch cycles, http://www.eoearth.org/view/article/154612.

Lisiecki L.E. and Raymo M.E. 2005 "A Pliocene-Pleistocene stack of 57 globally distributed benthic δ^{18}O records", Paleoceanography vol. 20 PA1003 doi:10.1029/2004PA001071.

Lockwood C. 2007, "The Human Story", published by the Natural History Museum, London. ISBN 13 978 0 565 09214 6.

Lowe J. and Walker M. 2015, "Reconstructing Quaternary Environments", Third Edition published by Routledge, Abingdon UK and New York, USA. ISBN 978-0-131-27468-6.

Mann et al 2008, "Proxy-based reconstructions of hemispheric and global surface temperature variations over the past two millennia", Proceedings of the National Academy of Sciences USA vol. 105 (2008) number 36 pp. 13252–13257.

Marcott S.A., Sharlem J.D., Clark P.U. and Mix A.C., 2013, "A Reconstruction of Regional and Global Temperature for the Past 11300 years", Science vol. 339 pp. 1198–1201.

Miller S.L. and Urey H.C. 1959 "Organic compound synthesis on the primitive Earth", Science vol. 130 pp. 245–51.

Petit J.R. et al., 1999 Vostok Collaboration "Climate and atmospheric history of the past 420000 years from the Vostok ice core, Antarctica", Nature vol. 399, pp. 429–436.

Petrelis F., Besse J. and Valet J-P., 2011, "Plate tectonics may control geomagnetic reversal frequency", Geophysical Research Letters vol. 38 L19303.

Scotese C.R. et al, 1994, "Phanerozoic CO2 levels and global temperatures inferred from changing paleogeography", Geological Society of America Special Papers volume 288 pp. 57–74.

Exercises.

1. A planet accretes mass by material falling onto it so that it reaches a radius R. Show that the total energy gained from such falling material is $E = \frac{16\pi^2}{15} G R^5 \rho^2$ where ρ is the density of material (assumed to be approximately constant) and where G is the Newtonian Gravitational constant . Hence show that if the mean specific heat capacity is S Jkg^{-1}K^{-1} that the temperature rise, T, of the planet at birth is $T \approx 4\pi G R^2 \rho / 5S$, assuming that the formation time of the planet is short enough that heat losses can be neglected. Estimate the temperature rise of the Earth after it was formed. How accurate do you think that this estimate is? (Answer 10^4K)

2. Estimate the time it will take the Earth's crust to cool from a temperature of order 10^4K when it formed to a temperature of 300K. Assume that the main heat loss is from thermal radiation and that the Earth acts as a black body. (Mean density of the Earth is 5500 kg/m^3, radius=6350 km and its mean specific heat capacity is 4000 J kg^{-1}K^{-1}). (Answer 3 10^5 years)
3. As can be seen from problem 2 the Earth's crust cooled quickly to a temperature $\sim$300 K following its formation. In 1863 Kelvin assumed that the only contribution to the Earth's loss of heat from the core would be by thermal conduction. He then showed from the theory of thermal conduction that near the surface the rate of change of temperature with depth would be $\frac{dT}{dx} = a\, t^{-1/2}$ where t is the age of the Earth and is a constant. It was known at the time from measurements in mines that $\frac{dT}{dx} = 0.04$°C per metre. He deduced from this that the age of the Earth was 100 million years. What value of dT/dx would you expect from conduction alone knowing that the true age of the Earth is 4.5 billion years. Estimate the fraction of the geothermal energy coming from such conduction and from radioactivity in the Earth from these figures.
4. Discuss the merits and relative accuracy in the dating techniques described in this chapter.

10 THE INTERGOVERNMENTAL PANEL ON CLIMATE CHANGE (IPCC)

The Intergovernmental Panel on Climate Change (IPCC) was set up when it was first realised in the late 20th century that increasing greenhouse gas concentrations could lead to significant global warming and thereby man-made changes to the climate. In this chapter the method of working of the IPCC is described. The chapter is a summary of an article by Sir John Houghton (Houghton and Tavner 2013) published in The Times Newspaper on 15 March 2010. Sir John was a founder member of the IPCC and acted as co-Chairman of the Scientific Assessment Working Group from 1988–2002 (see also Houghton 2015).

10.1 INTRODUCTION TO THE IPCC

The IPCC was founded in 1988 by two UN agencies, the World Meteorological Organization and the United Nations Environment Programme. Its mandate is to produce accurate and balanced assessments about human-induced climate change. Because this is a topic with a broad scientific scope that concerns all nations, the IPCC has ensured that many hundreds of scientists from many countries and a wide range of disciplines contribute to its assessments.

About 70 scientists from around the world attended the first meeting of the Group at Nuneham Courtenay near Oxford early in 1989. The task was to scope and draw up an outline of the first report due in 1990 (see endnote 5 page 202). At the beginning there was no preconceived agenda regarding the conclusions. In fact, at the start, a number of the scientists present argued that insufficient was known about human induced climate change to produce any significant report. However, it was agreed that what was known with reasonable certainty should be identified carefully and estimates of the uncertainties made and that these should be distinguished from what was much more uncertain – a general formula that has been followed through all subsequent reports.

10.2 CLIMATE FORCINGS

The climate system consists of components generally identified as the atmosphere, ocean, ice, land and biosphere. It is a chaotic system with large natural variability due to interactions within the climate system on all scales of space and time. The smallest scales of variability, up to days or weeks in time, are known as weather. Climate is also subject to external forcings that bring about changes in the radiation balance at the top of the atmosphere – hence called radiative forcings. These can arise from natural causes such as variations in incident solar radiation (its amount or its distribution due to regular changes in the Earth's orbit), or volcanic activity (due to large amounts of aerosol that enter the atmosphere). Human induced forcing of climate arises from the greenhouse effect (known for over 200 years) of the main greenhouse gases – CO_2, CH_4, N_2O etc – as they change concentration and radiative forcing from anthropogenic aerosols (e.g. sulphate particles from power stations' emissions and black carbon from biomass burning etc).

10.3 COMPONENTS OF THE SCIENTIFIC TASK

The scientific task of the IPCC has five major components as follows.

1) Estimate human induced climate forcings and compare them in magnitude and scale with other external forcings and natural variability.
2) Address, through process studies allied with observations, effects on the climate system and its dynamics, of feedbacks, positive and negative, due to water-vapour, ice-albedo, clouds, ocean circulation, CO_2 fertilization, climate-carbon-cycle connections etc.
3) Add together the effects of all the radiative forcings, feedbacks, processes and dynamics through numerical computer modelling applied to all relevant time and space scales including simulations of past and present climate and projections of future climate.

4) Compare a wide range of model simulations from different modelling groups with the enormous range of observations that are available from past and present climates, and through these detailed comparisons, balance out the contributions to climate change from all external forcings together with their associated uncertainties.
5) Describe the likely future impact on human communities or ecosytems.

10.4 CLIMATE MODELLING

Commenting particularly on computer models mentioned in (3) and (4) above Sir John continued –

These are not empirical or statistical models attempting to extrapolate past climates. For the atmosphere they are based on integrations through time using the known dynamical and physical equations together with algorithms describing motions and phenomena on all scales that have been tested individually and collectively in a wide range of contexts. The models available for the first IPCC Report in 1990 were crude by comparison with models today that possess great sophistication and capability. Models provide a powerful means, in fact the only means, of adding together all the non-linear processes involved in the wide range of components included in (1) to (3) above. Models are tested as thoroughly as possible by comparison with observations of current climate, the climate of the 20th century, periods that include major volcanic eruptions and with past climates, including periods when changes in the Earth's orbit had altered the distribution of solar radiation at the Earth's surface. For the 20th century, for instance, agreement with observations can only be achieved when both natural and anthropogenic forcings are included (see figure 1.6).

Some of the parameters within models, for instance those concerned with clouds and aerosols, aspects of ocean circulation and ice dynamics, contain large uncertainties. Models provide a powerful tool to explore the sensitivity of climate to ranges of values of these and other parameters. Such changes are then included as numerical uncertainties.

10.5 THE 'BALANCING-OUT PROCESS'

The 'balancing-out' process, mentioned in (4) above, is key to the formulation of IPCC conclusions and is where the contribution of the IPCC process has been particularly crucial and effective. In preparing conclusions of individual chapters, taking into account the large number of review comments, meetings of lead authors debate at length the formulation of balanced conclusions on the most important issues, the numbers to be presented and the size of the uncertainties. A similar process occurs when the draft chapters are available and representatives of the chapters and other scientists meet to debate the conclusions of the overall Report. These debates are exciting occasions, long, thorough, even heated, but only scientific arguments are allowed – no influence from political or personal agendas can interfere. It is during these discussions that numerical values of probability are attached to uncertainties based on statistical analysis of model results together with judgements regarding other factors that the models do not include or address.

A key example of this balancing process concerns the best value of what is known as the climate sensitivity. This is defined as the increase in global average temperature associated with a doubling of atmospheric carbon dioxide. Unless severe mitigating action is taken such a scenario is likely to occur during the second half of the 21st century. The likely value of climate sensitivity has large relevance for consideration of the likely magnitude of impacts from climate change in the future. Relevant information regarding its value comes from observations of past climates (including the ice age period) and from model simulations. The IPCC 1990 report estimated its value as 2.5°C with an uncertainty range of 1.5 to 4.5°C. The largest uncertainty arises from the lack of knowledge of clouds, in particular the average magnitude of cloud-radiation feedback. Subsequent reports all gave detailed consideration to the value of climate sensitivity. The 1995 and 2001 Reports maintained the same best value and range as in 1990. The 2007 Report increased the best estimate to 3°C and reduced the range to 2.0 to 4.5°C, considering that evidence now makes it unlikely the value will be less than 2°C. The 2013 report AR5 presented a number of different estimates of the climate sensitivity depending on how the World decides to limit its emissions of greenhouse gases.

10.6 THE IPCC REVIEW PROCESS

Each chapter of an IPCC Report goes through three reviews before acceptance. The first is by a restricted number of expert scientists. For the second review, a general invitation to take part is sent to the international community of climate scientists and others with an interest (including industrial and 'green' NGOs) and the third review is by governments. The chapter authors consider all review comments, keep a record of them and of the actions taken for each comment. For the later IPCC Reports, during these review processes, each chapter's authors were assisted by a Review Editor chosen to be independent of the chapter authorship.

Finally, included in each IPCC Report is a Summary for Policymakers, the first draft of which is based on the chapters' summaries and prepared by a small group that includes a representative author from each chapter. It is then scrutinised sentence by sentence at an IPCC plenary meeting over a period of three or four days. Despite being a meeting of delegates from around 100 countries having a wide variety of political backgrounds (e.g. from oil-producing states like Saudi Arabia and Kuwait and also from some states with a strong 'green' ethos) it is a strictly scientific not a political meeting. Its purpose is to ensure that the Summary is clearly written, consistent, relevant to policy making and that it accurately represents scientific information without either under or overstatement. It provides an effective but very tough filter. In every case in Sir John's experience the meeting concluded with a Summary having greater clarity and accuracy than the version with which it began.

10.7 THE IPCC'S CAUTION

The IPCC has sometimes been accused of being alarmist in its conclusions. Others have complained that the IPCC has been too cautious. In general Sir John believes that the IPCC has come closer to the latter than the former – although the exposure of a mistake over the timing of disappearance of Himalayan glaciers is interpreted by some as suggestive of an alarmist attitude. For instance, the 1990 IPCC Report stated with some certainty that the increases in greenhouse gases were causing global warming but added that, because of natural climate variability, this warming could not be clearly detected in the observed record. As warming has continued at about the rate projected by the Reports, each subsequent Report has in general shown increasing confidence in its conclusions, but still retained appropriate caution. Further, the 2007 Report in estimating future sea level rise declined to make any estimate of the possible effect of accelerated melting of glaciers and ice sheets as it considered no reliable estimates were available in the literature at that time.

IPCC Assessments, because of their thorough process of preparation have been described as the most well researched and reviewed assessments carried out by the world scientific community. Because so many scientists and also governments are involved, the Reports possess a high degree of ownership by top scientific bodies and by governments.

10.8 THE IPCC REPORT AR5

Many hundreds of scientists contributed to the fifth assessment report, AR5, of the IPCC which was produced in 2013 and 2014. All papers relevant to the climate were reviewed before the report was released. There were three working groups (WG) each of which produced a long report. WG1 assessed the science, WG2 the socio-economic effects and the effects of adaptation to climate change. WG3 assessed the possibilities of mitigating the effects of climate change for example by limiting the production greenhouse gases. A Synthesis Report was then produced to provide an overview of the state of knowledge concerning the science of climate change, emphasizing the advances since the publication of the previous assessment report, AR4. The sum total of all the reports runs to thousands of pages and so a short summary of AR5 for policy makers of length about 30 pages was produced.

Since the First Assessment Report (FAR) confidence has grown in the conclusion that the production of greenhouse gases by mankind's burning of fossil fuels will contribute to climate change. In AR5 the IPCC assesses that it is extremely likely that human influence has been the dominant cause of the observed warming since the mid-20th century. Here extremely likely is defined as 95% probable. This statement implies that it is less than 5% probable that more than half the warming is due to natural causes. AR5 points out that such warming will lead to more extreme weather events. It will also lead to rising sea levels due to the thermal expansion of the oceans and to the melting of glaciers and of the Greenland and Antarctic ice sheets.

10.9 GOVERNMENTAL RESPONSES TO THE IPCC

As a result of the IPCC Assessment reports a series of intergovernmental meetings has taken place. These resulted in the treaty known as the Kyoto Protocol committing State Parties to reduce greenhouse gas emission. The protocol was adopted in 1997 and came into force in 2007. There were 192 parties to the protocol (Canada withdrawing from it in 2012). The Protocol is based on the principle of common but differentiated responsibilities. It puts the obligation on the developed countries to reduce current emissions since they are historically responsible for the current increased level of greenhouse gases. So far since industrialisation it is estimated that we have added 1000 gigaton (GT) of carbon equivalent to the atmosphere. It is estimated that there are of order a further 10000 GT which could result from burning the remaining World's reserves of fossil fuels.

The Protocol's first commitment period started in 2008 and ended in 2012. A second commitment period was agreed in 2012. This was known as the Doha Amendment, in which binding targets were set. However, there is some reluctance by several countries notably the United States and Canada to sign up to such legally binding targets. A further summit meeting took place in Paris 2015. The participating countries at this meeting undertook to limit greenhouse gas emissions to the level at which the ultimate rise in average global temperature will be less than 2°C with the hope that this could even be limited to 1.5°C.

To assist with the decision on which emission cuts to aim for, the IPCC in AR5 has considered various scenarios in predicting the future warming of the Earth. These are predictions for concentrations of 421, 534, 670 and 936 ppm of carbon dioxide in the atmosphere by the year 2100. These represent different emission cutting scenarios. The 421 ppm concentration is for a very severe and probably unattainable cut in emissions and the last figure is the projected level assuming no mitigating cuts i.e. business as usual with continued unfettered use of fossil fuels. The radiative forcing (see Chapter 7 section 6 for the definition of this quantity) resulting from these concentrations are 2.6, 4.5, 6.0 and 8.5 Wm^{-2}, respectively. The scenarios are labelled RCP2.6, RCP4.5, RCP6.0 and RCP8.5 where the term RCP stands for Representative Concentration Pathway. The climate models were studied in detail for each of these concentrations of carbon dioxide and the graphs shown in figures 10.1 and 10.2 give the results for RCP2.6 and RCP8.5 together with the averages at the end of the 21st century for all 4 scenarios. These results act as a guide to show the effects of future fossil fuel burning.

In conclusion the Earth is expected to see substantial warming by the end of the 21st century as well as a rise in sea level and other climatic effects such as increases in extreme weather events. This is confidently thought to be due to the continued use of fossil fuels by mankind. There are uncertainties in the amounts of these quantities both in the scientific predictions and in the political will to act on the warnings of the IPCC. There are two areas of hope for the future. The first is that governments will come up with binding agreements to limit the production of greenhouse gases from burning fossil fuels. The second is for technological innovations which will produce energy cleanly without the need for fossil fuels.

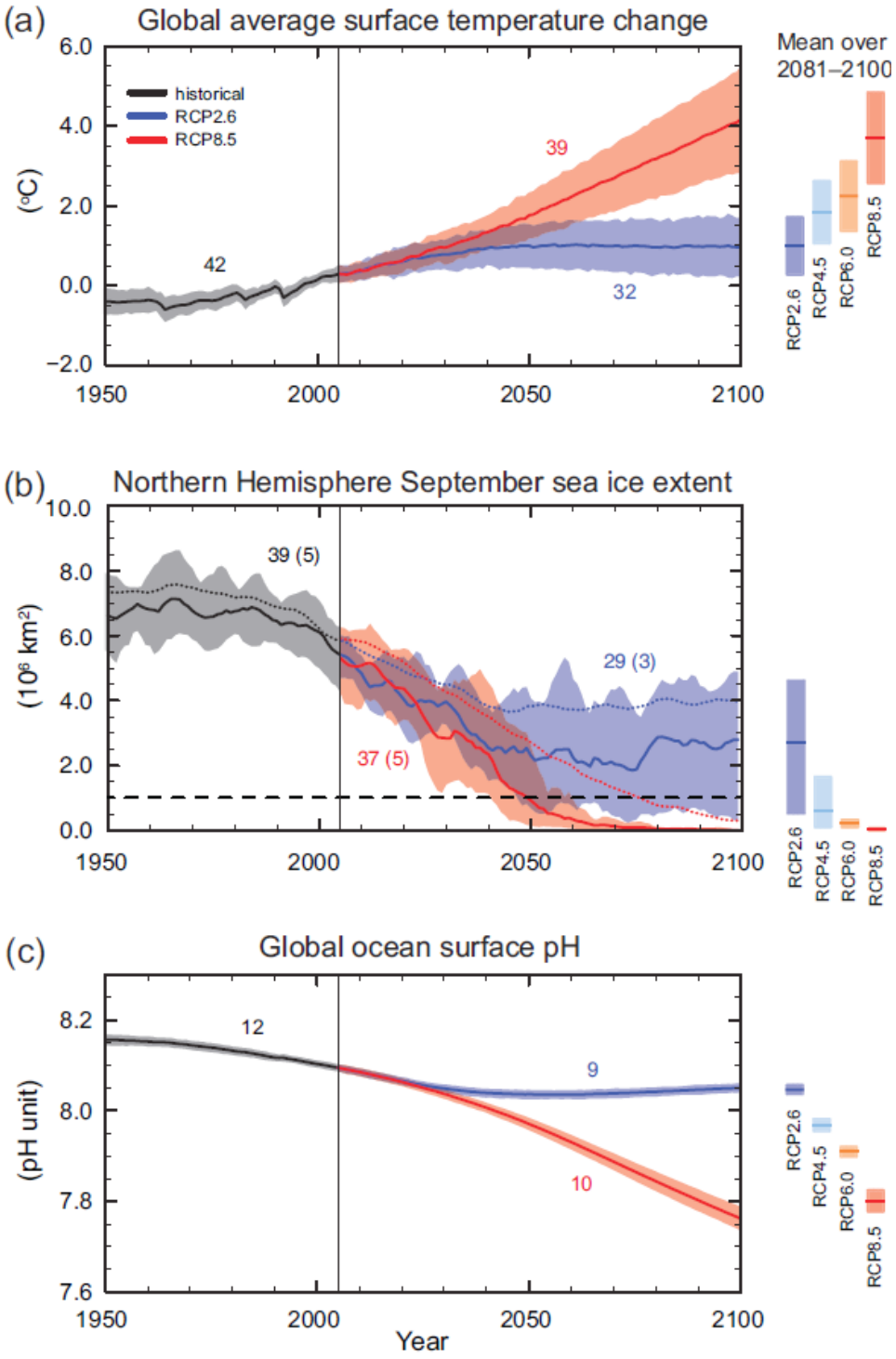

Fig. 10.1 The model predictions (labelled CMPI5) for the variation of a) global mean surface temperature for RCP2.6 and RCP8.5, b) Arctic sea ice extent (dashed line is the nearly ice free condition) and c) ocean acidity. The shaded regions show the uncertainties on these predictions i.e. the 90% confidence intervals. The numbers on each curve represent the number of models used to derive the averages. The bars on the right show the projected means of the all 4 forcings for 2081–2100. (Source IPCC AR5, Summary for Policy Makers fig. SPM 7).

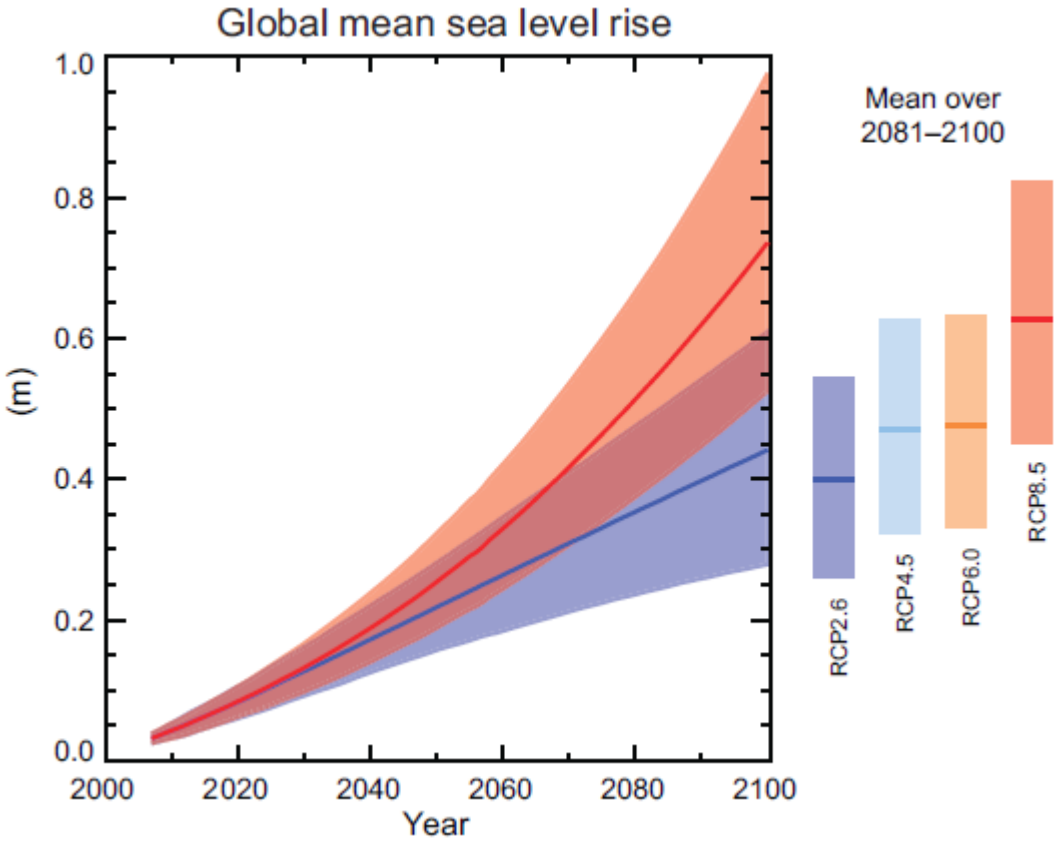

Figure 10.2 As figure 10.1 but showing the projected sea level rise. (Source IPCC AR5, Summary for policy makers figure SPM 9).

References

Houghton and Tavner 2013 "In the Eye of the storm, the autobiography of Sir John Houghton" by Sir John Houghton and Gill Tavner , published by Lion Hudson plc, Oxford, ISBN 978-0-7459-5584-1.

Houghton J 2015 "Global Warming: The Complete Briefing", fifth edition, Cambridge University Press. ISBN 9781107463790.

IPCC AR5 reports published in 2013 and 2014 are available at http://www.ipcc.ch/.

11 EPILOGUE

This book describes the science behind the reasons why increasing greenhouse gases in the atmosphere give rise to global warming and eventual climate change. As in all scientific measurements there are uncertainties. For example, the uncertainties in the calculations of radiative forcing allow a small probability of 5% that more than half the warming to date is natural rather than man made (see figure 7.6). This means that it is 95% probable that the warming is mostly man-made. On this basis the IPCC said in its 2013 report AR5 that it is extremely likely that most of the global warming seen since industrialisation is man-made.

It is for this reason that vast majority of expert climatologists accept the paradigm that increasing greenhouse gas concentrations due to burning of fossil fuels have created and will continue to create the global warming seen since industrialisation. There are few expert climatologists who disagree with this (Cook et al 2013). Furthermore most scientists from other disciplines also now accept this paradigm (Carlton et al 2015). However, surveys of opinion among the public at large show that about half the population either accepts that the Earth is warming but that this is natural rather than man-made or they do not accept that it is warming at all. Such a position is assisted by a generally hostile approach to the subject by the right wing press (Painter 2011 and Painter and Ashe 2012).

Suppose that the experts were wrong and the effect of greenhouse gases has been overestimated. Then the real climate should have experienced less warming from greenhouse gases than is seen. Hence the warming seen in the 20th Century would need a new, unknown phenomenon to explain it. Such a new, unknown process seems rather improbable given the many years of climate research that have taken place. Furthermore, the new phenomenon would need to produce warming rather than cooling. It can be seen that such a chain of events is stretching credibility and therefore must have rather a low probability to be true.

It seems obvious that if we burn off the fossil fuels laid down over several hundred million years in a time of order 200 years that damage to the climate will occur. However, a trawl of the World Wide Web (www) shows that there is a large number of people who deny either partially or totally that man-made global warming can happen. Presumably they are holding on to the small probability that such warming is natural in origin, despite the testimony of the experts in the field. Such doubts are reinforced by a generally hostile press which reports the blogs on the www as if they come from serious scientific research. Research shows that it is generally the press with a right wing bias which takes this line (Painter 2011).

There are also various think tanks around the World which encourage such doubt. These again usually support the political right wing. These think tanks often use the views of some scientists who are rarely experts on the climate but who advance alternative hypotheses for global warming rather the increasing concentrations of greenhouse gases. None of these scientists give reasons why increasing greenhouse gases do not cause global warming.

Various reasons have been advanced for such denial. For example it is the right wing which fears Government interference and global warming and climate change is seen as giving governments a means to interfere in free market economics (Oreskes 2010). In other quarters global warming and climate change are seen as threats to current life styles so denial is adopted as a defence mechanism. Such reaction has happened in previous histories. For example, the Church in Italy in the 17th century responded in much the same way to Galileo when he presented incontrovertible evidence that the Sun was the centre of the Solar System rather than the Earth. Presumably the Church in Italy saw this as a threat to its position. The tobacco industry responded in much the same way in the 1960s when it was first realised that smoking and ill-health were connected. It followed a similar line to the current climate change denial i.e. impugning the honesty of the scientists reporting their finding and inventing pseudo-scientific arguments to make the public believe that the findings were controversial amongst the scientific experts.

Most of the arguments given by such doubters of man-made climate change are either pseudo-scientific or political (see for example http://www.express.co.uk/news/uk/146138/100-reasons-why-climate-change-is-natural). An example of a political argument is that the scientists find positive effects so that they can protect the funding of their future research. This impugns the honesty of the scientists by implying that they find false results. Such false results are quickly found out when other scientists join the investigations. It also assumes that they are willing to do research which will not lead anywhere. These accusations come from people who do not know science and scientists. It will be very hard to find scientists who would do either of these things.

Examples of pseudo-scientific arguments are

1. There has been no global warming since 1998.
   While it is true that the average global surface temperature increase seems to have slowed since 1998 (up to 2015) this must be only a temporary phenomenon since the greenhouse gas concentrations are increasing apace. Furthermore, the oceans continue to warm rapidly (see ocean heat content figure 5.7) with much more heat going there than to the atmosphere. The oceans continue to become more acid due to the increasing greenhouse gas concentrations (see figure 11.1) and glaciers continue to melt at an increasing rate. The sea level continues to rise (see figure 5.7) mostly due to melting glaciers and polar ice and the remainder from thermal expansion of the ocean due to warming (Llovel et al 2014). The early 21st century slow-down is therefore temporary and is due to natural variability of the many other factors which govern the climate as well as greenhouse gases. There was a similar slow-down in the 1940s. One theory is that it is due to increased heat sinking to a depth of order 1500m in the ocean (Chen and Tung 2014). This theory predicts that warming will occur in cycles with alternate rapid and slow warming trends.

2. The climate has always been changing naturally and the twentieth century change is another natural variation.
   It is true that the climate has seen many changes during the Earth's history, as we saw in Chapter 9. However, during the last 10000 years or so the climate has been relatively stable (see figure 1.1 and Marcott et al. 2013 and the graph at http://cdn.theatlantic.com/static/mt/assets/science/marcott-B-CD.jpg). This has allowed mankind to flourish and civilisations to grow. Before this time mankind was a hunter-gatherer. The IPCC in AR5 (AR5 2013) predicts an increase in the frequency of extreme weather events and a large rise in sea levels as a result of unfettered global warming from increasing uses of fossil fuels. This will interfere in the long run with the stable climate which we have grown to expect with uncomfortable consequences for the present World population, especially for developing countries who have limited resources to adapt.

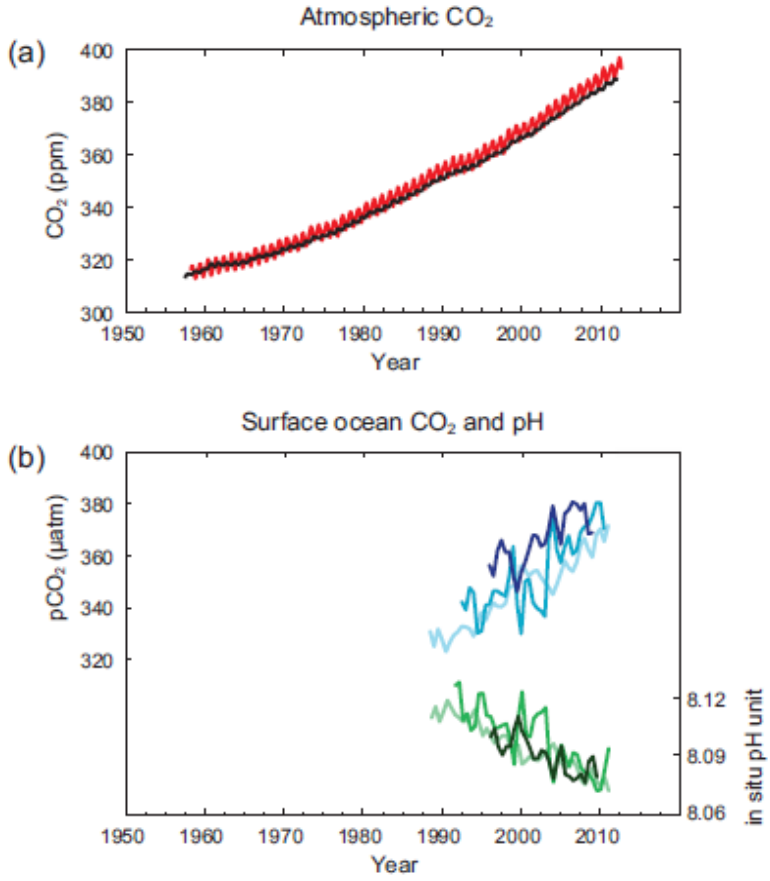

Figure 11.1 a) carbon dioxide concentration variation with time from Mauna Loa, Hawaii, b) partial pressure of dissolved CO2 at the ocean surface (blue curves) and acidity of the sea water (measured by its pH) at locations in the Atlantic Ocean (dark blue, dark green) and in the Pacific Ocean (light blue, light green) (Source IPPC AR5 figure SPM.4).

3. The arguments are based on unreliable computer models.
   As shown in Chapter 7, the models are based on sound physical principles. While it is true that complicated models are needed to obtain a precise prediction of the global temperature rise with greenhouse gas concentration, the underlying first order process described in chapter 7 shows that there is a bona fide effect present. Complicated models are not necessary to understand this first order process.

There are many other less plausible pseudo-scientific arguments given by the doubters. Hopefully, after having read this book, the reader will be in a better position to recognise the pseudo-science, to understand the true situation and to explain it to others.

References

AR5 2015 The fifth Assessment report of the IPCC available at the IPCC web site (http;//www.ipcc.ch/).

Carlton J.S., Perry-Hill R., Huber M., Prokopy L.S. 2015, "The climate change consensus extends beyond climate scientists", Environmental Reseacrh Letters 10 094025.

Chen X. and Tung K.T., 2014, 'Varying planetary heat sink led to global-warming slowdown and acceleration', Science Vol. 345, pp. 897–903. Doi:10.1126/science.1254937.

Cook J. et al. 2013 "Quantifying the consensus on anthropological; global warming in the scientific literature", Environmental Research Letters Vol. 8 (2), 024024.

W. Llovel et al 2014, 'Deep-ocean contribution to sea level and energy budget not detectable over the past decade', Nature Climate Change, Vol 4 pp 1031–1035. Doi 10.1038/NCLIMATE2387.

Marcott S.A., Sharlem J.D., Clark P.U. and Mix A.C., 2013, "A Reconstruction of Regional and Global Temperature for the Past 11300 years", Science vol. 339 pp. 1198–1201.

Oreskes N. 2010, Lecture http://www.fas.harvard.edu/~hsdept/bios/oreskes.html and "Merchants of Doubt", Bloomsbury Press, NY).

Painter J. 2011, "Poles Apart", published by Reuters Institute for the Study of Journalism, Oxford UK. ISBN 978-1-907384-07-03.

Painter J. and Ashe T.A. 2012, "Cross-national comparison of the presence of climate scepticism in the print media in six countries, 2007–2010", Environmental Research Letters 7 044005.

ENDNOTES

(1. The absolute temperature in degrees Kelvin (K) is frequently used in this book i.e. the temperature in degrees C plus 273 degrees. A temperature of zero K is that at which the motion of atoms and molecules essentially ceases (neglecting quantum mechanical effects).)

(2. $\boldsymbol{\Omega}$ is a vector in the direction of a right handed screw moving in the sense of the Earth's rotation with a magnitude of the angular velocity of the Earth in radians per second ($7.27\ 10^{-5}$ radians per second). The vector product $\boldsymbol{\Omega}\times\boldsymbol{v}$ is a vector pointing in the direction of a right handed screw moving from the vector $\boldsymbol{\Omega}$ to vector $\boldsymbol{v}$ and of length $|\boldsymbol{\Omega}||\boldsymbol{v}|\sin\theta$ where the || sign means the length of the vector and θ is the angle between vectors $\boldsymbol{\Omega}$ and $\boldsymbol{v}$.)

(3. The notation is used that 1 Ma=1 million years, 1 Ga= 1000 Ma or 1 billion years.)

(4. ppm = parts per million in concentration.)

(5. This became known as the First Assessment Report or FAR. This was followed by the Second Assessment Report (SAR, 1995), the Third Assessment Report (TAR, 2001). The fourth and fifth Assessment Reports known as AR4 and AR5 followed in 2007 and 2013. All the reports are available at www.ipcc.ch.)